PROPERTIES OF POLYCRYSTALLINE GaAs FILMS GROWN BY THE CLOSE SPACED VAPOUR TRANSPORT TECHNIQUE ON Mo SUBSTRATES

by

BLAIR RUSSEL

B.A.Sc., University of British Columbia, 1972

A THESIS SUBMITTED IN PARTIAL FULFILMENT OF
THE REQUIREMENTS FOR THE DEGREE OF
MASTER OF APPLIED SCIENCE

in the Department
of
Electrical Engineering

We accept this thesis as conforming to the
required standard

THE UNIVERSITY OF BRITISH COLUMBIA
September 1976

In presenting this thesis in partial fulfilment of the requirements for an advanced degree at the University of British Columbia, I agree that the Library shall make it freely available for reference and study. I further agree that permission for extensive copying of this thesis for scholarly purposes may be granted by the Head of my Department or by his representatives. It is understood that copying or publication of this thesis for financial gain shall not be allowed without my written permission.

Department of Electrical Engineering

The University of British Columbia
2075 Wesbrook Place
Vancouver, Canada
V6T 1W5

Date Sept. 25/76.

ABSTRACT

This thesis is a study of the properties of thin GaAs films grown on molybdenum substrates by the close spaced vapour transport (CSVT) deposition technique with the intention that the GaAs/Mo structure would be used as the semiconductor and substrate for economic solar cells. The GaAs films were polycrystalline cubic crystals with no preferred orientation. The crystallite area increased with the temperature at which the substrate was held during growth and at 710°C grain sizes of 100 μm^2 were observed. The crystallites formed a columnar-like structure with crystal size comparable to the film thickness. No impurities of foreign instrusions existed in the films in quantities observable on the electron microprobe.

The resistivity of the GaAs films was 220 Ω cm, hence acceptable for thin film solar cells, however, the GaAs/Mo contact was mildly rectifying. Diodes were fabricated by the deposition of Au onto the GaAs films and the resulting barriers showed values of barrier height of approximately 0.8 eV, ideality factor n = 1.5 to 2, and depletion-layer majority carrier concentration of roughly 10^{16} cm^{-3} as measured by J-V and C-V methods.

The GaAs films show promise for use in solar cells provided that the Mo/GaAs interface resistance can be reduced.

TABLE OF CONTENTS

LIST OF ILLUSTRATIONS

LIST OF TABLES

LIST OF SYMBOLS

Symbol	Description	Unit
AM0	Solar spectrum in outer space	
AM1	Solar spectrum at earth's surface for optimum conditions at sea level, sun at zenith	
A	contact area of diode	cm^2
A	first element of a compound	
A*	modified Richardson's constant = $\frac{4\pi qm^*k^2}{h^3}$	amps $cm^{-2}{}_oK^{-2}$
a_o	crystal lattice constant	Å
$\alpha(\lambda)$	absorption coefficient	cm^{-1}
$B_{(S)}$	second element of a compound (in solid phase)	
$B_{(V)}$	second element of a compound (in vapour phase)	
C	capacitance	farads
C_e	edge capacitance	farads
C'	equivalent capacitance measured by capacitance meter	farads
c	speed of light = 2.998×10^{10}	cm sec^{-1}
D_S	density of surface states	$eV^{-1}cm^{-2}$
$D_{B\delta}$	density of negative acceptor type boundary states (discrete energy level)	$eV^{-1}cm^{-2}$
D_{Bu}	net density of boundary states (uniform distribution)	$eV^{-1}cm^{-2}$
d	crystal interplanar spacing	Å
E	energy	eV
E_C	conduction band energy	eV
E_F	Fermi energy	eV
E_M	maximum electric field in the depletion region of MS diode	volts cm^{-1}
E_V	valence band energy	eV
$\mathcal{E}(\lambda)$	terrestrial solar energy radiation	watt sec m^{-2}

Symbol	Description	Unit
ε_S	- static value of the semiconductor dielectric constant	farad cm^{-1}
η_{SC}	- solar cell efficiency	%
G	- conductance	mho
I	- current	amps
I_M	- current delivered by solar cell at max. power	amps
I_S	- saturation current from ideal diode equation	amps
I_{Ph}	- photo generated current	amps
J	- current density	amps cm^{-2}
J_{rec}	- recombination current density	amps cm^{-2}
J_S	- saturation current density in diode equation	amps cm^{-2}
J_{ST}	- saturation current density for thermionic emission	amps cm^{-2}
J_{Srec}	- saturation current density for recombination current	amps cm^{-2}
k	- Boltzmann's constant = 8.62×10^{-5}	eV $°K^{-1}$
ℓ	- thickness	μm
ℓ_B	- length of intercrystal region	Å
ℓ_C	- length of crystal region	Å
λ	- wavelength	Å
m_o	- free electron mass = 9.108×10^{-31}	kg.
m*	- effective mass of electrons	kg.
ν	- frequency of photons	Hz
N_A	- concentration of acceptor stator	cm^{-3}
N_C	- effective density of states in the conduction band	cm^{-3}
N_D	- concentration of donor states	cm^{-3}
$N(\lambda)$	- irradiance	watts m^{-2}

Symbol	Description	Unit
N_V	- effective density of states in valence band	cm^{-3}
N_u	- net number of acceptor and donor surface states per unit energy	$eV^{-1}cm^{-2}$
N_δ	- number of acceptor type surface states per unit area at energy ϕ_δ ωrt E_V	$eV^{-1}cm^{-2}$
n	- an integer in Bragg's Law	
n	- empirical factor in the diode equation $J = J_S[\exp \frac{qV}{nkT} - 1]$	
p	- perimeter of metal contact on semiconductor	cm
ϕ	- potential height of barrier formed between 2 crystals	eV
ϕ_B	- metal-semiconductor barrier height	eV
ϕ_{Bn}	- metal-n type semiconductor barrier height	eV
n_i	- intrinsic carrier concentration	cm^{-3}
ω	- angular frequency = $2\pi\nu$	Hz
P_L	- power across load	watts
P_M	- maximum solar cell power	watts
ϕ_o	- energy level below which all surface states are filled for charge neutrality at the surface (before equilibrium)	eV
ϕ_δ	- the boundary states energy above E_V (E_V at the grain boundary)	eV
Q_B	- charge at the grain boundary arising from surface states	coul.
q	- magnitude of electronic charge = 1.6×10^{-19}	coul.
R	- resistance	ohms
R_L	- load resistance	ohms
R_S	- series resistance of semiconductor device = $r_{Sb} + r_C + r_M$	ohms
R_{SH}	- shunt resistance across diode	ohms
$R_{(V)}$	- reactive agent in vapour phase	

Symbol	Description	Unit
r_C	– resistance of back contact	ohms
r_M	– resistance of Schottky barrier metal film	ohms
r_{Sb}	– resistance of semiconductor bulk	ohms
ρ	– resistivity = σ^{-1}	ohm-cm
ρ_B	– resistivity of intercrystal region	ohm-cm
ρ_C	– resistivity of crystal region	ohm-cm
ρ_{Sb}	– resistivity of semiconductor bulk	ohm-cm
σ	– conductivity = ρ	mho cm^{-1}
σ_{SC}	– conductivity across a single crystal	mho cm^{-1}
$\bar{\sigma}$	– macroscopic conductivity (conductivity across a polycrystalline sample)	mho cm^{-1}
T	– temperature	°K
T_C	– cooler temperature at which reaction proceeds to left	°C
T_H	– hotter temperature at which reaction proceeds to right	°C
τ	– effective lifetime of carriers due to traps	secs
V	– voltage	volts
V_{bi}	– metal-semiconductor junction built in voltage	eV
V_i	– voltage intercept of C-V curves	volts
V_L	– voltage across a load	volts
V_n	– the energy difference between the Fermi level and the bottom of the conduction band in the semiconductor bulk	eV
$v_{ph(\lambda)}$	– spectral density of photons	m^{-2}
W	– space charge depletion width	cm
x	– displacement in x direction	cm

ACKNOWLEDGEMENT

I wish to thank my research supervisor, Dr. D.L. Pulfrey, for his encouragement and guidance throughout the course of this investigation.

Grateful acknowledgement is given to Mr. J. Lees for fabricating the quartz reaction chamber, Mr. Arvid Lacis for his instruction and assistance with the electron microscope instruments, Prof. R.G. Butters for the x-ray spectrometer analysis, and H. Stuber for his technical assistance.

The work described in this thesis was financially supported by the National Research Council (Grant No. A-7248).

Finally, I would like to thank my fellow graduate students in the Solid-State Group for their helpful discussions and also Miss Sannifer Louie for typing this thesis.

I INTRODUCTION

The photovoltaic solar cell is being given serious consideration as a supplier of a significant portion of the world's future energy demands (see appendix AI1). The success of terrestrial solar cells relies on developing new forms of materials and manufacturing processes which can bring about greatly reduced costs and increased production rates. The cost and production rate goals that will have to be met if photovoltaic electricity is to be competitive with other existing methods of generation have been estimated by Wolf [75 W1] at \$15-60/m^2 and 5×10^8 m^2/year. In comparison the 1975 values were \$2,000/m^2 and 2,000 m^2/year respectively.

The two fundamental requirements for conventional photovoltaic devices are; 1) a material that absorbs light while generating mobile charge carriers, 2) a potential barrier that separates the carriers so that they cannot recombine. Semiconductors with appropriate band gap fulfil the first requirement and junctions like p-n, hetero, metal-semiconductor (MS), and metal-insulator-semiconductor (MIS) fulfil the second.

The semiconductor is the most expensive component of the solar cell and viable terrestrial photovoltaic systems will have to improve the present \$/watt rating by using either high purity, high efficiency cells with concentrators, or reduced grade (purity and crystallinity) semiconductors in a thin film form suitable for large area coverage. In the former scheme Si and $Ga_{1-x}Al_xAs$ are already available but are prevented from immediate implementation by the high production cost and the need for cheap, suitable concentrator systems with heat sinking. In the latter scheme suitable materials and cell configurations are still

being developed and the existing problems are still of a fundamental, materials science nature. Junction formation in thin film cells is also a major area of investigation as the conventional p-n diode construction may not be applicable to the almost inevitably polycrystalline form of the thin semiconductor films on account of grain boundary diffusion.

This thesis seeks to contribute to the development of thin film semiconductor solar cells by evaluating the preparation and properties of a thin film semiconductor grown directly onto a metal substrate. The factors leading to the selection of the semiconductor material and its growth process are outlined in the following sections.

I-A Film Preparation Techniques

The price of single crystal semiconductors that are normally used for solar cells is from $2 to $4 for a 2 inch diameter by 10 mil thick wafer. This large thickness is only necessary for support not absorption. If an inexpensive metal foil could be used as both a substrate and electrode onto which a thin semiconductor film of only 5 μm. thick could be deposited, this would reduce the volume, and hence cost of semiconductor material used by about 100 times.

It is doubtful whether metal foils can seed single crystal films, but it has been shown by Fang [74F1] and Vohl et al [67V1] that Si and GaAs can be grown on metals in a polycrystalline form that shows promise for use in solar cells. The great advantage to thin film growth is the avoidance of the slow and costly Czochralski crystal growth method and the subsequent slicing, dicing and polishing of wafers.

Thin film deposition methods can be grouped into three categories; vacuum evaporation, sputtering, and chemical deposition.

Vacuum evaporation of semiconductors such as Si, Ge, and GaAs is usually done by electron beam evaporation. This method produces the purest results because interactions between evaporant and support material are greatly reduced (over the conventional resistance heater method). Substrate heaters are required to avoid amorphous films and after the evaporation a slow cool down cycle is necessary to minimize formation of dislocations. This lengthy procedure in conjunction with complex electron guns and related focusing equipment makes this method impractical in the present context. In addition the electron beam emits x-rays and produces secondary electrons on striking the surface of the evaporant which can cause radiation damage to the semiconductor.

Sputtering can also lead to radiation damage caused by ion beam bombardment. Fang ([74F1], p. 26) found, for Si in particular, that sputtering would not be economical for solar cells because of the slow rate of deposition ($\approx$ 1 μm/hr.). Other semiconductors are likely to sputter as slowly, leaving sputtering as an uneconomical process.

Chemical methods form the largest group of film preparative procedures, but most of them, e.g., electroplating, chemical reduction, anodization etc. are suitable only for amorphous film growth. However, chemical vapour or liquid phase growth does produce crystallinity. The most familiar chemical vapour deposition (CVD) technique is the pyrolysis of silane, but the resulting films are almost as expensive as single crystal Si. The simplest and most direct method of growing GaAs by CVD is the close spaced vapour transport technique developed by Nicoll [63N1]. A preliminary investigation of this technique by Vohl et al [67V1] showed that GaAs can be deposited by Nicoll's method onto metals in polycrystalline form. The well-known liquid phase epitaxy of GaAs has only been

used to grow crystals from other single crystal seeds and it is uncertain what kind of films liquid phase epitaxy would produce on metals.

I-B Semiconductor Selection

Three semiconductors, CdS, Si and GaAs, are currently being intensively investigated as bases for thin film semiconductor solar cells.

From a low cost, large area point of view the CdS based device would seem to be an ideal cell for terrestrial applications. It is a thin film polycrystalline cell fabricated by either evaporating or spraying a CdS layer on an inexpensive substrate and overlaying a Cu_2S film by a chemical dipping process. Unfortunately, the cell has several major problems. The photovoltaic properties of Cu_2S are a strong function of its stoichiometry which is difficult to control in fabrication and degrades in the presence of minute quantities of moisture. Also, despite more than a decade of development, the efficiencies are still only 5-7%. This is still below the minimum value of 10% efficiency that a recent preliminary cost analysis has indicated to be required for terrestrial applications (see Wolf [75W1] Fig. 2).

Single crystal Si cells have monopolized space applications for the past 20 years, and this development has led to present AM1 efficiencies of 19% as reported by Lindmayer and Allison [73L1]. Inexpensive thin film cells have been only moderately developed. Fang [74F1] has deposited Si films on a variety of substrates by evaporation and pyrolysis of silane and has investigated their properties. Chu et al [75C1] have made polycrystalline solar cells by the thermal reduction of trichlorasilane on graphite and metallurgical grade silicon substrates. Efficiencies were still very low, namely 2.5 and 4% respectively.

In the past GaAs solar cells have been only a laboratory curiosity. However, recently the $Ga_{1-x}Al_xAs$ heterostructure has been reported [75E1] with AM1 efficiencies of 21% and the good thermal stability of this arrangement leads to an expectation of its use in conjunction with concentrators. Vohl et al [67V1] are the only investigators who have worked with thin film GaAs cells and their Pt/GaAs cells on Mo foil produced 4.5% efficiencies.

GaAs thin films are the natural choice over Si considering their greater absorption of energy and higher potential efficiencies. Fig. I-1 shows that Si cells generally require more than 10 times as thick material as GaAs in order to realise comparable efficiencies. Although Ga is more expensive than Si at present market values, it is still more profitable to use GaAs for absorptions up to 95% of incident energy. Prices can be compared in Table IA-1. Details of the program and data used in obtaining Fig. IA-1 are given in appendix AI 2.

Other advantages are:

1) GaAs has a better high temperature performance compared with materials like Si which have smaller band gaps.
2) MS structures are well suited to thin film GaAs because the high absorption in GaAs generates most carriers near to the metal in the field region.
3) In polycrystalline form GaAs cells have been estimated by Woodall and Hovel ([75W2], p. 1005) to have a 3:1 cost advantage over poly. Si at 10% efficiency.

The authors arrived at this factor by assuming that the carrier diffusion lengths were equal to the grain size (for the purpose of accommodating the effect of recombination at the grain boundaries) and by modelling

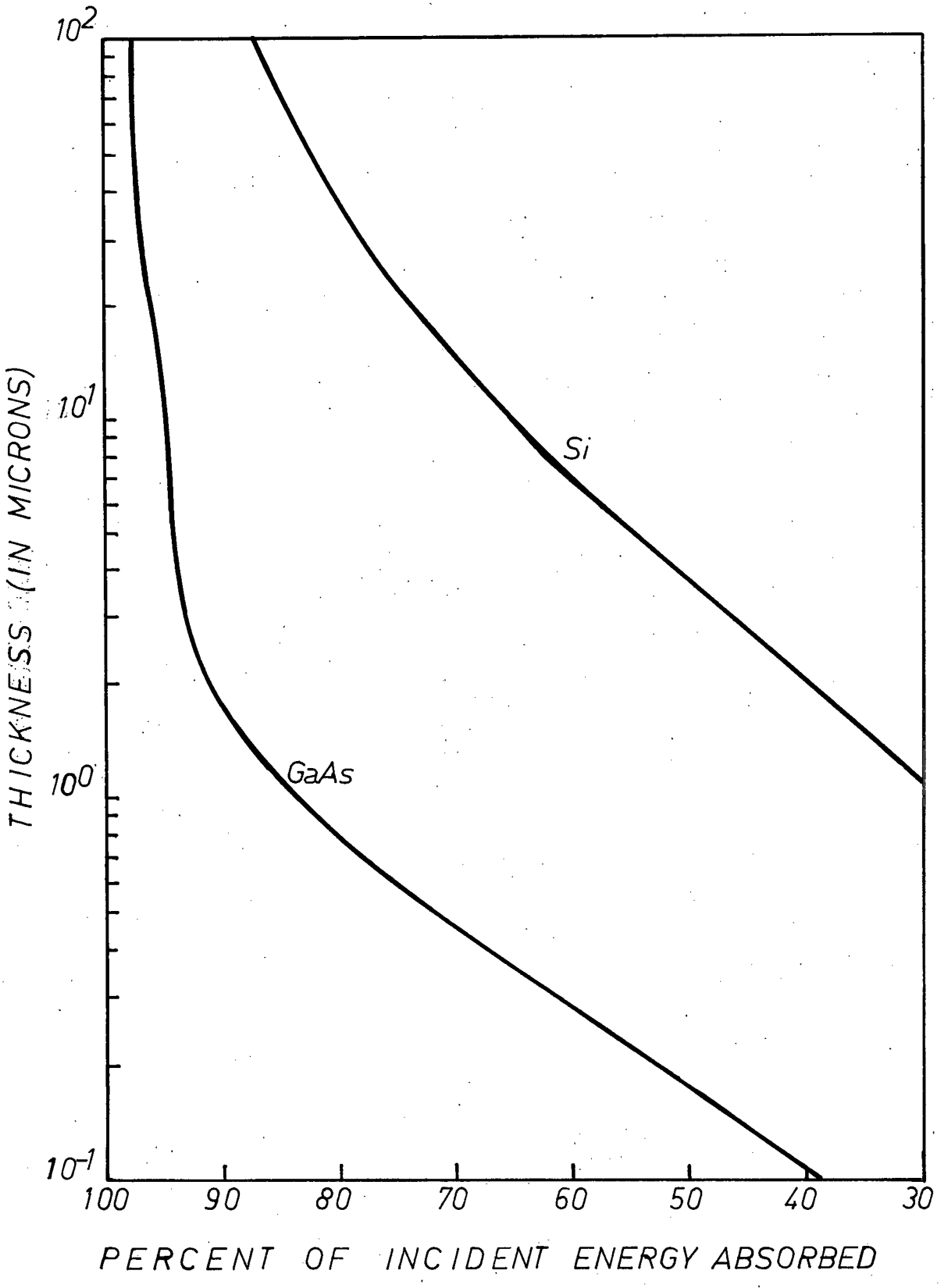

Fig. IA-1 Percent of Incident Energy Absorbed versus Semiconductor Thickness

Cell	Element	U.S. Production (in 1,000 kgm)	Cost $/kgm.	% Purity
Si	Si	1250 (1974)	60	.2 PPB
GaAs	Ga	.3 (1968)	750	10 PPB
	As	19×10^3 (1968)	1.21	pure

Table IA-1 Semiconductor Market Prices
(Taken from [75W2] table 24)

the cell as a single vertical crystal cell (parallel combination of filamentary crystals). The resulting calculations revealed that poly. GaAs cells were better than poly.Si cells in sustaining their efficiencies with decreasing grain size.

I-C Summary

Vohl et al.'s work showed that CSVT GaAs solar cells were feasible but at that preliminary stage inadequate. Efficiencies were only about 5% and contact and stability problems were apparent. Nevertheless the technique shows promise and it is clear that investigations into the microstructural and electrical properties of the GaAs films are required before improvements can be made. It is the aim of this thesis to perform these investigations and to further evaluate the CSVT method as a possible method for fabricating thin film solar cells.

Chapter II reviews the CSVT technique and summarizes previous work in this area using GaAs. Chapter III analyses the microstructure of the chemical vapour deposited GaAs thin films and Chapter IV deals with the electrical properties of Schottky barriers formed by deposition of Au onto the thin film GaAs. J-V and C-V measurements are used

to find resistivity, barrier height, quality factor, and majority carrier concentration in the diodes. The conclusions to be drawn from this work and recommendations for further research are given in Chapter V.

II THE CLOSE SPACED VAPOUR TRANSPORT TECHNIQUE

II-A Close Spaced Vapour Transport Theory

Vapour phase growth or vapour plating is the deposition of a film on a substrate by means of a chemical reaction involving the vapour phase. The material to be deposited is vaporized and transported by convection or diffusion to the substrate where, under the correct conditions, a solid phase film can be seeded and grown (see e.g. Fig. IIA-1).

The close spaced vapour transport (CSVT) technique is vapour phase growth with the substrate placed a short distance from the source as shown in Fig. IIA-2. A slow flow of a carrier gas containing a reactive agent is introduced between the source and substrate. The source is held at a high enough temperature (T_H) in order that the reactive agent can oxidize the source producing the vapours shown on the right of equation IIA-1

$$\underset{\left(\begin{smallmatrix}\text{source}\\ \text{compound}\end{smallmatrix}\right)}{AB_{(s)}} + R_{(v)} \underset{T_C}{\overset{T_H}{\rightleftharpoons}} AR_{(v)} + B_{(v)} \qquad \text{(IIA-1)}$$

These gases transport easily bby diffusion to a cooler substrate (T_c) where the reactive agent is reduced so that A and B can nucleate on the substrate as a film of the original source material, i.e. reaction proceeds to the left in eq. IIA-1. Ideally, the source and substrate should be independently heated, but this is difficult to achieve in practice. A reasonable method is to obtain the heat required by absorption of high intensity light incident on relatively massive heater blocks which are in thermal contact with either the source or the substrate (see Fig. IIA-2). Non-conducting inert spacers between source and substrate are used for separation and thermal isolation. Source and

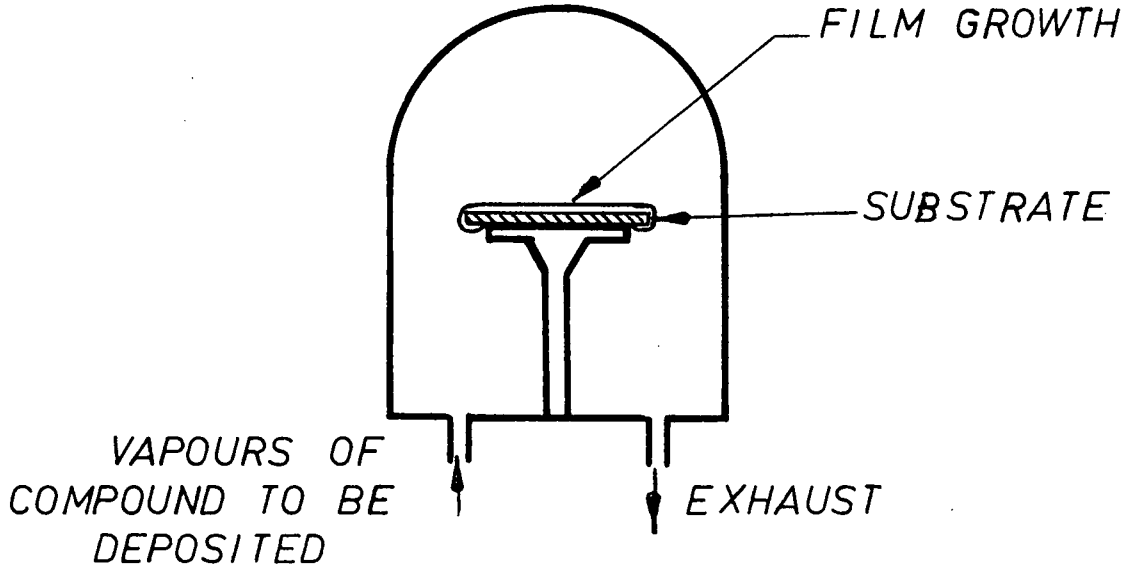

Fig. IIA-1 Simplified Chemical Vapour Growth Chamber

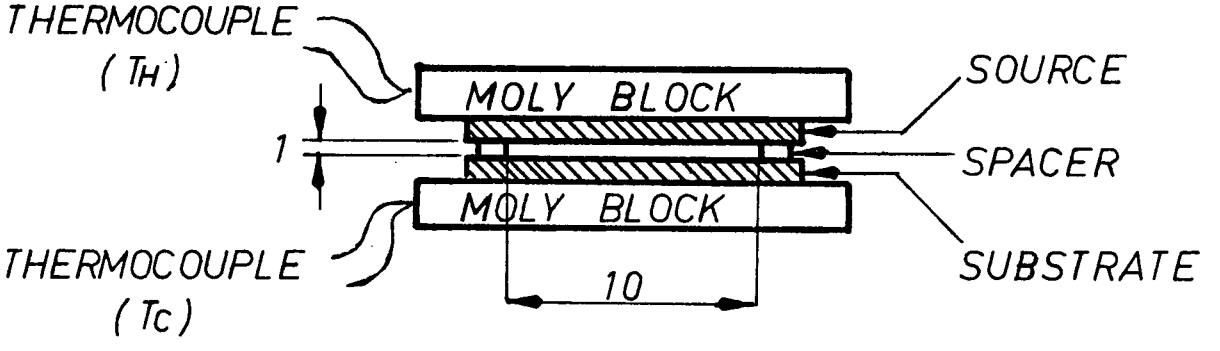

Fig. IIA-2 Source and Substrate Arrangement for CSVT

substrate temperatures are monitored by thermocouples inserted into the heater blocks.

As a deposition system this technique's main advantage is simplicity and the ability to be used at atmospheric pressure. For solar cell fabrication the benefit from using close spacing is the relatively unlimited area on which a film may be grown. Only the spacing is critical so that cells could be mass-produced in large sheets using a powdered source. Another advantage results from the efficient use of the reactive agent. After each transport R returns to its original form after deposition. It therefore can be used again and again for transport since the source is close to the substrate. This multiple use of reactive agent reduces the required amount of both transport and reactive agent yielding reported mass-utilization efficiencies of 90-98% (see Robinson [63R1]).

GaAs has been grown by the CSVT technique using a H_2O reactive agent transported on pure H_2 gas. The chemical reaction is believed to proceed as in equation IIA-2 (from Frosch and Thurmond [62F1]).

$$2GaAs_{(s)} + H_2O_{(v)} \underset{T_C}{\overset{T_H}{\rightleftharpoons}} Ga_2O_{(v)} + H_{2(v)} + As_{2(v)} \qquad \text{(IIA-2)}$$

II-B Review of Previous Work

The CSVT technique for the deposition of GaAs has been studied in some detail at RCA by Nicoll [63N1], Robinson [63R1], and Gottlieb and Carboy [63G1]. The main thrust of this work was to investigate the parameters affecting the growth of GaAs on single crystal Ge. The following paragraphs are summaries of the results.

1. Flow Rate

Gottlieb and Carboy investigated the effect of the H_2 flow rate

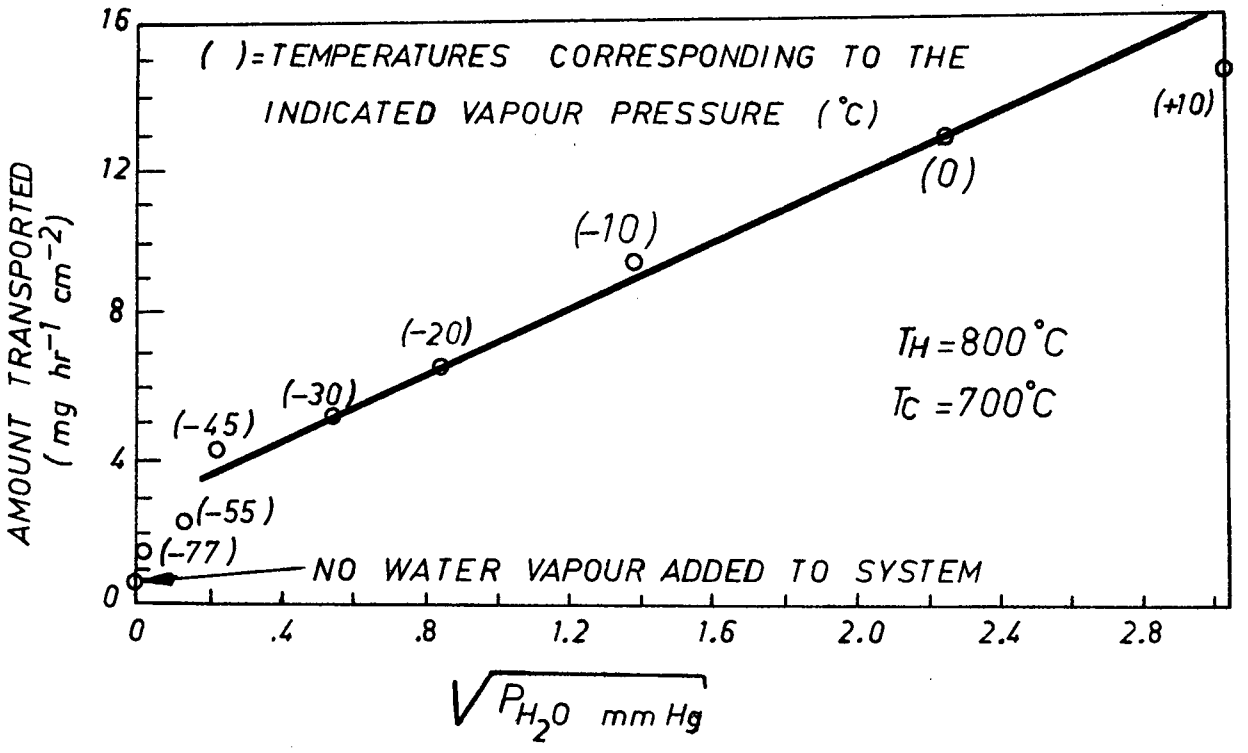

Fig. IIB-1 Amount of GaAs Transported as a Function of Water-Vapour Pressure (from Gottlieb and Carboy [63G1], p. 586)

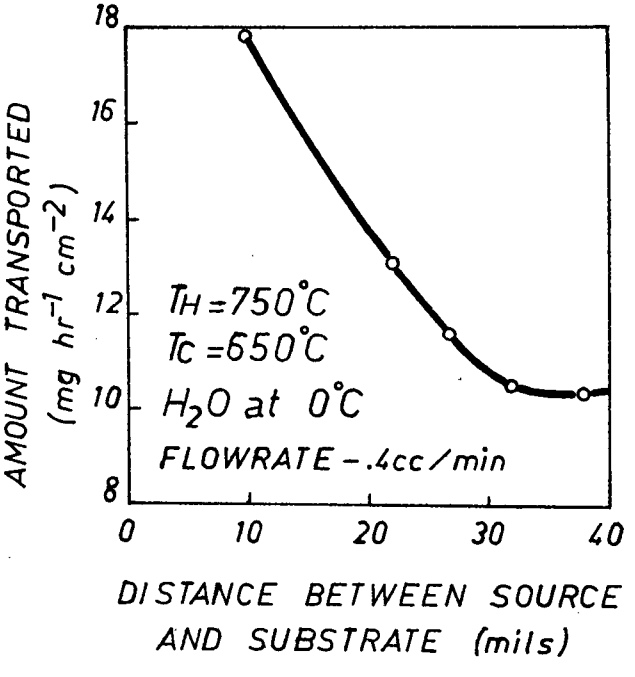

Fig. IIB-2 Amount of GaAs Transported as a Function of Spacing (from Gottlieb and Carboy [63G1], p. 591)

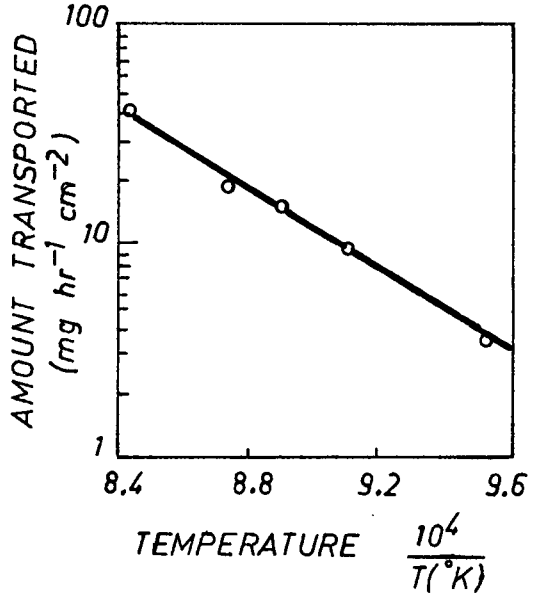

Fig. IIB-3 Log Rate of Transport vs Temp. (from Robinson [63R1], p. 579)

on the amount of GaAs transported (weight loss of GaAs source). It was found that the H_2 flow rate had little bearing on the transport rate. However, an increase in water vapour pressure caused an increase in transport rate, see Fig. IIB-1.

2. Spacing

As the name implies the 'close spaced vapour transport' technique relies on the short distance between source and substrate for transportation effectiveness. Nicoll ([63N1], p. 1165) stated that a spacing of less than 1/10th the diameter of the source area was necessary for efficient transfer. Gottlieb and Carboy [63G1] grew samples with different spacing and produced the plot in Fig. IIB-2. If most of the samples were about 1 cm. in diameter (380 mils) it can be seen from this graph that transport efficiency increases once Nicoll's criterion is satisfied.

3. Temperature

Temperature affects the reaction and it would be expected that higher source to substrate temperatures would speed up the kinetics of the film growth. Robinson [63R1] plotted the log rate of transport versus reciprocal of source temperature (substrate temperature held constant) and as expected mass transport increased with temperature (see Fig. IIB-3) and from this plot an energy of activation of 43 kcal per mole can be calculated. Substrate temperatures tended to control the surface nature of the films; rough and dendritic for high temperatures and smooth for low temperatures. Growth rates were restricted by an upper bound imposed on the source-substrate temperature difference by the heater arrangement.

4. Surface Topography and Crystal Orientation

The authors did not report in detail on surface topography and crystal orientation; however, there is some evidence that the smoothest layers were obtained on the smoothest substrates. It was found that the best deposits were on chemically polished and vapour phase etched Ge wafers. Robinson [63R1] observed some source orientation effects and found that a [100] GaAs surface facing the Ge substrate yielded films with the smoothest surfaces.

5. Doping

The films reported by the RCA workers [63N1], [63R1], and [63G1] were invariably n-type regardless of any attempt to obtain the contrary, i.e. p type. This was likely due to the low vapour pressure of the common p-type dopant oxides and to Ga autodoping. A Zn-doped source also failed to produce p-type GaAs [63G1]. Controlling the amount of n-type doping was attempted with T_e and H_2S included in the H_2O vapour, but no quantitative results were reported.

All the authors did some work with source materials other than GaAs, notably GaP, InAs, CdS, ZnS and Ge. These sources all gave results similar to GaAs when deposited on substrates with similar crystal size and shape. However, all the above source materials, including GaAs, deposited as polycrystalline films onto quartz or metal foils. Structural properties like preferred orientation, crystal size and shape were not investigated.

II-C The Apparatus

The design of the apparatus used to grow GaAs by the CSVT technique for the present investigation stemmed from a consideration of the apparatus and results previously discussed (II-B). The reaction

chamber was made from quartz male and female 1 inch diameter ground junctions closed at the ends (see Fig. IIC-1). The female end could be removed to replace the source, substrate or spacers. A quartz tube connected through the male end supplied the source and substrate with the reactive agent as well as furnishing support. Two 625 watt Sylvania "Sun Guns" supplied the necessary energy to heat the molybdenum heater blocks which were in thermal contact with source and substrate.

The peripheral equipment is shown in Fig. IIC-2. A medical grade hydrogen source supplied the gas which was blown over ice, in order to absorb water vapour, and then was introduced into the quartz r reaction chamber. The ice, which was kept close to 0°C by a salt ice bath, produced a controlled partial pressure of H_2O in the H_2 gas stream. Two thermocouples attached to the molybdenum blocks monitored the source and substrate temperature with the aid of associated voltmeters. A water trap was connected onto the reaction chamber exhaust for protection against backup, as a scrubber, and as a means of checking H_2 flow rates. The latter function was achieved by counting the number of bubbles per minute and calibrating this rate with a soap bubble flow meter. The bubble count method was convenient because the rates used were very slow and close to the limit of satisfactory continuous operation of the soap bubble flow meter.

II-D Choice of Substrate Material

The criteria for choosing a suitable substrate involved its cost, stability, and thermal expansion compatibility with GaAs. The list below includes all the common substrate materials that were considered.

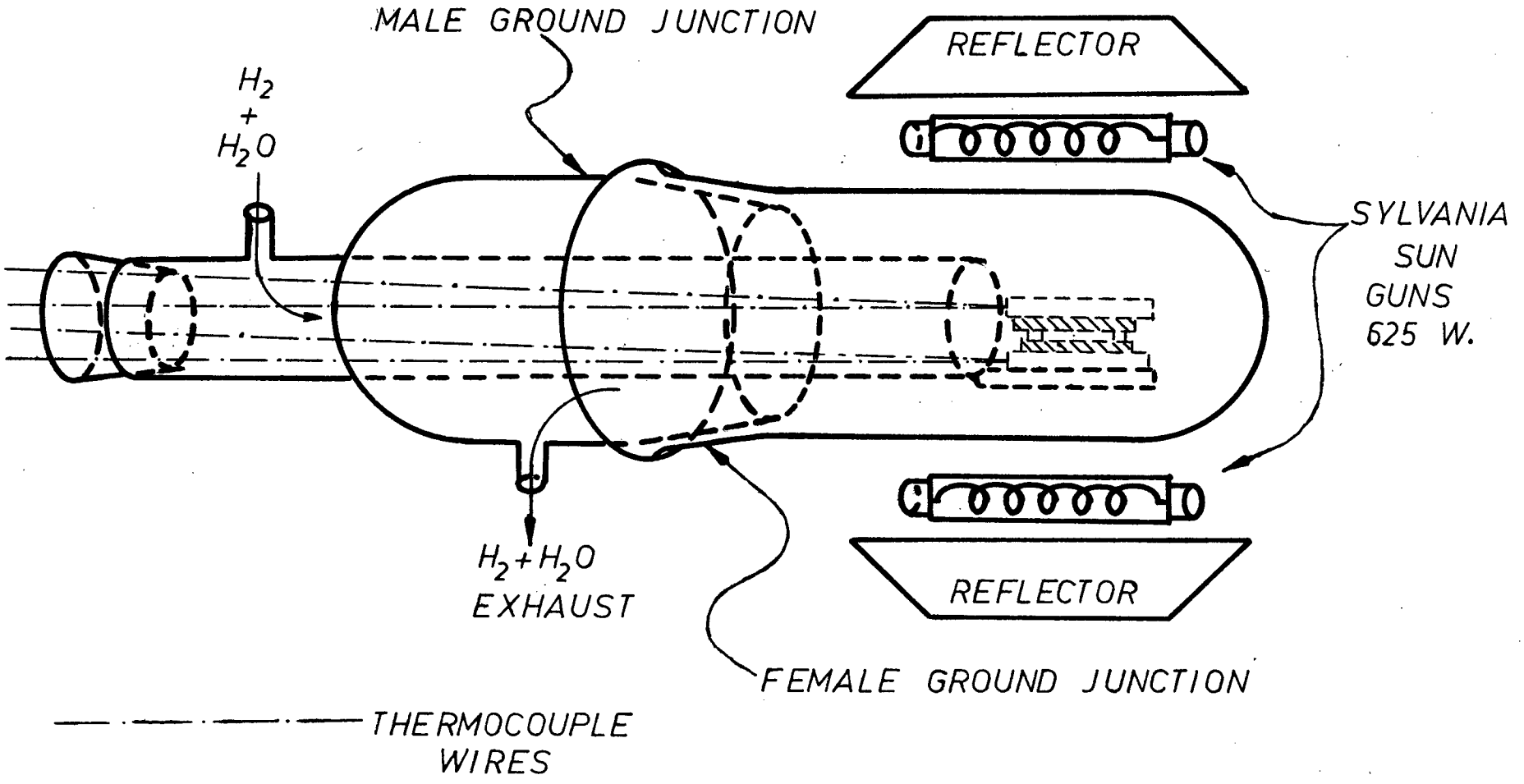

Fig. IIC-1 The Basic CSVT Apparatus

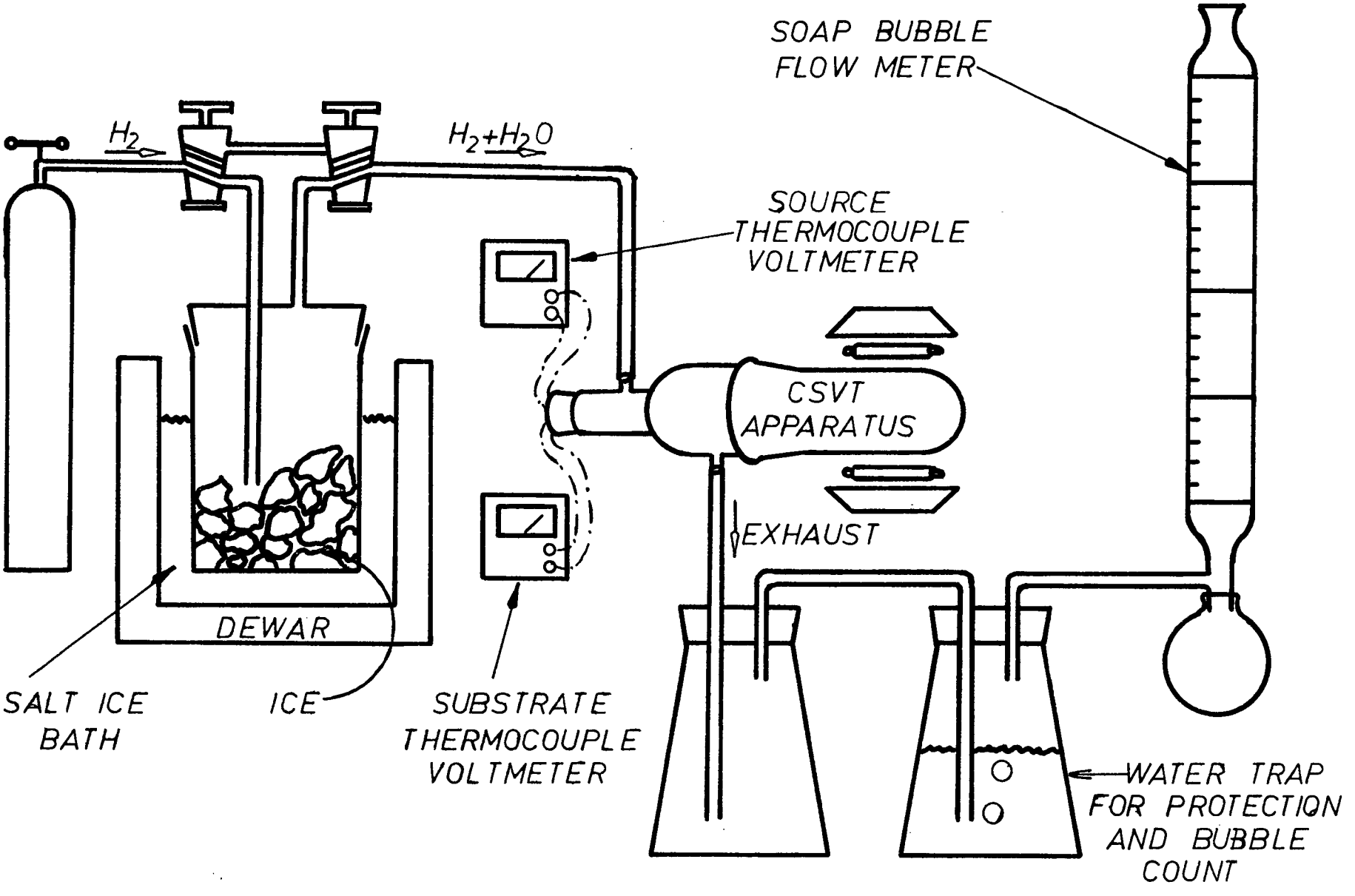

Fig. IIC-2 The CSVT Peripheral Equipment

1. Aluminum
2. Tin
3. Copper
4. Bronze (95% Cu, 5% Sn)
5. Brass (70% Cu, 30% Zn)
6. Steel
7. Stainless Steel
8. Kovar
9. Invar
10. Nickel-Iron Alloys
11. Tantalum
12. Tungsten
13. Molybdenum
14. Alumina (coated with metal electrode)
15. Fused Silica (coated with metal electrode)

The first and most important task was to find stable substrates. The high growth temperatures of the GaAs CSVT technique ($\approx$700°C) make the GaAs film particularly sensitive to diffusion or reactions with elements from within the substrate. Also the melting points of the base materials must be greater than approximately 750°C. Tin and aluminum have values below this and therefore would not, alone, support a GaAs film. Substrates that are "wetted" by Sn and Al could be used but most of the possible substrates could be used by themselves and therefore tin and aluminum are excluded.

Copper is a known dopant in GaAs (see Madelung [64M1], pp. 229, 230). Fuller and Whelan [58F1] found it diffused very rapidly especially along dislocations or surfaces. This type of diffusion would create shorting of a solar cell from heavily doped grain boundaries, therefore Cu and Cu alloys are to be avoided.

The principal component of steels and other Fe alloys is iron which acts as a deep acceptor in GaAs (Cunnell et al. [60C1], p. 103). Impurity diffusion information is unavailable for iron but it is thought not to be as rapid a diffuser as Cu. Diffusion could be prevented by coating these Fe alloys with passivation layers of SiO or metals such as

Ta, Mo, or W. In the case of SiO, a second film would be required to furnish the metal electrode. All these film formations require expensive electron beam evaporation or sputtering equipment and added processing steps which reduce their economic feasibility.

Kovar, Invar and other Ni-Fe alloys contain appreciable amounts of nickel and cobalt which have ionization energy levels deep in the band gap and thus form effective trapping centers ([64M1], p. 231). Therefore prevention of Ni and Co diffusion is also mandatory (and probably expensive).

The remaining metals Ta, W, and Mo are the most costly in the list. However, as outlined above, the inexpensive metals require passivation and thus their final cost would also not be cheap. There are two methods that would reduce the high price of Ta, W and Mo sheets. The first requires cold rolling the metals to their thinnest possible thickness ($\approx$.02 mm), thereby stretching them and reducing cost to a level where the substrate price could become comparable to that of the thin film semiconductor (see Table IID-1). The second method involves deposition of thin layers of inert metals onto cheap substrates. A 2000 Å layer sputtered or evaporated onto a smooth, high temperature material would furnish an electrode with electrical properties similar to that of the bulk metal.

Using the first substrate formation technique, it seems reasonable to consider Ta, W and Mo for use in the present investigation and molybdenum (.1 mm thick foil, 99.9% pure) was finally chosen as its coefficient of thermal expansion resembles most closely that of GaAs (see graph in Fig. IID-1). An initial attempt to smooth the roll marks in the molybdenum foil by electropolishing in 175 ml. methyl alcohol and 25 ml. sulfuric

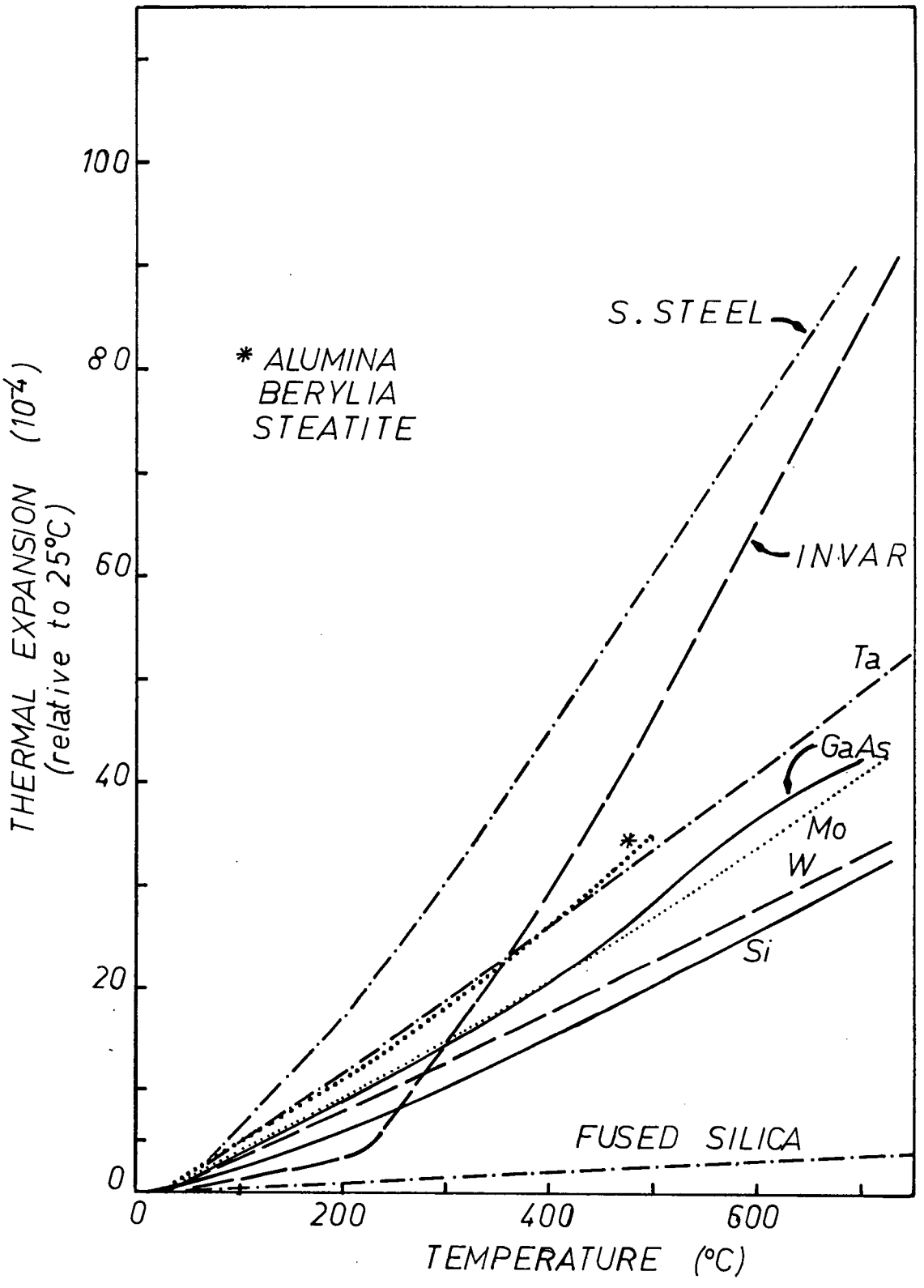

Fig. IID-1 Relative Thermal Expansion of Different Metals

acid at current densities varying from 0.6 to 1.0 amp/sq. cm resulted in the pitting and etching of all substrates. This was probably a result of contaminants present in the Mo reacting, unfavourably, with the acid. The smoothest and cleanest Mo surfaces were prepared by sputter etching the foils for 20 min. at 100 watts in argon at a pressure of 1.5×10^{-2} torr. The foils were precleaned in hot detergent and water, rinsed first in distilled water then hot methanol, and blown dry before insertion in a Perkin-Elmer r.f. sputtering system for the sputter etching.

The second method of substrate formation consisted of Mo (of the type and purity described above) sputtered onto fused silica slides. The same Perkin-Elmer sputtering system was used with a 6 inch Mo foil target. Fused silica slides were precleaned as outlined above and outgassed in the sputtering chamber at 10^{-6} torr for 10 min. 2000 Å of Mo (as later measured on a Sloan Angstrometer) was sputtered onto the quartz slides at 1.5×10^{-2} torr argon pressure with 100 watts forward power for 30 minutes. Films prepared under these conditions had a sheet resistance (measured by the 4 point probe method) of roughly 0.3 Ω/square. This value is equivalent to a film resistivity of 6×10^{-6} Ω cm and is only about 10% higher than the bulk value.

II-E Experimental Conditions

The experimental conditions used to grow GaAs by the CSVT technique in this present work were derived from the results of the RCA workers [63N1], [63R1], [63G1] summarized in Chapter II section C, and also from experience gained by using the particular experimental arrangement at U.B.C. Table IIE-1 lists the parameters used during each growth unless otherwise stated in the text.

A H_2 gas flow rate of 4 cc/min. gave a steady flow with adequate H_2O vapour for growth. The ice bath was held at 0°C for convenience and to give high transportation yield (see Fig. IIB-1).

Substrates and sources were roughly 1 cm^2 in area, therefore by Nicoll's criterion the spacing should be less than 1 mm. 500 μm was chosen.

For the particular experimental arrangement with Mo on fused silica substrates, temperatures were adjusted to establish optimum growth. The source temperature was varied from 650°C to 750°C whilst maintaining a 100°C temperature difference between source and substrate. At 650°C the GaAs film was not continuous but grew in isolated islands. At 750°C the film peeled or consisted of large dendritic growth. A substrate temperature of 710°C gave the smoothest results with an acceptable transport rate. The transport of GaAs reduces with lower source to substrate temperature. Therefore the maximum obtainable temperature difference was used (i.e. 100°C for this particular experimental arrangement). For the experiments using sputter etched Mo foil substrates the maximum temperature difference attainable was only 90°C.

The GaAs sources were obtained from Monsanto and were in the form of boat grown single crystal wafers 15 mils thick. They were n-type doped with Si to a carrier concentration of 2.0×10^{17} cm^{-3} (10^{-2} Ω cm).

Material (.25 mm thick)	Cost (10^6 \$/km^2)	Reference
Kovar	400	([74F1], p. 15)
Molybdenum	240	"
Tantalum	68	"
(42% Ni.) Fe alloy	1.1	"
Steel	.3	"
Cu (and Cu alloy)	7.8	"
Aluminum	.2	"
Fused Silica	> 400	
Alumina	> 400	
Si (100 μ thick)	14.	([74F1], p. 15)
GaAs (10 μ thick)	22.8	([75W2], p. 1005)

Table IID-1 Cost of Substrate Materials, Si, and GaAs

Description of Parameter	Quantity or Remarks
H_2 Flow Rate	4-5 cc/min.
H_2O Vapour Pressure (ice bath temp.)	5.3 mmHg (0°C)
Source and Substrate Area	1 cm^2
Spacing	500 μm
Source Temperature	810°C
Substrate Temperature	710°C
Time	1 hour
GaAs Source Orientation	[100] facing substrate
Substrate	Mo. on fused silica

Table IIE-1 Summary of CSVT Technique Conditions for Optimum Growth

III MICROSTRUCTURAL ANALYSIS OF THE GaAs FILMS

In this chapter the structure and topography of the polycrystalline GaAs films are examined by x-ray diffraction and scanning electron microscopy. X-ray diffraction techniques were employed to determine crystallinity and preferred orientations. The SEM was used to study the crystal sizes and shapes as a function of growth temperature. In addition to the crystal investigations, electron microprobe analyses of impurities were performed on the surfaces and at the cross sections exposed from cleaving the samples.

III-A X-ray Diffraction

Ordinary x-ray diffractometry can be used to analyse GaAs films up to 10 μm thick and several mm^2 in surface area. This technique was chosen to investigate the structure of the films on a macrovolume scale.

In a cubic lattice, the interplanar spacing d corresponding to a set of Miller indices (h k ℓ) is

$$d = \frac{a_o}{\sqrt{h^2 + k^2 + \ell^2}} \qquad \text{(IIIA-1)}$$

where a_o is the lattice constant. Crystalline GaAs is generally cubic with a lattice constant of a_o = 5.6535 Å ([76H1], p.333). The Bragg angles, 2θ, that produce constructive interference in cubic GaAs are listed in Table IIIA-1.

1. Crystallinity

a. Apparatus

A Philips type 12046 x-ray diffraction machine with CuKα radiation of wavelength λ = 1.542Å was used to study the crystallinity.

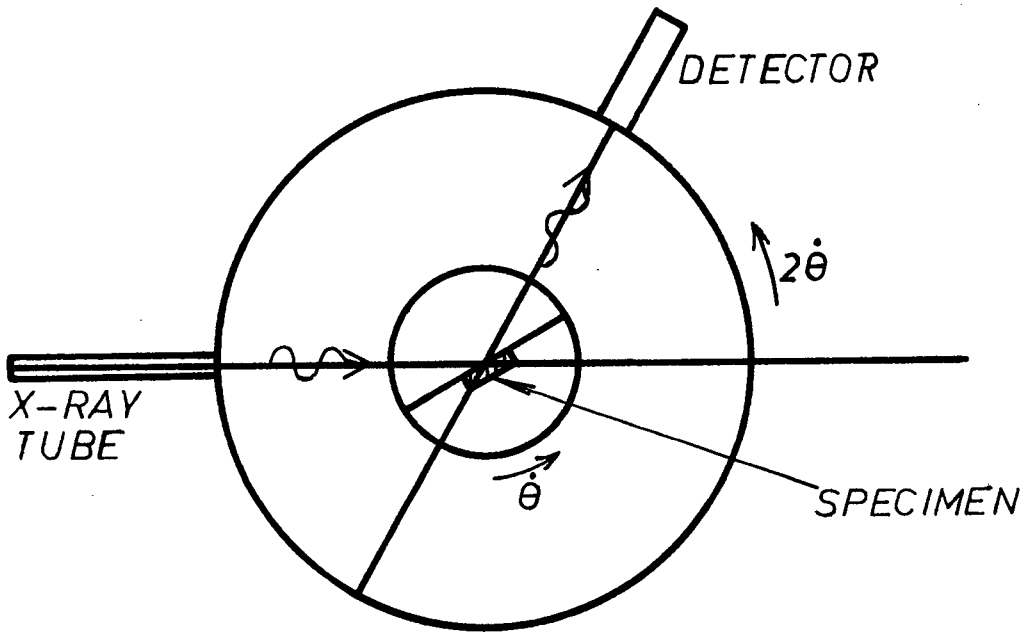

Fig. IIIA-1 X-ray Diffraction Goniometer

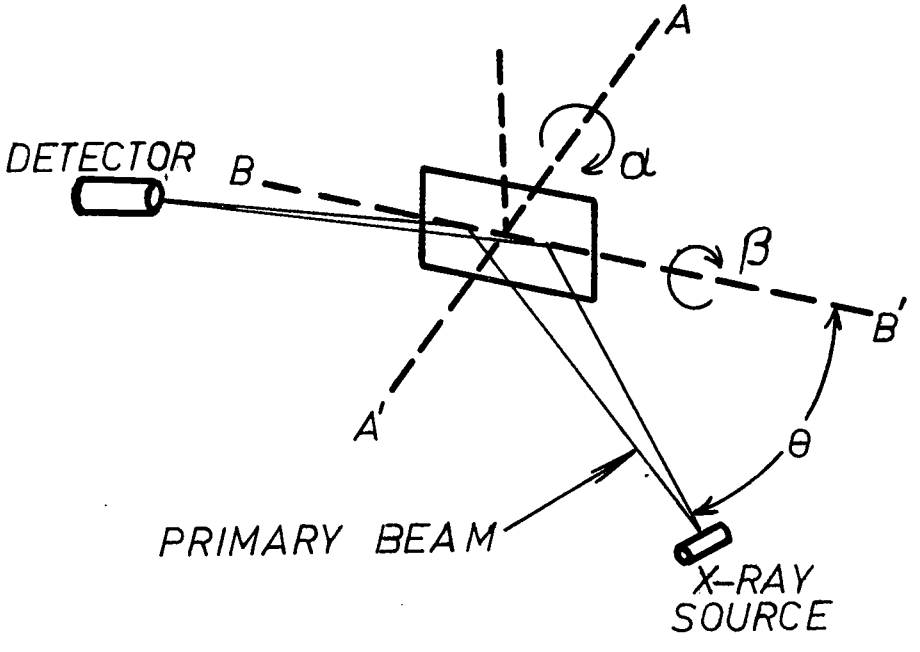

Fig. IIIA-3 Texture Goniometer

X-rays emitted from the CuKα source were reflected from the GaAs crystal planes and collected at a detector. The x-ray detector was a xenon filled proportional counter capable of handling extremely high count rates without need for any dead time correction. The detector and specimen were fitted to a goniometer (Philips type 42202), i.e. the detector was made to move in a circle around the sample at twice the angular speed of the sample as shown in Fig. IIIA-1.

Bragg's Law is satisfied whenever

$$n\lambda = 2d \sin \theta \qquad \text{(IIIA-2)}$$

where

λ = wavelength of radiation source (CuKα = 1.54051 Å)

n = an integer ≥ 1

θ = angle of incident radiation on specimen

Pulses from the detector were conveyed via a Tennelec TC 214 Linear amplifier to a Tennelec TC 592P Digital Ratemeter that summed the pulses every 2 seconds. Each sum was traced on a calibrated chart recorder (Minneapolis-Honeywell Reg. Co. model no. 153X17V-X-6A3P4). The chart recorder rate was set at 1/2 inch per min. The goniometer revolved so that 2θ moved 1° in 1 min. Therefore the chart scale was 2 degrees per inch (or division).

b. Results

Two specimens were tested, each grown on a different substrate, namely: i) moly foil, ii) moly sputtered on quartz, and the results obtained were identical. A diffractogram of the GaAs on Mo/quartz specimen is shown in Fig. IIIA-2. The observed angles of the peaks are listed alongside the theoretical values in Table IIIA-1. (Note when reading the graph of Fig. IIIA-2 that the chart recorder pen reflected on overshoot and thus the relative intensity magnitudes cannot be directly compared to Table IIIA-1.)

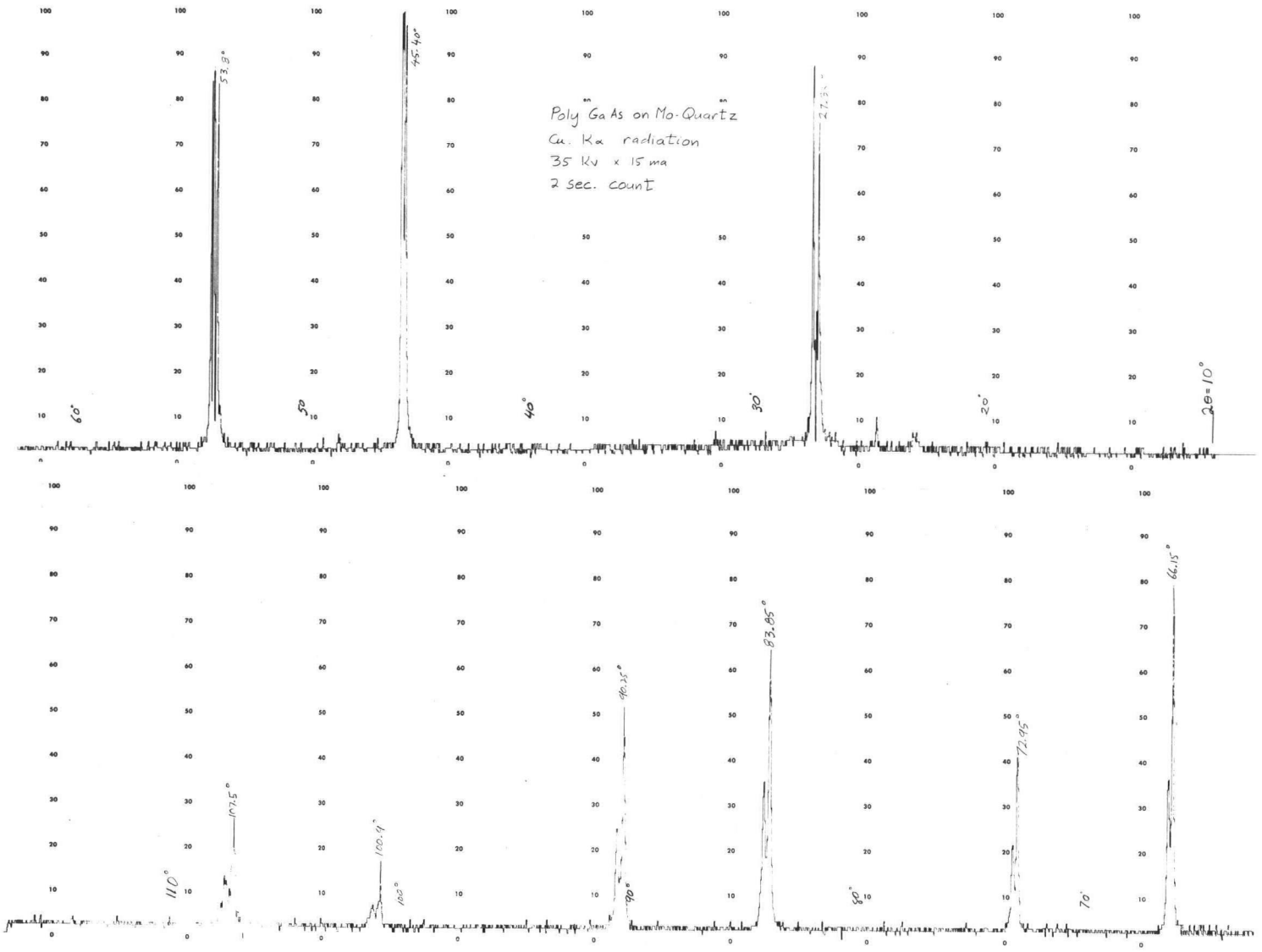

Fig. IIIA-2 X-ray Diffraction of Polycrystalline GaAs on Mo-Quartz

	Theory for a_o = 5.6535		Poly GaAs Results	
Miller Indices h k ℓ	Bragg Reflection 2θ in degrees	Relative Intensity I/I_o	2θ (tolerences ±.05°)	Calculated Lattice Constant a_o (Å)
111	27.33	100	27.35	5.643
220	45.38	90	45.40	5.645
311	53.78	80	53.80	5.646
400	66.12	60	66.15	5.646
331	72.95	70	72.95	5.648
422	83.84	70	83.85	5.648
511,333	90.25	50	90.25	5.648
440	100.97	40	100.90	5.651
531	107.57		107.50	5.651

Table IIIA-1 Bragg Reflection Angles for Cubic GaAs and CSVT Grown GaAs

c. Analysis

The positions of the observed x-ray diffraction peaks were, within the bounds of experimental error, identical to cubic lattice GaAs. At higher Bragg angles, where the accuracy of the machine was best, the calculated lattice constant approached its expected value within .04%. No hexagonal phase reflections were observed as was the case for the vacuum deposited GaAs films of Pankey and Davey ([66P1], p. 1513). These authors had encountered a weak hexagonal close packed (1010) reflection at $2\theta = 25.90°$. No other major peaks were observed in the present work. The films were therefore GaAs cubic crystals.

2. Preferred Orientation

a. Apparatus

The specimens were inspected for preferred crystal orientation using a Schulz type texture goniometer. The texture goniometer incorporated the same Philips x-ray diffractometer (Philips type 12046) as described above but with a more complex sample holder. The sample holder rested on a motorized gyro with two axes of rotation. The first axis rotated about the sample's center and perpendicular to its face, i.e. axis A'A shown in Fig. IIIA-3. The second axis B'B revolved about a line in the plane formed by the intersection of the primary and diffracted beams and at an angle θ to the primary beam. When the primary beam is at an angle 2θ from the diffracted beam where 2θ corresponds to a Bragg reflection from an interplanar spacing, x-ray intensity peaks occur at the detector. These peaks appear only when the sample is orientated so that the perpendicular to crystal planes bisect and are in the plane formed by the primary and diffracted beams.

The gearing was arranged so that for every 360° revolution of

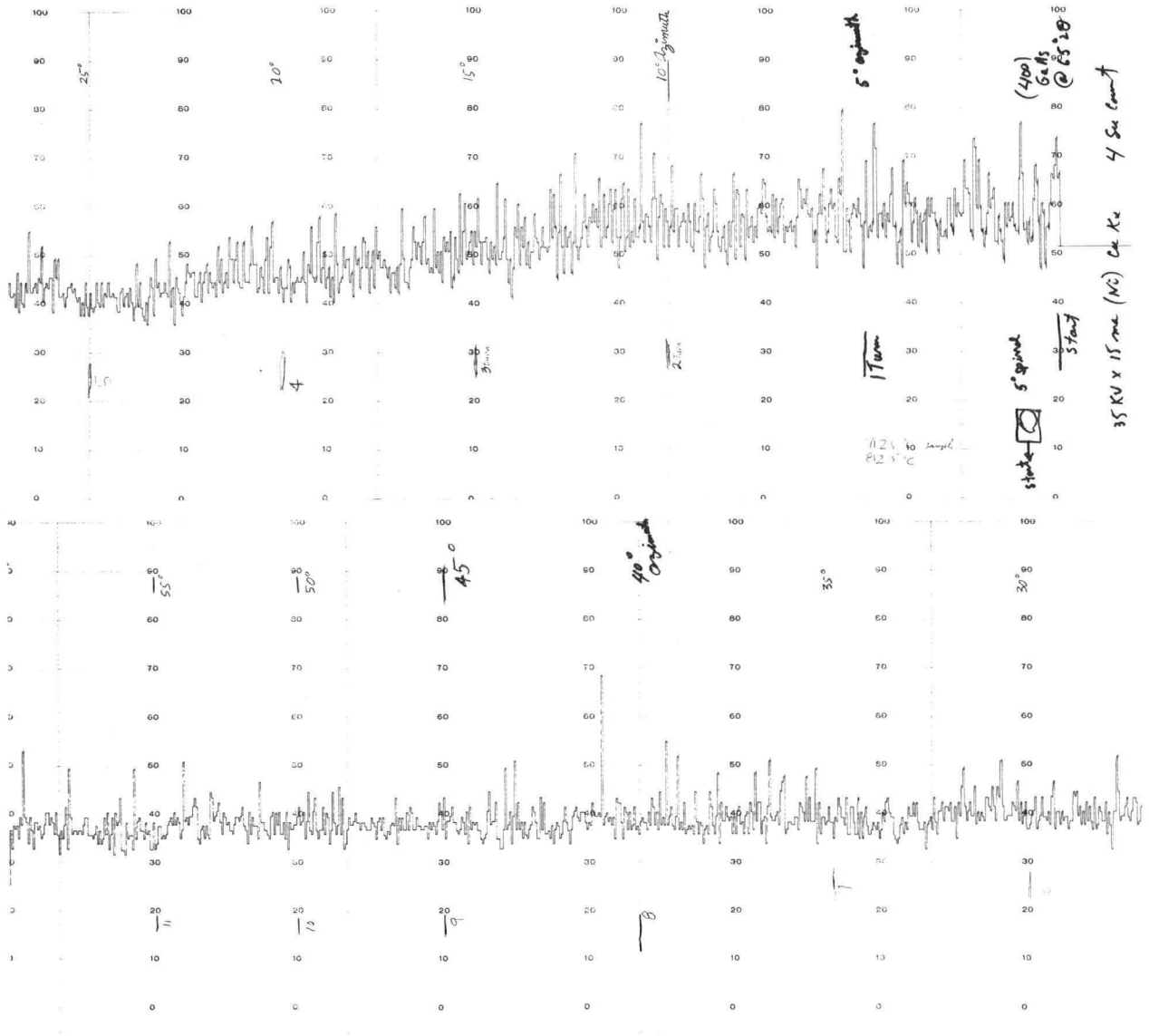

Fig. IIIA-4 Texture Goniometer Chart of Polycrystalline GaAs on Mo-Quartz

α, β advanced 5°. In this way the primary beam searched through a wide range of angles with respect to the surface of the sample. For films with preferred crystal orientations, peaks occur at the detector for certain α_o and β_o when Bragg's Law is satisfied. The results are similar to those from Laue analyses but easier to interpret. When a peak occurs, one set of α_o and β_o are defined which yield the direction of that preferred crystal orientation. The strength of any peak compared to another gives a qualitative indication of the relative magnitude of the preferred orientation.

b. Results

No peaks were observed. The results comprised a slightly decreasing waving output that corresponded to the rotation of the sample about AA'. This was due to the projection of the x-ray beam on the sample becoming larger than the surface area of the GaAs film for low 2θ angles. The chart from the GaAs on Mo/quartz substrate is shown in Fig. IIA-4. Again the GaAs on Mo foil specimen yielded identical results.

c. Analysis

Since no distinct peaks were observed the films were random crystallites with no preferred orientation.

III-B Scanning Electron Microscopy

1. Introduction

For good solar cell efficiency using polycrystalline semiconductor films, it is necessary that the photocarriers avoid the polycrystalline grain boundaries so that conduction is not hindered by grain boundary barriers. In other words, growth conditions should be arranged to produce a film of semiconductor crystals with preferably one crystal between the base substrate and the top electrode. This type of cell,

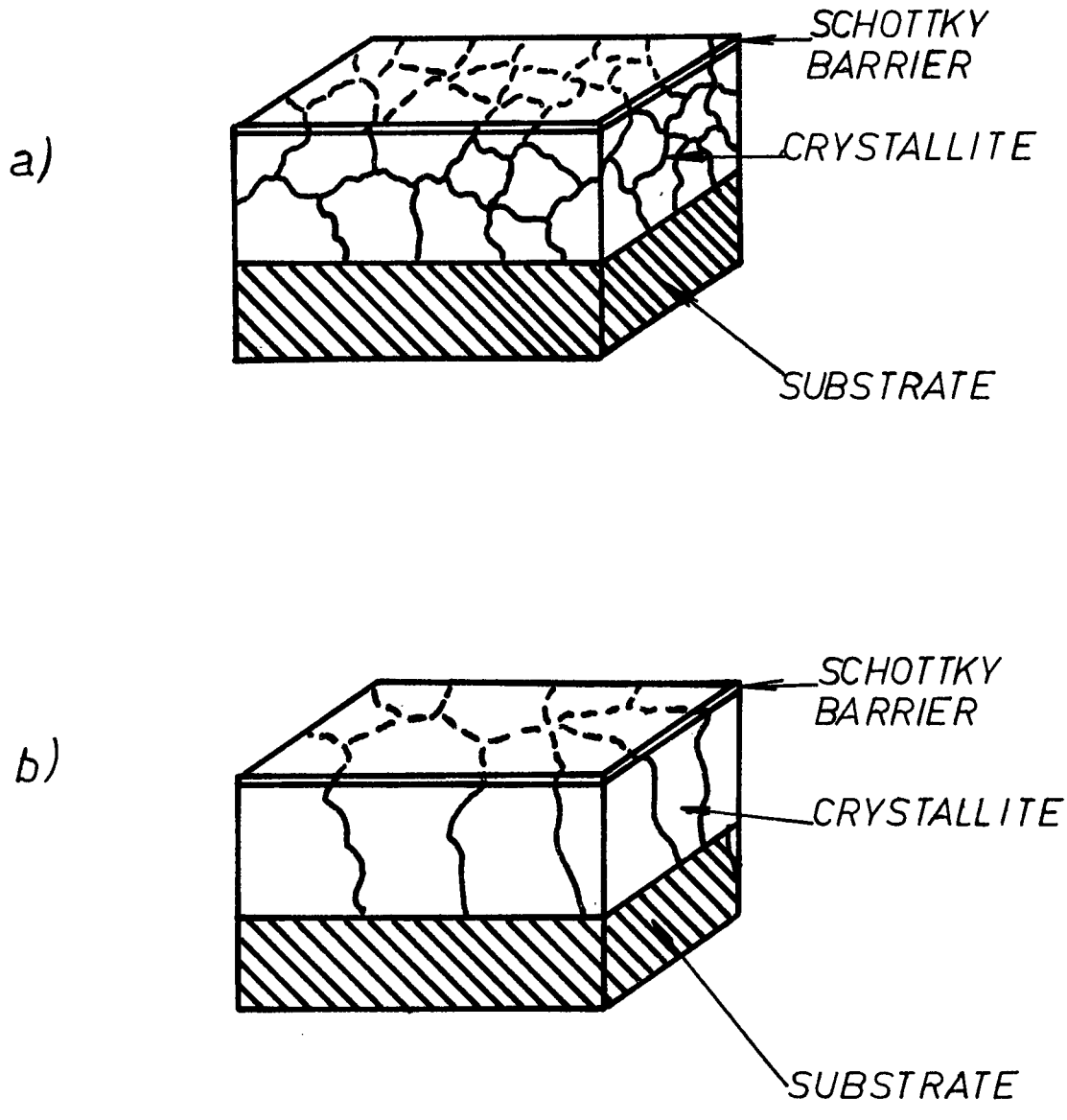

Fig. IIIB-1 Schematic Diagram of Polycrystalline Films:
a) multiple vertical crystals
b) single vertical crystals

the single vertical crystal polycrystalline solar cell is shown in Fig. IIIB-1b. The most important parameter affecting the crystallite size and shape is growth temperature. In the following experiments, GaAs films were grown on Mo on quartz substrates at different temperatures ranging from 675°C to 725°C. The scanning electron microscope (SEM) was used to study the crystal size and shape principally because of its large depth of field.

2. Theory

The scanning electron microscope (SEM) uses a fine electron beam to strike the specimen. At the point of impact, a variety of phenomena occur as shown in Fig. IIIB-2. The electron beam is scanned in a raster pattern across the specimen surface in synchronization with a cathode ray tube (CRT). Secondary electrons, which are dependent on topography, are detected and used to produce an image of the specimen on the CRT.

3. Procedure

The temperature experiment utilized 5 samples all grown on Mo sputtered on quartz substrates. A substrate temperature range of 675 to 725°C was covered in increments of 12.5°C. The temperature difference between substrate and source was kept at 100°C.

After the CSVT film growth step, the quartz substrates were scribed, then diced, in order to produce cross sections of the GaAs films. (Attempts to view cross sections of the films on Mo foil were unsuccessful because the shearing chipped away the films at the cut edge of the substrate.)

The exposed side views were too flat to distinguish the grains on the SEM easily so the following grain boundary etches were investigated.

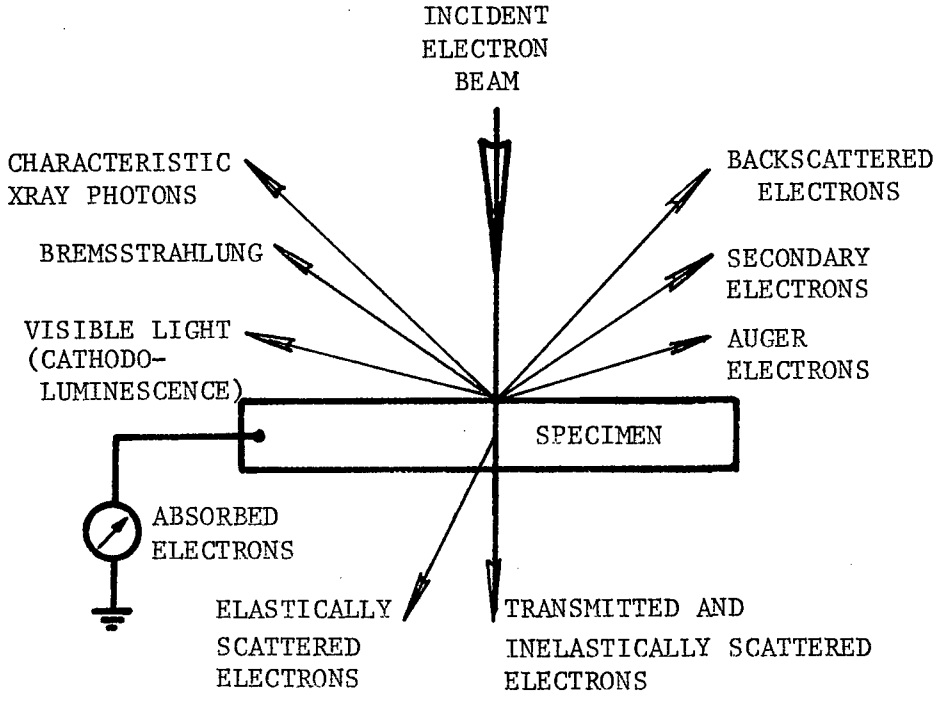

Fig. IIIB-2 Phenomena Generated from an Incident Electron Beam

(i)	HNO_3 : HF : H_2O	in ratio 1 : 1 : 1	for 10 secs
(ii)	H_2O_2 : HF : H_2O	in ratio 2 : 1 : 6	for 1.5 mins
(iii)	H_2O_2 : H_2SO_4	in ratio 1 : 1 : 8	for 10 secs

Etch number 1 exposed grains that could be seen on the SEM. It etched deepest at the crystal boundaries and was least subject to fluctuations in temperature, freshness and=time. No. 2 etch did not attack the grains and no. 3 left a worm-eaten surface that was less comprehensible than the original.

An Etec Autoscan SEM with 20 kV accelerating voltage and 2000 lines per frame picture resolution was used to produce the photomicrographs shown in Fig. IIIB-3 through to Fig. IIIB-7. A thin layer, less than 100 Å, of gold-palladium had to be sputtered onto the quartz surfaces to reduce charge build up and haze.

4. Results

The topography of the samples grown at different growth temperatures, as shown in Figs. IIIB-3 and 4, illustrated that the crystallite surface areas increased with temperature and thickness. The mean crystallite areas at the surface and their standard deviations are listed in Table IIIB-1. The film thicknesses were measured on the SEM from the cross-sectional view of the diced specimens; see for example Figs. IIIB-5 and 6. The etched sample clearly revealed that the film commenced growth with the nucleation of small crystals that grew to a 2-5 μm diameter. Further growth consisted of every second or third crystal outgrowing its neighbours and covering the surface with larger crystals in the 10-100 μm diameter range.

The films grown on Mo foil had surface features similar in shape but not as large as the films on Mo/quartz substrates. The

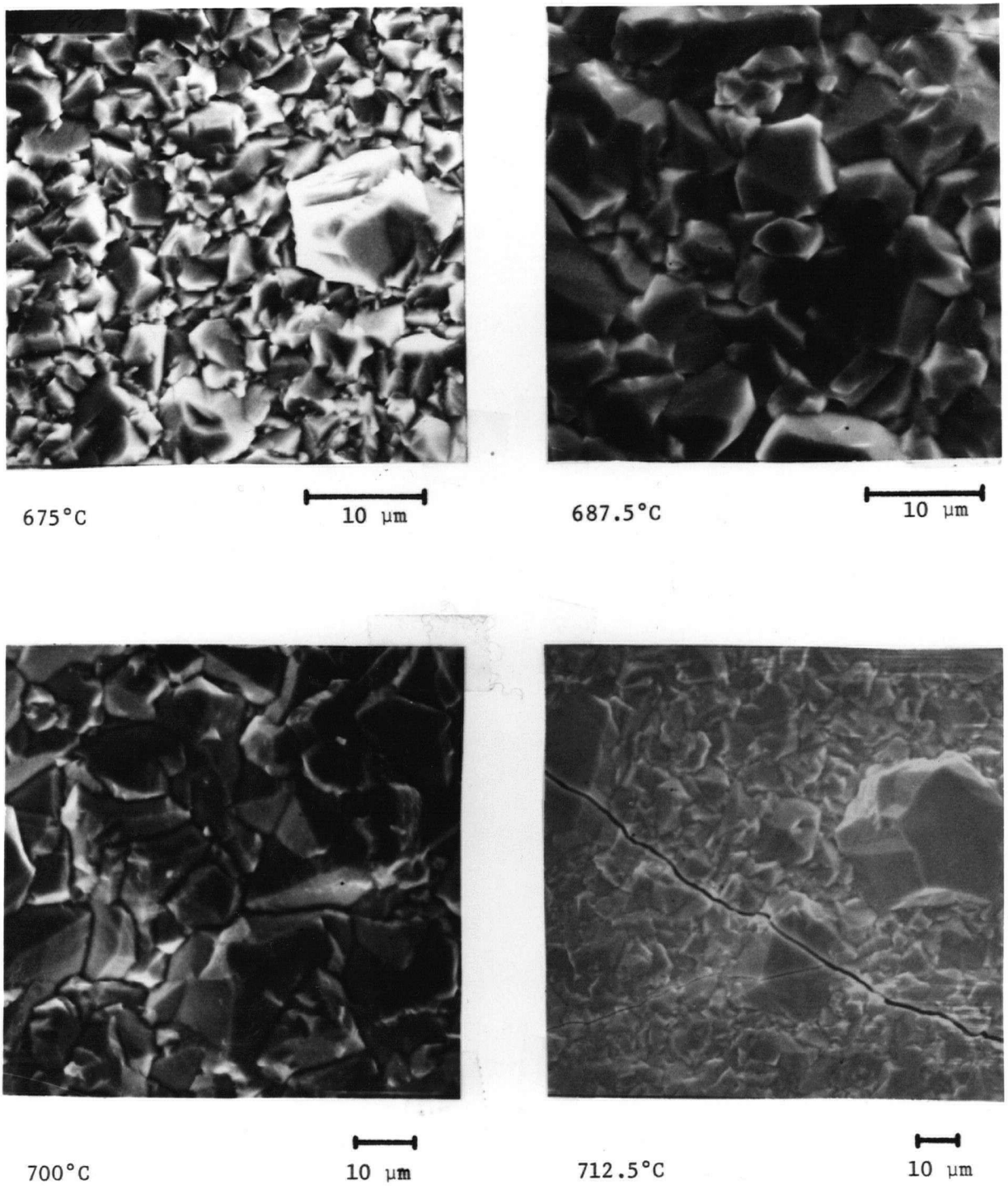

Fig. IIIB-3 SEM Photomicrographs of GaAs Film Surfaces Grown on Mo-Quartz at Different Substrate Temperatures

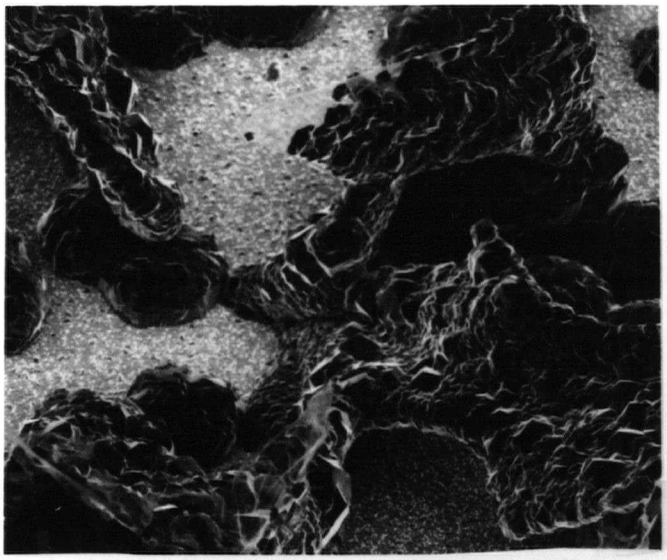

10 μm

Fig. IIIB-4 SEM Photomicrograph of Noncontinuous GaAs Grown on Mo-Quartz at 725°C

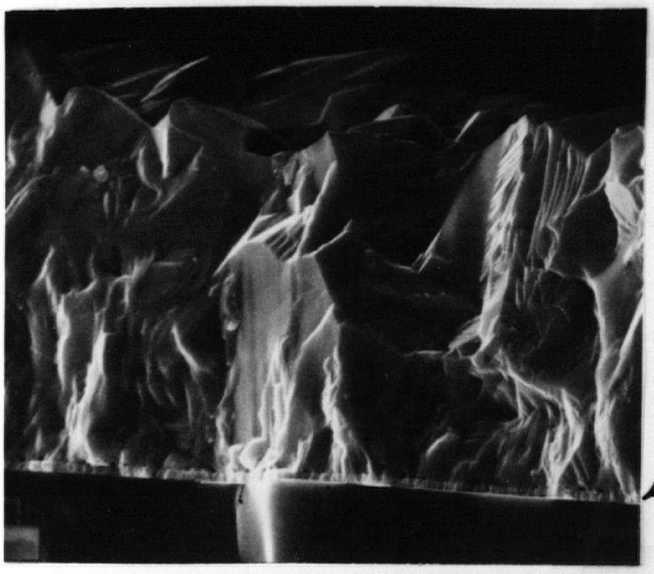

10 μm

Fig. IIIB-5 SEM Photomicrograph of Cleaved Side View of GaAs Grown on Mo-Quartz at 700°C

(Interfacial layer is 3000Å of sputtered Mo.)

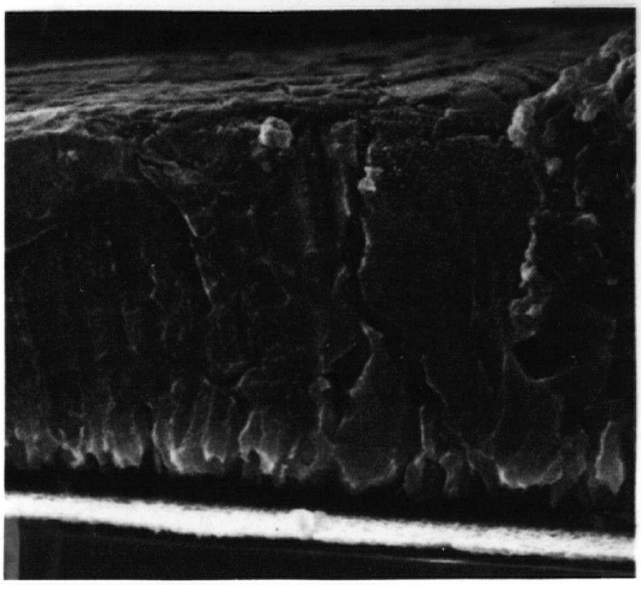

1 μm

Fig. IIIB-6 SEM Photomicrograph of Sample Etched in HNO_3:HF:H_2O

average crystal size of the films on the former substrates was 60 μm^2 and 100 μm^2 for films on Mo/quartz. The larger crystals on the latter substrates were probably due to a higher temperature at the quartz surface resulting from a temperature gradient across the insulating quartz.

The surface roughness on the bulk of all the samples was approximately 10% of the thickness. The exceptions occurred on high temperature growths and selected areas of films grown on Mo foil. In the former case (see e.g. Fig. IIIB-4), discontinuous films resulted. In the latter case, occasional clusters of dendrites would grow out of the films, see for example Fig. IIIB-7. This phenomenon was probably related to inhomogeneous seeding from the Mo foil.

	Crystal Size at Surface		Crystal height at Cleaved Edge		
Substrate Temperature (°C)	Mean Area (μm^2)	Standard Deviation (μm^2)	Mean Height (μm)	Standard Deviation	Film Thickness (μm)
675	20	33	6.7	2.9	10
687.5	45	52	8.8	4.7	22
700.0	105	88	9.2	5.4	22
712.5	100	440	10	10	19
725.0	not continuous				

Table IIIB-1 Effect of Growth Temperature on Crystal Size (For films grown on Mo on quartz.)

Fig. IIIB-7 GaAs Dendritic Growth on Mo Foil

III-C Electron Microprobe

A semi quantitative analysis of the impurity content of the CSVT GaAs films was made using an electron microprobe.

1. Theory and Apparatus

The electron microprobe consists of an electron beam probe and an x-ray spectrometer detector. The specimen can be brought into position under the electron beam with the aid of an optical microscope. Characteristic x-rays and other phenomena result from the electron bombardment (see Fig. IIIB-1). The angle of the spectrometer is set for maximum intensity diffraction of characteristic x-rays from a known standard. The intensity of the x-rays from the specimen being analysed

is then compared with that of the standard. The mass concentration of the standard element in the specimen can be determined from the ratio of these intensities and calibration curves. (A detailed description of the microprobe is given by Birks [63B1].)

The analysis was performed on a JEOL Co. JXA-3A microprobe with a variable fraction of a percent sensitivity for elements of atomic number eleven and above. The resolution of the probe was 1 to 2%

2. Results

The CSVT film specimens were encapsulated in plastic and cross sections were diamond-polished down to a 1/4 μm finish. The surfaces were scanned and no peaks occurred other than those associated with Ga and As. Particular impurities that might be expected on account of their presence in the reaction chamber were oxygen, molybdenum and aluminum. Specific scans were made to look for each of these possible impurities.

The oxide test involved the scanning of a 1 μm diameter electron beam across the specimen with a count every second. The accelerating voltage was 5 kV and a lead stearate crystal diffracted the oxygen $K\alpha_1$ radiation. The results are superimposed over an absorbed electron image of the film (see Fig. IIIC-1). The counts were low enough to make it unnecessary to correct for dead time. No oxygen was present in concentrations greater than one part in 100 (probe is about 1% sensitive for O_2). The intensity increased only at the plastic indicating oxygen was present there.

In the Mo test, the electron beam stepped 1.25 μm every 10 secs. The accelerating voltage was 25 kV and a mica crystal diffracted the Mo $K\alpha_1$ radiation. The results show (Fig. IIIC-2) that no Mo existed

across the thickness of the film in concentrations greater than 1 part in 1000 (probe is .01-.1% sensitive for Mo). Aluminum was not found in quantities greater than 0.1% using an accelerating voltage of 25kV and a mica crystal diffracting the Kα radiation.

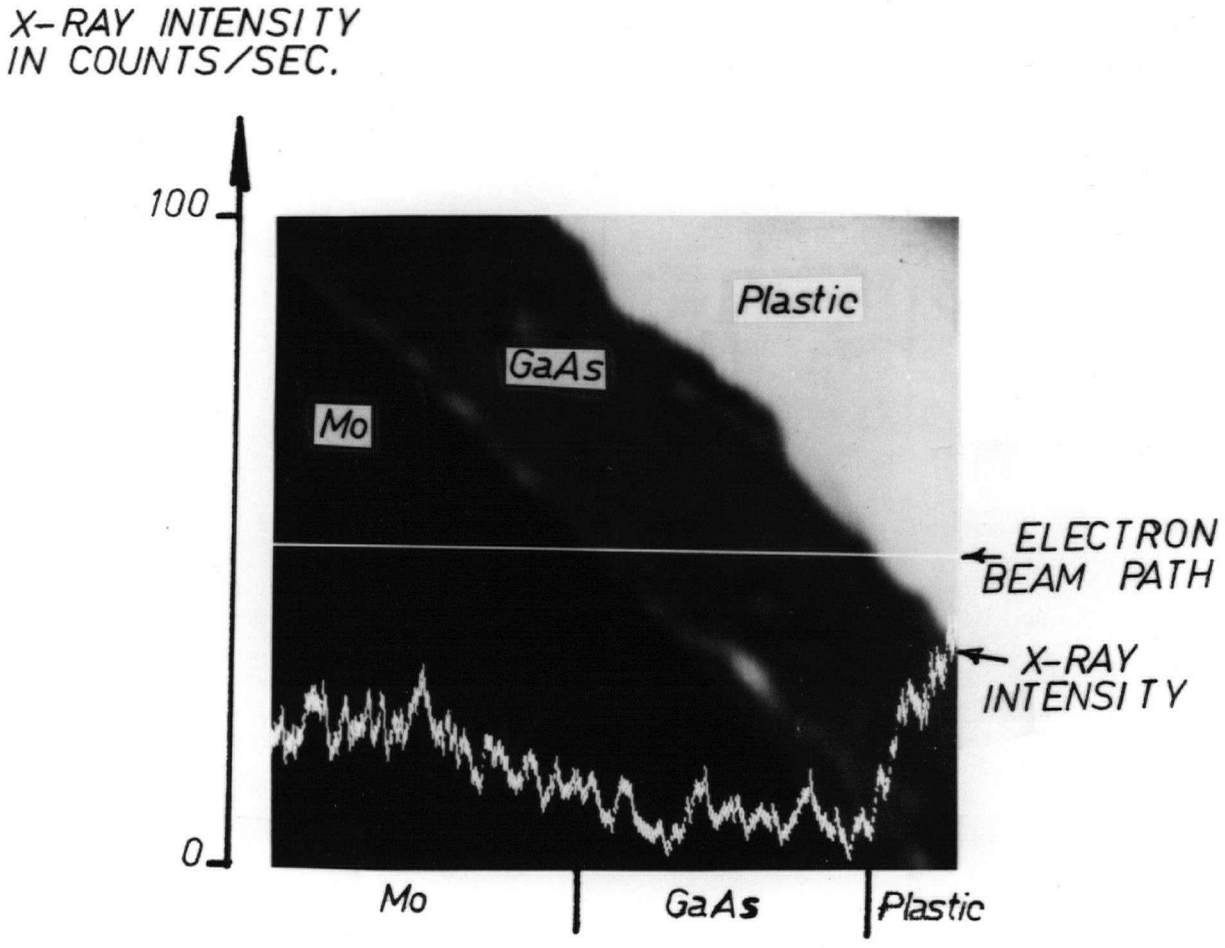

Fig. IIIC-1 Microprobe Analysis of Oxygen Concentration.

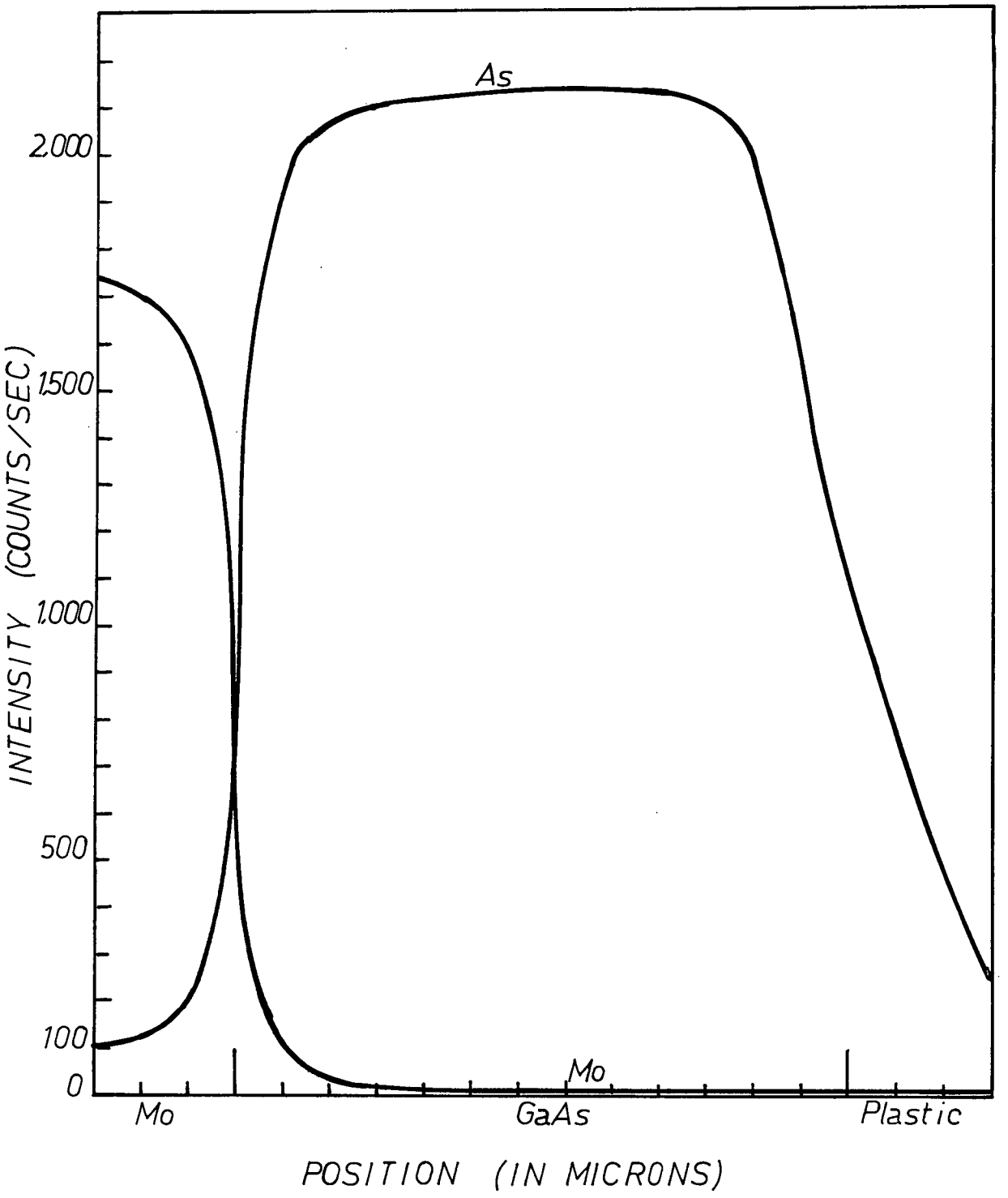

Fig. IIIC-2 Microprobe Analysis of Mo Concentration

III-D Discussion

The films prepared in this present work were cubic crystals of GaAs with no preferred orientation. Continuous crystal growth on Mo substrates was found to take place over the substrate temperature range of 675-725°C with the grain size increasing with temperature up to a maximum of around 100 μm^2. The growth rates varied from 15 to 40 μm/hr. Films were essentially a layer of columnar single crystals 10-100 μm^2 in area with a sparse bed of smaller (stunted) crystals at the Mo-GaAs interface. Hovel [75H1] has shown using a 'filament lifetime' model for GaAs single vertical solar cells 1 μm thick, that efficiencies, short circuit current, and open circuit voltage all have maximum values comparable to single crystal values for grain sizes in excess of 2 μm. This columnar growth, then, would be highly suitable for thin film solar cells.

The surface topography indicates a roughness on the scale of 10% of the film thickness and this would be an advantage in subsequent solar cell fabrication as such a surface would present a textured plane to incoming radiation, leading to the possibility of improved radiation absorption. Such surfaces are being deliberately introduced into Si single crystal cells and have led to a marked reduction in reflection losses.

No impurities resided in the films in quantities observable on the electron microprobe. In particular Mo, O_2, and Al could have perhaps been expected in the films but in fact were not present, at least not in concentrations greater than 1 part per 1000, 100, and 1000, respectively.

IV ELECTRICAL PROPERTIES OF THE GaAs FILMS

The microstructural properties of the GaAs CSVT-prepared films discussed in chapter III indicate that films prepared by this method have a grain size and crystal structure well suited to photovoltaic applications. For solar cell use the semiconductor must be incorporated in a diode structure. This can be achieved by doping the semiconductor to form a homojunction or by the application of a dissimilar material onto the semiconductor to form a heterojunction. Certain semiconductors, metals or metal-thin insulator structures can be used for this latter function. For the GaAs films under consideration, and indeed for most thin film non-single crystal semiconductors, homojunction fabrication is difficult to achieve on account of the non-uniform doping likely to result from dissimilar rates of diffusion along the grain boundaries and in the bulk of the crystals. Of the remaining heterojunction possibilities the metal/semiconductor structure was selected for this investigation on account of its simplicity and relevance to economical terrestrial photovoltaic systems.

In this chapter, the important features of metal semiconductor solar cells are enumerated and the results of measurements on Au/GaAs Schottky barrier diodes presented.

IV-A Solar Cell Theory

Efficiency, η, of solar cells is a matter of prime concern for commercial terrestrial applications and, as has been mentioned in chapter II, a minimum requirement of 10% has been suggested [75W1] as being necessary for photovoltaic systems to be competitive with the other methods of power generation. The important factors that control the solar cell efficiency η can be both process- and material-dependent and

are shown in the equivalent circuit of Fig. IVA-1. They are the series resistance R_S, shunt resistance R_{SH}, diode ideality factor n and barrier height ϕ_B. The latter term is the principal component in J_S, see eq. IVA-1.

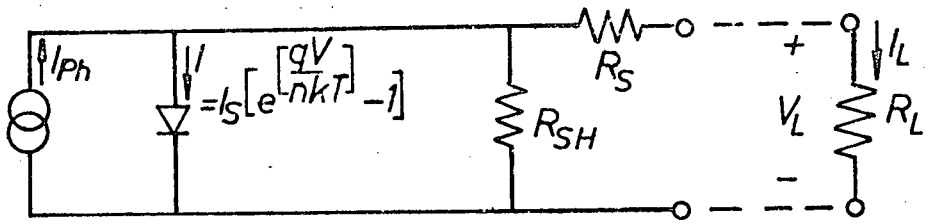

Fig. IVA-1 Equivalent Circuit of a Solar Cell

The series resistance in polycrystalline GaAs is not expected to be negligible. Grain boundaries will cause recombination and barriers that will reduce the effective number of carriers in the first case and hinder their flow through the thickness of the film in the second case. Ohmic and thin rectifying contacts also contribute to series resistance. The effect of R_S on η has been evaluated in appendix IVA-1 using Au/GaAs Schottky diode parameters (see appendix IVA-1). The results, as illustrated in Fig. AIV1 show that series resistances greater than 1.0 Ω begin to degrade solar cell efficiency markedly and values greater than 10 Ω would not be acceptable for commercial cells.

Shunt resistance is expected to occur due to shorting between electrodes via low resistance paths such as heavily doped grain boundaries or metallic bridges in microcracks. The effect of R_{SH} on η for AMO radiation on single crystal solar cells has been evaluated by Hovel ([75H1], Fig. 51) where it was shown that R_{SH} less than 10^3Ω just begins to degrade efficiency until the point where $R_{SH} \approx 100$ Ω at which cells would become uneconomic ($\eta < 10\%$).

The effect of the diode junction on η depends, in the calculations,

on the model chosen. For the Au/GaAs Schottky diode format utilized in this investigation, the Thermionic Emission theory was considered most appropriate as outlined in chapter IV-B. The diode equation can be expressed as (see equations IVB-8,9,11)

$$\frac{I}{A} = A^*T^2 \exp\left[-\frac{q\phi_B}{kT}\right]\left[\exp\frac{qV}{nkT} - 1\right] \qquad \text{(IVA-1)}$$

The barrier height ϕ_B and diode ideality factor n are the two main parameters dependent on fabrication processes. Pulfrey and McOuat [74P1] have calculated the effect of ϕ_B on η for n-type GaAs using a model with zero reflection and resistance losses, and a quantum efficiency of unity. The results showed that efficiency increased monotonically from 10% at ϕ_B = .9 eV to as high as 25% at $\phi_B = E_g$ = 1.43 eV. Au-Schottky barriers have already been fabricated with a ϕ_B = .9 eV by Padovani and Sumner ([65P1], p. 3747). Still higher effective barriers and efficiencies are actually possible using the metal-thin insulator-semiconductor structure as evidenced by the 15% efficient solar cell announced by the Jet Propulsion Laboratory [75S1].

The empirical factor n has the same effect on efficiency as ϕ_B because it also resides in an exponential term of the diode equation and efficiency can therefore be expected to increase monotonically as n increases from 1. However, it must be realised that n > 1.2 means other conduction mechanisms are present in the metal-semiconductor barrier besides thermionic emission, for example, recombination and interfacial layer effects. Therefore, a cell with high n does not necessarily mean a high η will result.

R_S, R_{SH}, η and ϕ_B can be extracted from J-V measurements of Au/GaAs Schottky barrier diodes and used as a preliminary evaluation of the suitability of the CSVT GaAs films for terrestrial solar cells.

IV-B Electrical Contacts to the GaAs Films

In this section, the theory of metal-semiconductor contacts is briefly reviewed and the fabrication procedures used to make ohmic and rectifying contacts to the CSVT-grown GaAs films are presented.

1. Rectifying Contacts

a. Schottky Barrier Theory

The fundamental theory of Schottky diodes has been reviewed in many books ([69S1], chapter 8), ([72M1], chapter 6 and 7), and ([57H1], chapter 7). The energy band diagram for a metal in contact with an n-type semiconductor at 0 bias is shown in Fig. IVB-1. The barrier height for a

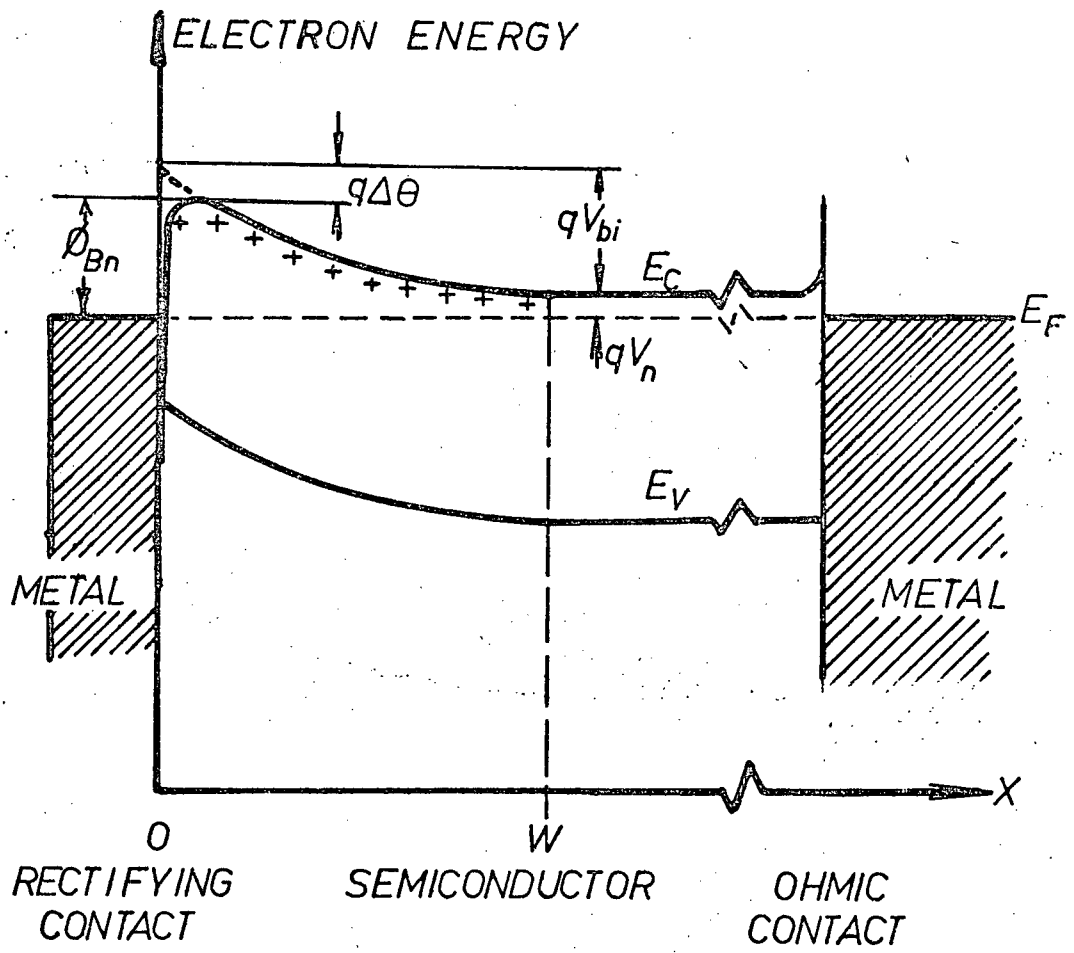

Fig. IVB-1 Energy Band Diagram of a Metal/n-type Semiconductor/ Ohmic Contact Structure at Thermal Equilibrium

semiconductor with a doping concentration N_D is:

$$\phi_{B_n} = V_{bi} + V_n - \Delta\phi \qquad \text{(IVB-1)}$$

where V_{bi} is the built in voltage, V_n is the difference between the fermi level and the bottom of the conduction band in the semiconductor bulk, and $\Delta\phi$ is the barrier lowering due to the image force. The image force lowering at bias V is related to the maximum electric field E_m by

$$\Delta\phi = \sqrt{\frac{q\,E_m}{4\pi\varepsilon_S}} \qquad \text{(IVB-2)}$$

where

$$E_m = 2(V_{bi} - V - \frac{kT}{q})/W \qquad \text{(IVB-3)}$$

and ε_S is the static value of the semiconductor dielectric constant, q is the electron charge, and kT/q arises from the effect of the reserve layer ([57H1], p. 177). The width of the space charge region is denoted by W:

$$W = \sqrt{\frac{2\varepsilon_S}{qN_D}(V_{bi} - V - \frac{kT}{q})} \qquad \text{(IVB-4)}$$

Therefore the Schottky capacitance relation becomes

$$\frac{A^2}{C^2} = 2(V_{bi} - V - \frac{kT}{q})/(q\varepsilon_S N_D) \qquad \text{(IVB-5)}$$

and V_{bi} can thus be determined from a plot of A^2/C^2 vs V, so enabling calculation of ϕ_B from eq. IVB-1. It also follows that the doping concentration N_D in the depleted region can be given by

$$N_D = -\frac{2}{q\varepsilon_S}\left(\frac{d(A/C)^2}{d\,V}\right)^{-1} \qquad \text{(IVB-6)}$$

For non-uniform impurity content, the slope of $\frac{A^2}{C^2}$ versus V is no longer a straight line. Equation IVB-6 can still be used; however, $N_D(W)$ is the value of the doping concentration at x = W (the space charge width),

where

$$W = \frac{\varepsilon_S A}{C} \qquad \text{(IVB-7)}$$

The current transport in metal-semiconductor barriers is mainly due to majority carriers. Two theories have been proposed to describe the process, Schottky's diffusion theory and Bethe's thermionic emission theory. Both have similar J-V characteristics.

$$J = J_S[\exp \frac{qV}{kT} - 1] \qquad \text{(IVB-8)}$$

However, the thermionic emission theory has a saturation current density J_S that is more temperature dependent and less sensitive to voltage than J_S of the diffusion theory. Sze has shown that the thermionic emission theory is valid for transport in GaAs Schottky barrier diodes at room temperature with an electric field range between 9×10^3 V/cm and 1×10^5 V/cm ([69S1], p. 390). This encompasses the useful forward bias range of Schottky barriers for doping concentrations less than $N_D \approx 10^{16}\,cm^{-3}$ (which are generally used in photovoltaics).

The saturation current density J_{ST} for thermionic emission is given by

$$J_{ST} = A^*T^2 \exp(-\frac{q\phi_{B_n}}{kT}) \qquad \text{(IVB-9)}$$

where A* is the modified Richardson's constant

$$A^* = \frac{4\pi\, m^* k^2}{h^3} \qquad \text{(IVB-10)}$$

where h is Planck's constant and m* is the carrier effective mass. For GaAs $m^* = 0.068\, m_o$ ([69S1], p. 20) therefore $A^* = 8$ Amp $cm^{-2}\,{}^\circ K^{-2}$.

In practice, both A* and ϕ_B are functions of voltage; therefore, the forward J-V characteristics (for $V > 3\ kT/q$) should be represented by

$$J = J_{ST} \exp(\frac{qV}{nkT}) \qquad \text{(IVB-11)}$$

where

$$n = [1 + \frac{\partial \Delta\phi}{\partial V} + \frac{kT}{q} \frac{\partial(\ell n\ A^*)}{\partial V}]^{-1} \qquad \text{(IVB-12)}$$

when $1 < n < 1.2$

The barrier height can be obtained from the saturation current J_{ST} (found by extrapolating J to zero voltage) inserted in the following equation.

$$\phi_{B_n} = \frac{kT}{q} \ell n\ (\frac{A^* T^2}{J_{ST}}) \qquad \text{(IVB-13)}$$

b. Schottky Barrier Fabrication

In order to prepare a rectifying contact to the polycrystalline films grown on Mo by the present CSVT technique the following procedure was adopted. Immediately after removal from the growth chamber, hydrocarbons and other gross contaminants were removed by an ultrasonic wash in hot distilled water and detergent. The GaAs was then dipped for a minute in chloroform, rinsed for 5 minutes in hot methyl alcohol, etched for 10 seconds in freshly prepared $H_2SO_4 \cdot H_2O \cdot H_2O_2$ in a 16·3·1 ratio, rinsed in boiling distilled water and blown dry. Each sample was put directly into a Veeco vacuum chamber which was then pumped down to a base pressure of 1×10^{-6} torr. The GaAs was heated to slightly above 100°C in order to evaporate water vapour from the surface.

Au barrier films were deposited by evaporation through a metal mask, forming circular Au contacts of 7.85×10^{-3} cm^2 in area in order to investigate different regions of the film. The edge capacitance C_e from Goodman ([63G2], eq. 7)

$$C_e < \varepsilon_S \pi\ p/2 = .4pf \qquad \text{(IVB-14)}$$

is negligible for this size of contact (p is the perimeter of the contact). As this area of contact was not suitable for light collection purposes, no attempt was made to fashion photosensitive diodes and, indeed, the Au

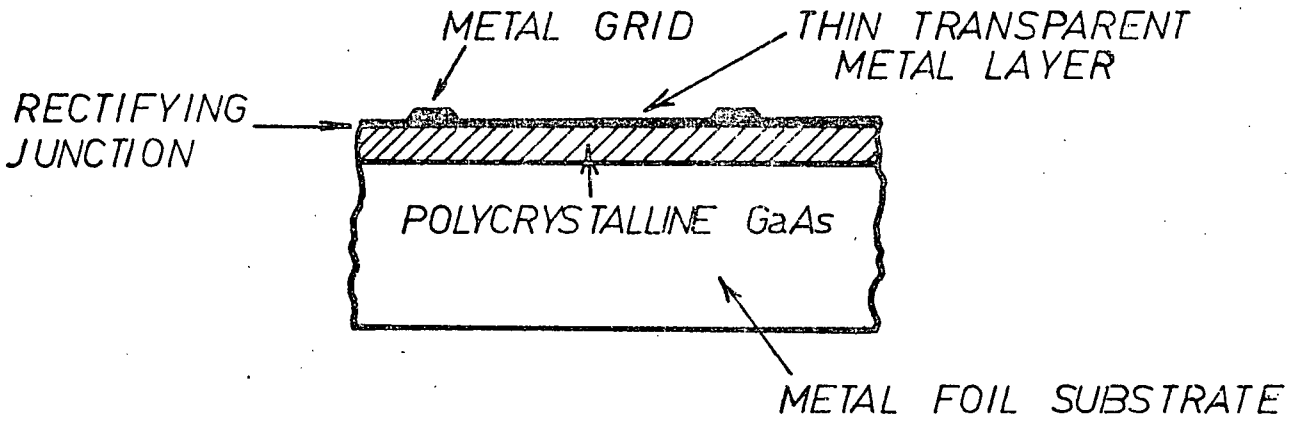

a. FRONTWALL CELL STRUCTURE

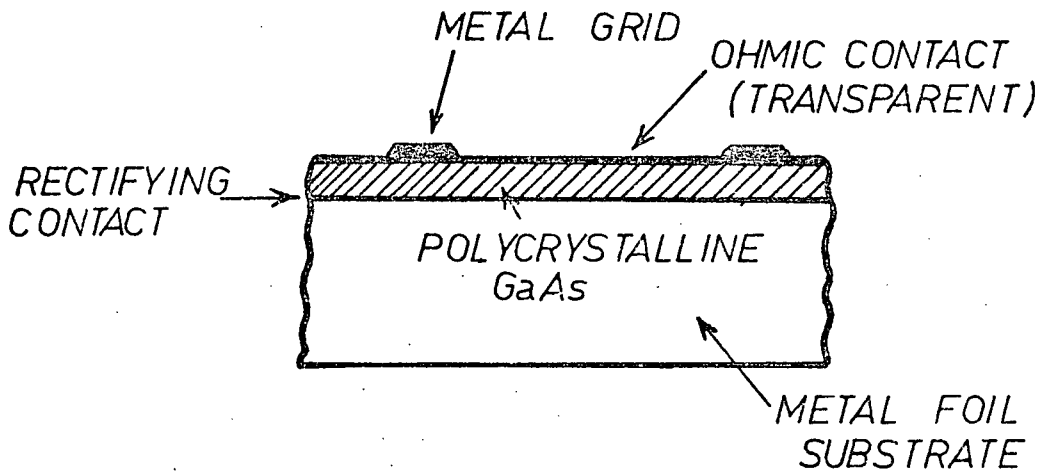

b. BACKWALL CELL STRUCTURE

Fig. IVB-2 Poly GaAs Solar Cell Configurations

film was made thick ($\approx$ 2000 Å as measured by an Inficon 321 film thickness monitor) to ensure that there would be no contribution to R_S from this region.

2. Ohmic Contacts

Schottky barrier solar cells are normally furnished with ohmic contacts to the non rectifying side of the semiconductor. The CSVT GaAs films could be used in either a frontwall or a backwall cell configuration as shown in Fig. IVB-2. The frontwall cell requires an ohmic contact between the substrate and GaAs film. The backwall cell depends on the substrate - GaAs interface being rectifying and an ohmic contact is fitted to the surface of the GaAs. The next section contains the theory of ohmic contacts followed by a section outlining the fabrication process used to place ohmic contacts on the GaAs films.

a. Ohmic Contact Theory

Any conductor (metal) brought in contact with a semiconductor will produce an electrostatic barrier. This is due to the presence of surface states and the difference between the work function of the metal and the electron affinity of the semiconductor. The equation that describes the potential energy distribution of the barrier is

$$q\ V(x) = \frac{q^2 N_D x^2}{2\varepsilon_S} - \frac{q^2}{16\pi\ \varepsilon_D (W-x)} \qquad \text{(IVB-15)}$$

from Rideout and Crowell ([70R1], p. 996).

In order that this contact become ohmic, the barrier must be reduced so that adequate current densities can flow with a voltage drop negligible compared to that in the Schottky barrier region. An obvious way to lower the barrier is by the image force effect. Note that for low barriers the contact voltage will be near zero and the barrier lowering is

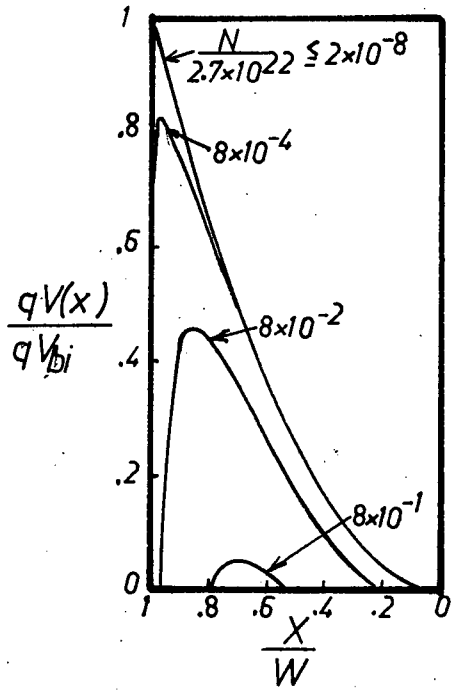

Fig. IVB-3 Effect of Image Force on the Potential Barrier at a Metal-Semiconductor Interface for n type GaAs with Band Bending V_{bi} = 1 eV. Taken from ([75R1], Fig. 6)

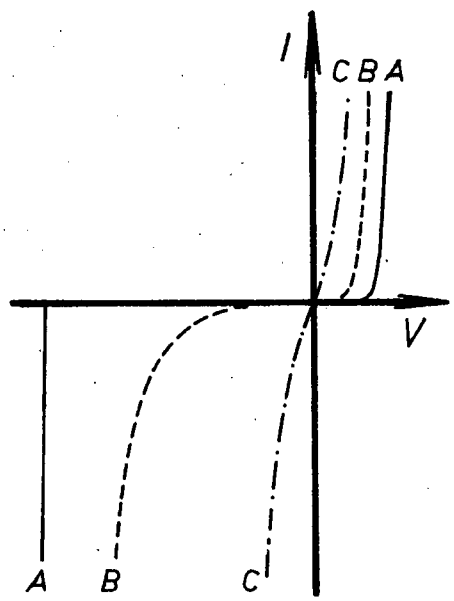

Fig. IVB-4 Illustration of the Current-Voltage Relationship for a Metal-Semiconductor Contact for Progressively Higher Carrier Concentrations

A) $N \leq 10^{17}cm^{-3}$ Thermionic Emission Dominates

B) $N \approx 10^{18}$-$10^{19}cm^{-3}$, Thermionic-Field Tunneling Dominates

C) $N \geq 10^{19}cm^{-3}$, Field Emission Tunneling Dominates

$$\Delta\phi = \left[\frac{q^3 N_D \phi_B}{8\pi^2 \varepsilon_S^3}\right]^{1/4} \qquad \text{(IVB-16)}^*$$

Equation IVB-16 is derived from equations IVB-1,2,3 with $\frac{kT}{q}$ assumed negligible. The effect of image force on the shape of the potential barrier is shown in Fig. IVB-3. The image force lowering equals the band bending V_{bi} for GaAs when

$$N_D = 2.7 \times 10^{22} \frac{cm^{-3}}{volts} V_{bi} \qquad \text{(IVB-17)}$$

For most GaAs contacts $V_{bi} \approx .7$ volts and zero barriers would require impurity concentrations greater than the solubility limit of GaAs.

Besides the image force, the electric field in the barrier controls conduction and Sze has shown that for $E_m \geq 10^5$ v/cm ([69S1], p. 388) thermionic field emission occurs. In effect the current component due to tunneling rapidly increases for fields above 10^5 v/cm and barrier width less than 3000 Å. The field and the width are related to N_D by

$$E_m \propto \sqrt{N_D} \text{ and } W \propto (\sqrt{N_D})^{-1} \qquad \text{(IVB-18)}$$

Rideout specified $N_D \geq 10^{19}$ cm^{-3} as the doping density required for field emission tunneling ([75R1], p. 545). Fig. IVB-4 illustrates the I-V characteristics of the three modes of metal-semiconductor conduction. In conclusion, very heavily doped semiconductors produce a tunneling situation that gives symmetric I-V relationships and low contact resistance, i.e. an ohmic contact.

b. Ohmic Contact Fabrication

The ohmic contacts were formed by evaporation of gold germanium nickel and annealing at 450°C in H_2 gas for a short period of time.

---

* The image force dielectric constant $\varepsilon_D \approx$ the static value ε_S from Sze's argument ([69S1], p. 367).

The films of GaAs were cleaned for 1 minute in boiling chloroform then 5 minutes in hot methyl alcohol, then blown dry. The clean pieces were placed in contact with a mask in a Veeco vacuum chamber that was pumped down to a maximum pressure of 10^{-6} torr. 100 mg. of Au Ge alloy in a 88% to 12% ratio with 8 mg. of 99.98% pure Ni added was evaporated through the mask to form round dots roughly 1 x 10^{-2} cm^2 in area. After removal from the vacuum system, the sample was placed in the furnace shown in Fig. IVB-5. The furnace was designed to produce rapid thermal cycling required for good ohmic contacts ([73H1], p. 836).

The fast annealing was made possible by the use of a specially made magnetized trolley. The specimens were attached to the end of a long quartz rod which was supported at the nose of a truck. This truck

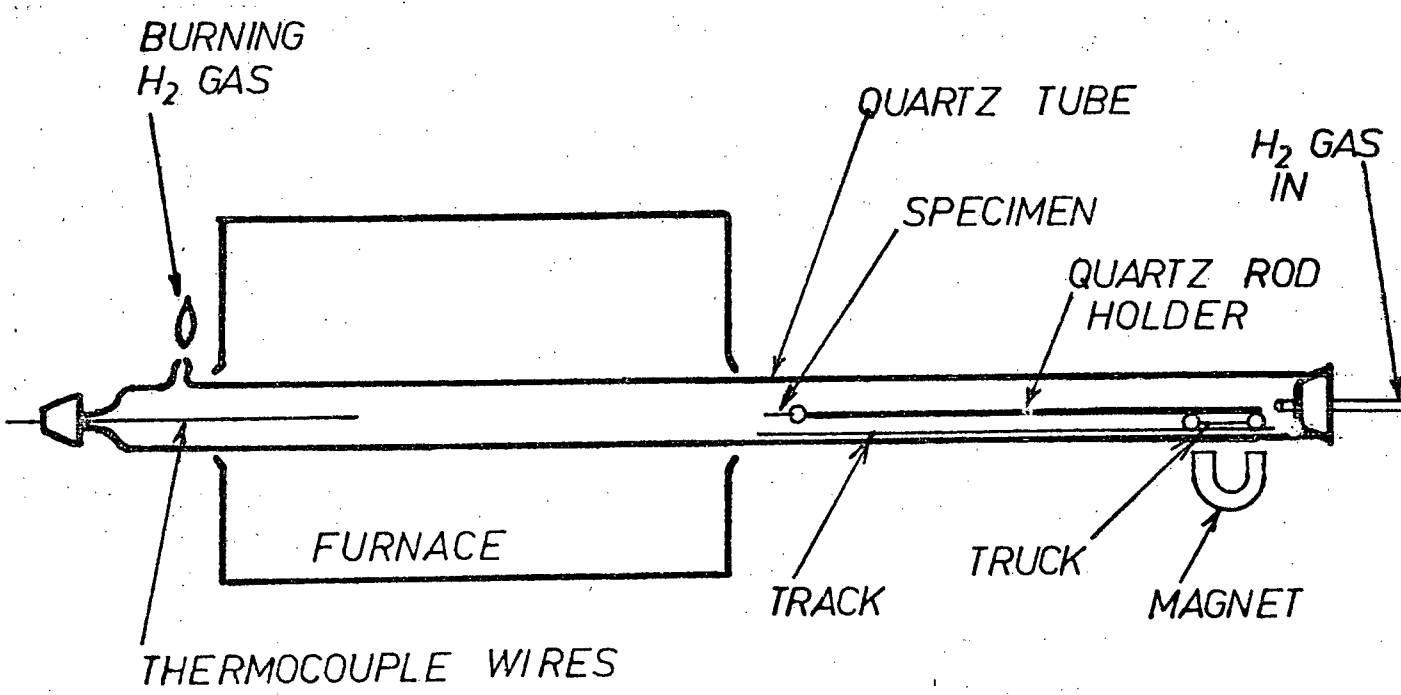

Fig. IVB-5 Ohmic Contact Annealing Furnace

could be moved along a track lying in the quartz furnace tube but outside the furnace (see Fig. IVB-5). The specimen was run into the hot section of the furnace and up to a thermocouple by pulling the truck down to the track with a magnet. The thermocouple measured the rise in temperature of the GaAs to 450°C, 20 seconds after which the truck was pulled back and the GaAs allowed to cool.

Good ohmic contacts with contact resistance r_c less than 3×10^{-2} Ω cm^2 have been reported by Robinson ([75R2], p. 335) using this method.

IV-C Electrical Measurements

In the first section of this chapter, the parameters R, R_{SH}, n and ϕ_B were defined and shown to be important in determining solar cell performance. Information on all these parameters can be gained from measurement of the dark I-V relationship of a Schottky barrier diode. Such measurements were performed on Schottky barrier diodes fabricated from the CSVT grown GaAs films and are described below.

As a check on the barrier height determination and also to obtain information on the doping density of the GaAs films C-V measurements were performed on the completed Schottky barrier diodes. All the electrical measurements were made on GaAs films grown at a substrate temperature of 710°C. Diodes were fabricated on three such films and a range of behaviour was observed. Results are presented from 8 diodes which serve to illustrate the range of the data obtained.

1. Measurement Apparatus

The current-voltage measurements were made in a grounded metal chamber. The Mo side of the diodes were pressed into contact with a gold plated disc using micrometer probes on the substrate edges. The top contact

was made via a gold wire probe. The test fixture was connected to the measuring instrument by RG-58 coaxial cables. Forward and reverse voltage bias was supplied by an Ambitrol regulated DC power supply model 5005R. Voltages were measured across the specimen with a Fluke DCC. differential voltmeter to ensure infinite resistance at the meter for low biases. A Keithley 417 high speed picoammeter and a Fluke digital multimeter model 8000A measured currents less than and greater than 3×10^{-5} amps respectively.

The capacitance-voltage measurements were made in the same test fixture as for the J-V characteristics. The contact probes were connected to the test terminals of a Boonton Capacitance/Inductance meter model 71A by RG-58 coaxial cables. The combined length of the cables was less than 2 ft. The correction for error in capacitance measurement owing to series inductance for this length of cables was less than 0.1 pf. (0.1% of results). The model 71A instrument provided capacitance measurements by means of a 15 mv test signal at 1 MHz. The DC bias was applied to the specimen by an external source and a Fluke differential voltmeter model 881AB measured the bias voltage to greater than 2 significant digit accuracy.

Measurements were performed in the dark 30 minutes after any exposure to light. These precautions prevented light induced trapping effects.

2. Current-Voltage Results

a. ϕ_B, n and R_{SH}

The forward bias semilog J-V plots of all the diodes tested exhibited three characteristic regions and Fig. IVC-1 curve c shows a typical example. The central region of the curve relates to the expected

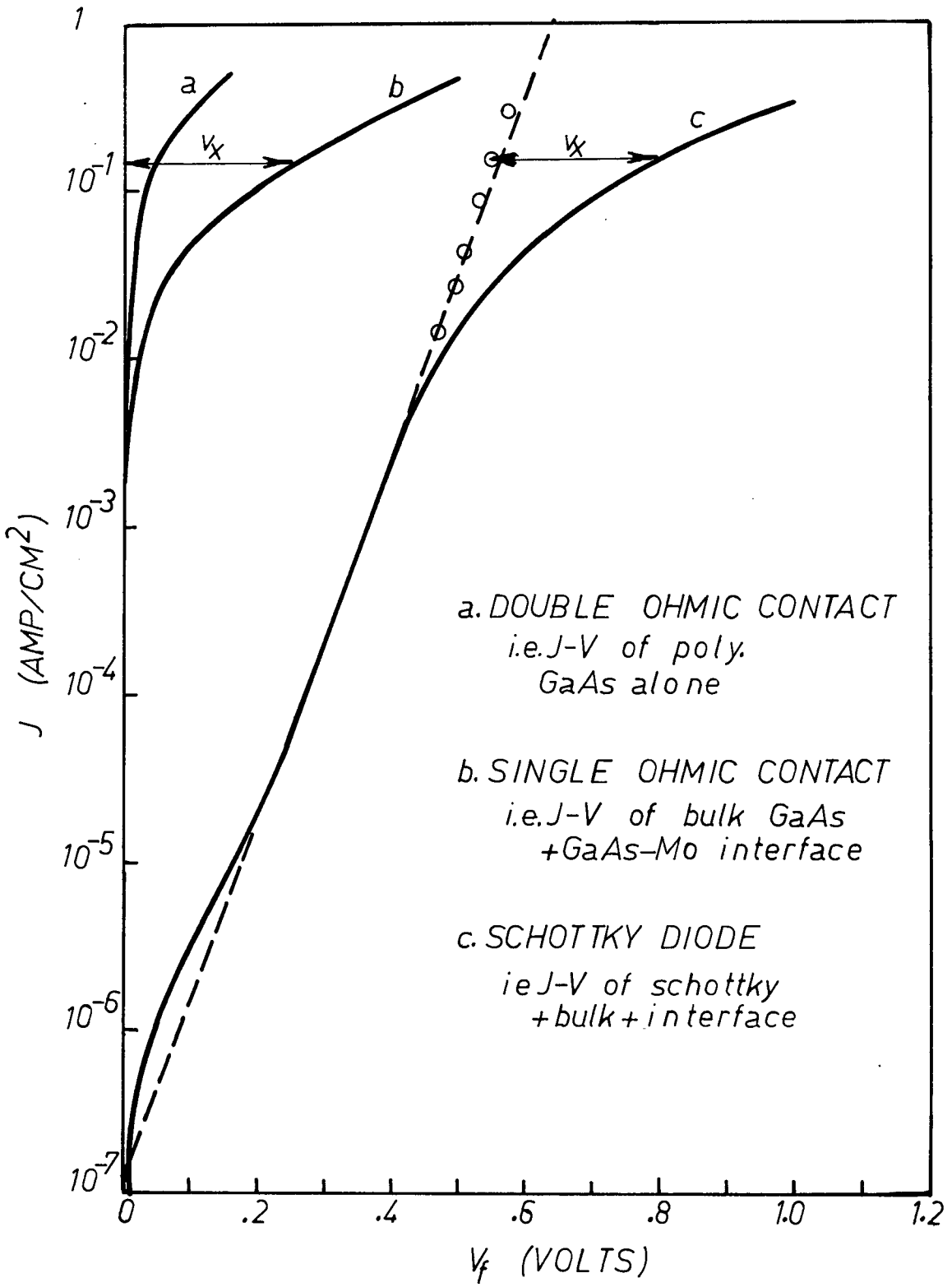

Fig. IVC-1 Series Resistance Model Check

experimental behaviour and from this portion and its extrapolation to zero bias the parameters n and ϕ_B were determined. n values in the range of 1.58-2.29 were encountered, whilst ϕ_B values fell within a range of 0.67 to 0.80. The results are tabulated in Table IVC-1.

n and ϕ_B did not vary appreciably over the surface of the films except for diodes with large values of series resistance. High series resistance tended to reduce the range of the linear region of the ℓn J-V plot to the point where it was difficult to make accurate straight line approximations. See, for example, Fig. IVC-2.

The low bias (< about 0.2-0.3v) portion of the ℓn J-V curves indicated the presence of recombination or other shunting currents. As described in section IV-A, these phenomena can be represented in the equivalent circuit by a shunt resistance R_{SH}. Values of R_{SH} were computed for the various diodes by measuring the slope of the I-V curve at values of reverse bias close to the origin. In the equivalent circuit of Fig. IVA-1,

$$J \approx J_S + \frac{V}{AR_{SH}} \qquad \text{(IVC-1)}$$

for the reverse bias case where $JAR_{SH} << V$. The above conditions lead to $R_{SH} = \frac{dV}{dJ}\Big|_{V_R \approx 0}$. The results are summarized in Table IVC-1 and show that R_{SH} values for the diodes were high and in the range of 3.9×10^5 to 3.2×10^7 Ω.

b. R_S

The deviation from linearity of the ℓn J-V plots at high bias values was accounted for by the presence of series resistance in the diodes. In this region of the curve, the current-voltage relation can be expressed as

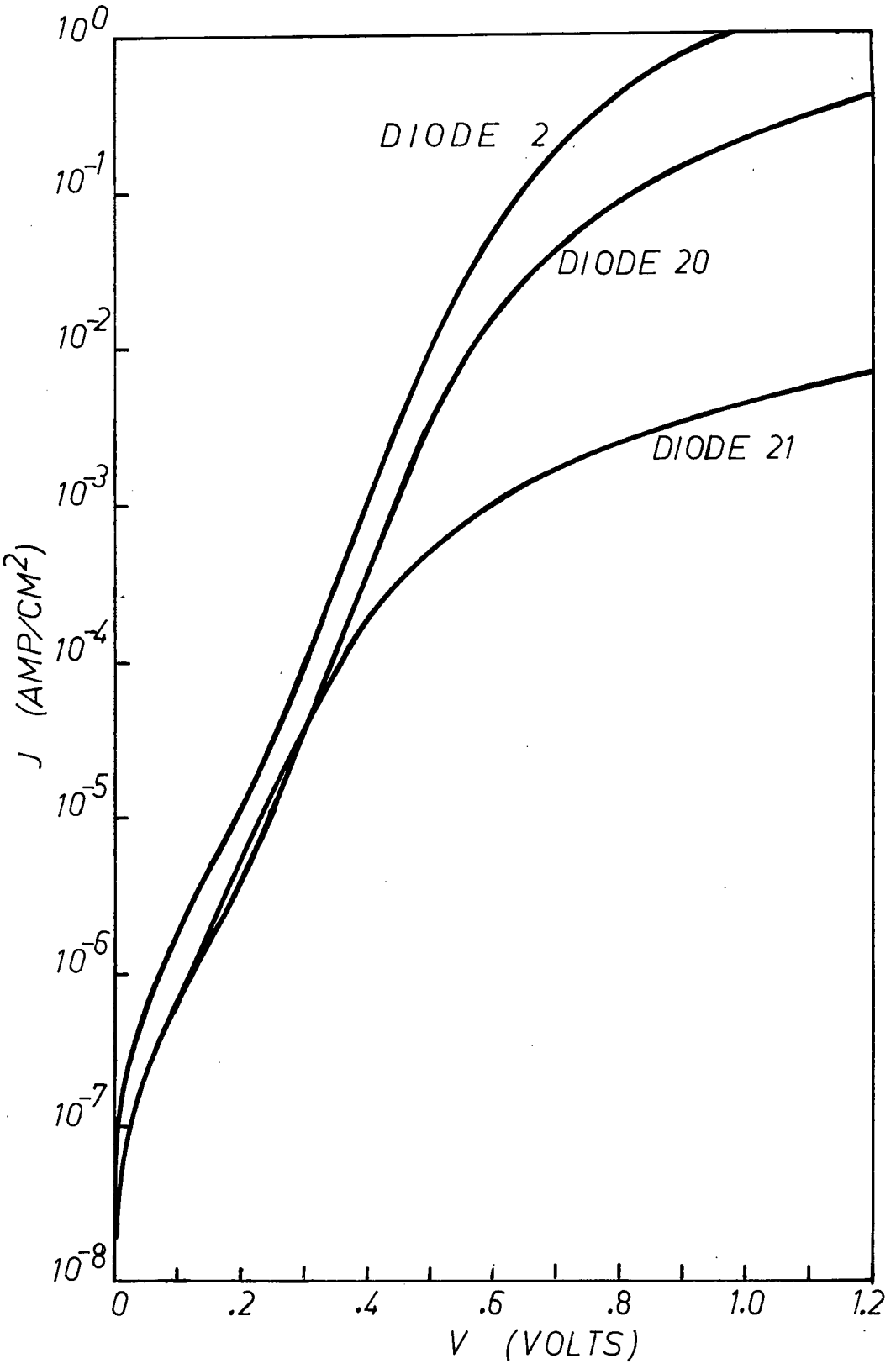

Fig. IVC-2 J-V Characteristics of Diodes on Samples B1/II with Different R_S
$R_S(2) = 120\Omega$, $R_S(20) = 550\Omega$, $R_S(21) = 35k\Omega$

$$J = J_S \exp \frac{q}{nkT} (V - JAR_S) \qquad \text{(IVC-2)}$$

Thus JAR_S is simply the voltage difference (ΔV) between the experimental curve and the straight line approximation to the ideal diode equation ($J = J_S \exp (qV/nkT)$) and therefore $R_S = \Delta V/JA$. Where appreciable dependence of this calculated series resistance on diode current occurred the highest value (worst case) of R_S was recorded. The results are summarized in Table IVC-1 from which it can be seen that R_S values covering the wide range of 20.5 Ω to 15.8 kΩ were obtained. Fig. IVC-2 shows some typical results.

These values of R_S would be too high in a solar cell. As the gold barrier films used here were at least 2000 Å thick the contribution to R_S from the barrier metal sheet resistance can be neglected. The high series resistance is thus related to the Mo contact and semiconductor film resistances and in an attempt to discern the relative magnitude of these components the following tests were made.

In the first test, GaAs chips were scribed and broken from several of the films and their substrates in order to measure the film resistively alone. In only one instance was this method successful (part of sample A5) and to this film ohmic contacts were deposited on opposing faces. The resulting current-voltage plot was linear over four decades in voltage as shown in Fig. IVC-3. The resistance R is the inverse of the slope and therefore the film resistivity is given by

$$\rho = \frac{1}{\text{slope}} \cdot \frac{A}{\ell} = 220 \ \Omega\Omega\text{cm} \qquad \text{(IVC-3)}$$

For a contact area of 7.8×10^{-3} cm^2 (as used for the diodes reported in Table IV-3), the series resistance due to the GaAs film would be 33 ohms. This is close to the lowest reported value of R_S, suggesting that the higher values of R_S may have been due to high resistance between

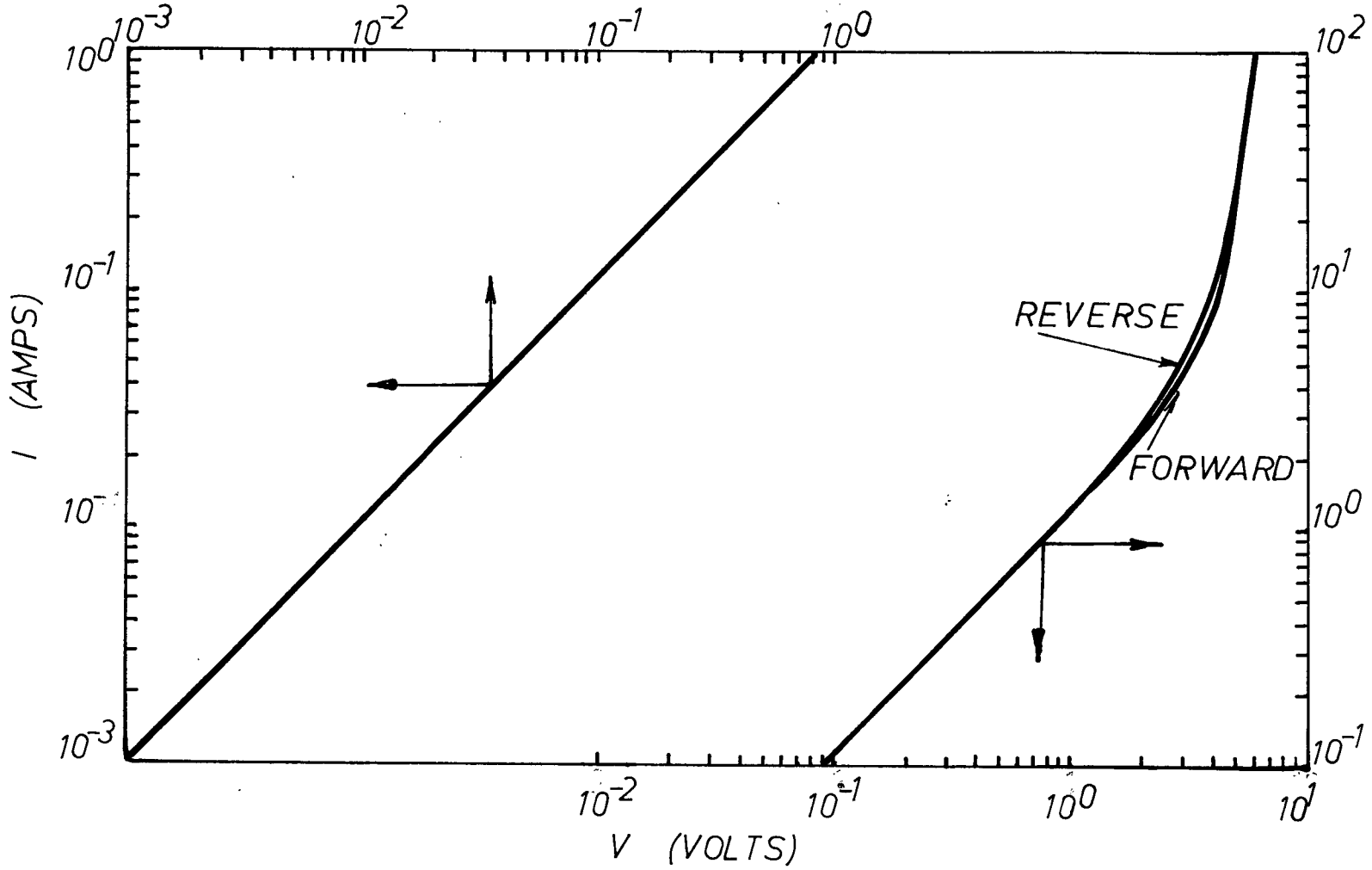

Fig. IVC-3 Relationship of Polycrystalline GaAs Chip with Ohmic Contacts on Both Sides

the GaAs film and Mo substrate. To investigate this possibility, the following test was carried out.

The sample used for this test was part of sample B1/III which had previously been scribed and broken into two pieces (the other of the pieces was used to obtain some of the data reported in Table IVC-1). Ohmic, instead of rectifying, contacts were applied to the free surface of the film and the range of J-V characteristics obtained is represented by the curves shown in Fig. IVC-4.

None of the curves is either linear or symmetrical about the origin. A variety of degrees of rectification is demonstrated and the more exponential nature of the characteristics when the Mo electrode was positive implies that the Mo-GaAs interface was rectifying. The equivalent resistances of the contacts were clearly voltage dependent, although over the range of -0.1 to +0.1 volts relatively constant values of series resistance could be implied (see Fig. IVC-5).

It is apparent that the Mo/GaAs interface exerts a large and variable influence on the total Au/GaAs/Mo diode characteristic. To further illustrate this point, it is interesting to plot on one graph the I-V characteristics from the three tests reported above. This is done in Fig. IVC-1 where the diode characteristics (c) came from contacts to sample B1/III and the ohmic contact characteristics (b) came from sample B1/II used to construct Fig. IVC-4 (both samples originated from the same film). The difference between curves (a) which is Fig. IVC-3 for dimensions equivalent to B1/III and (b) represents the contribution of the GaAs/Mo interface to the conduction characteristic. By subtracting this difference from curve (c) the linear region of curve (c) is extended to high bias levels. This shows the effect of the back contact

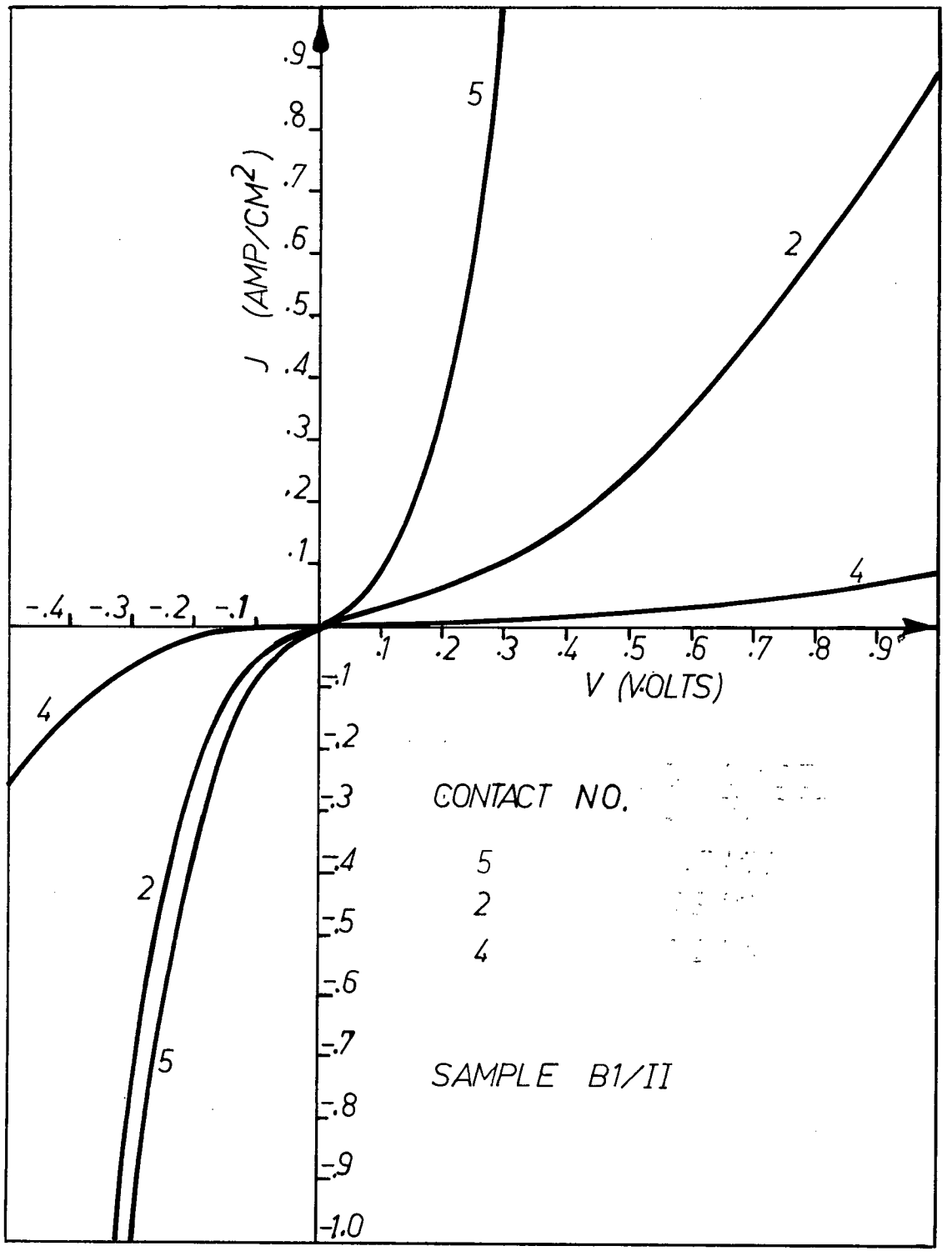

Fig. IVC-4 Current-Voltage Characteristic of Single Ohmic Contact to GaAs Mo

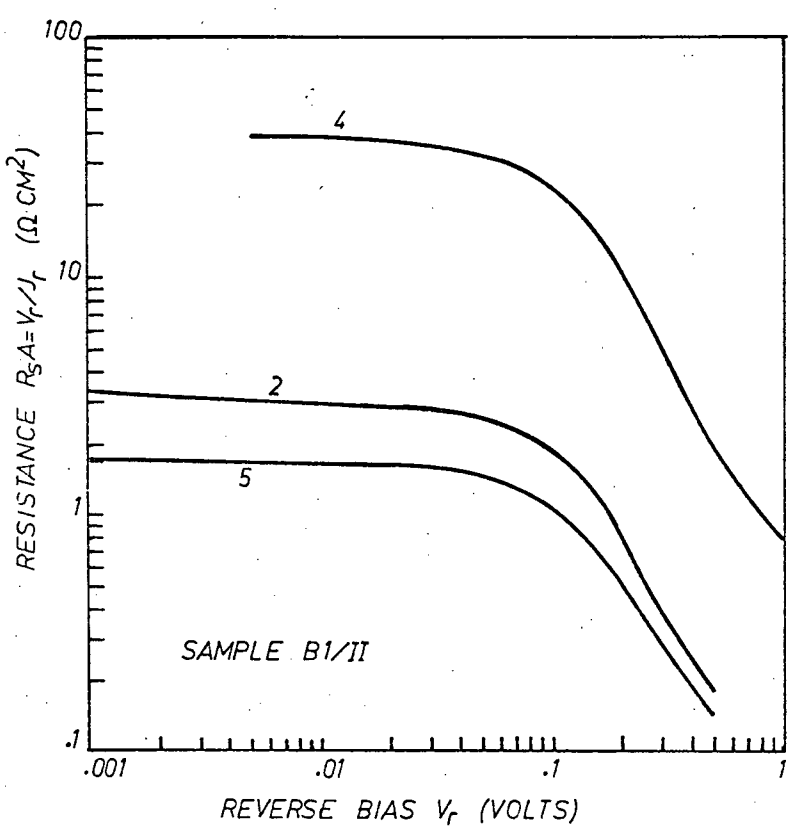

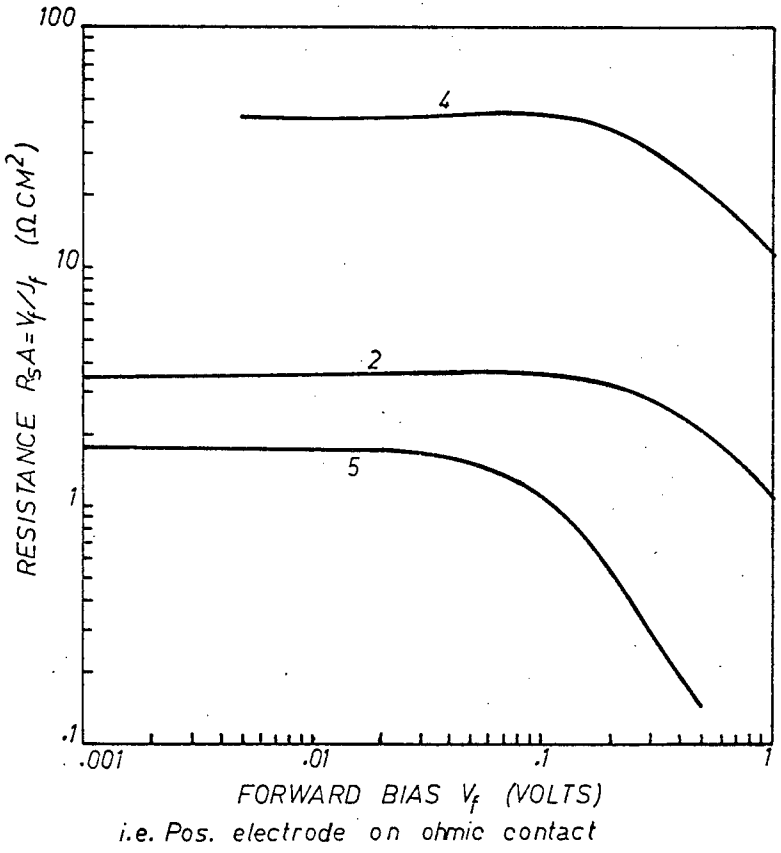

Fig. IVC-5 Series Resistance of B1/II Single Ohmic Contact Method

in causing the onset of a series resistance-dominated regime in the overall Schottky barrier diode conduction characteristic.

3. Capacitance Voltage Results

The zero-bias capacitance values for the eight diodessreferred to in section IV-C covered the range 8 - 250 picofarads, see Table IVC-1, and this variation is undoubtedly related to the non-uniformity in the back contact conditions described earlier. Because of the high effective series resistance of many of the diodes most of the measured C-V characteristics had to be corrected, after the fashion described below, for the presence of R_S before interpretation of the C^{-2}-V characteristics could be attempted.

The correction to the capacitance readings due to series resistance is illustrated through Fig. IVC-7a which shows how the Boonton capacitance meter characterizes the specimen as a parallel combination of conductance and capacitance. When the series resistance of the semiconductor bulk and Mo-GaAs contact is taken into account the circuit of Fig. IVC-7b results with the parallel branches representing the actual rectifying contact (Au/GaAs). The value R_S would be expected to vary only slightly over the normal range of C-V biasing (see Fig. IVC-5 and note that the voltage drop due to the Mo contact was much less than the rectifying contact over this range).

The steady state small signal equivalent capacitance of Fig. IVC-6 for angular frequency ω is given by equation IVC-4.

$$C' = C/[(R_S G + 1)^2 + \omega^2 R_S^2 C^2] \qquad \text{(IVC-4)}$$

Goodman ([63G2], p. 330) introduced a useful approximation for the case where $0.005 < (\omega R_S C)^2 < 0.1$ and $R_S G << 1$ by inserting equation IVC-4 (with $R_S G = 0$) into IVB-5 giving

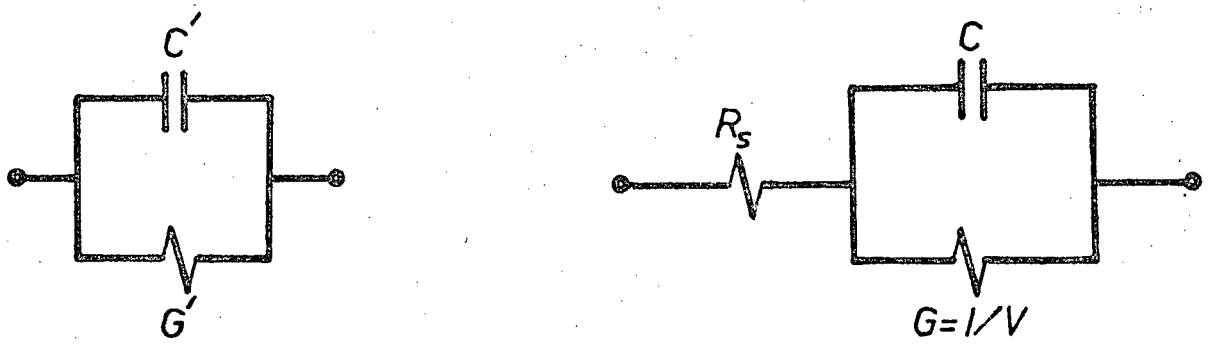

a. METER MEASURES THIS CIRCUIT

b. POLYCRYSTALLINE DIODE CIRCUIT

Fig. IVC-6 Equivalent and Actual Circuit for a Polycrystalline Metal-Semiconductor Diode

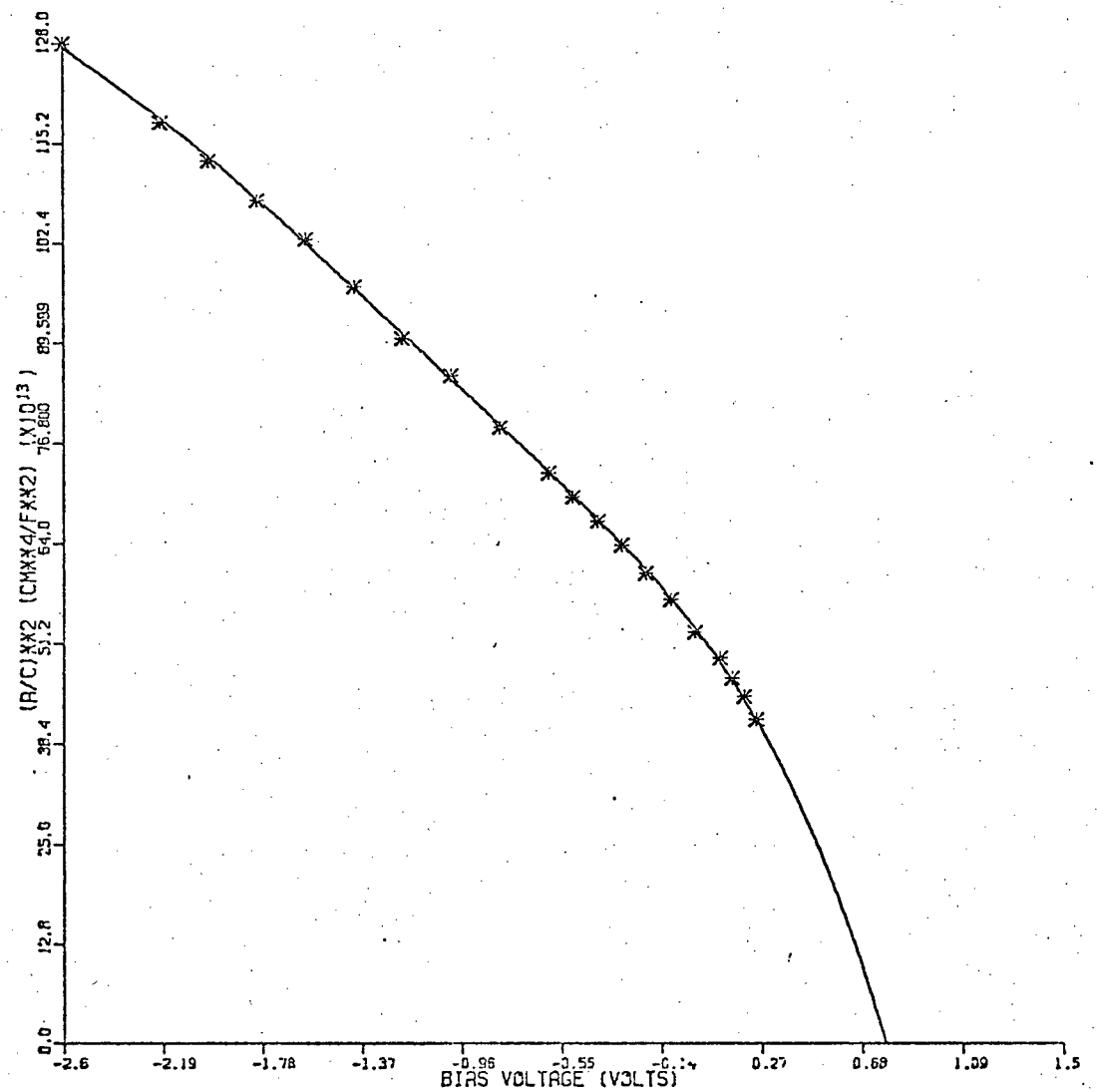

Fig. IVC-7a $(A/C)^2$ vs V of Specimen B1/II, Diode 2, Corrected for R_S and Approximated by a 5th Degree Chebychev Polynomial

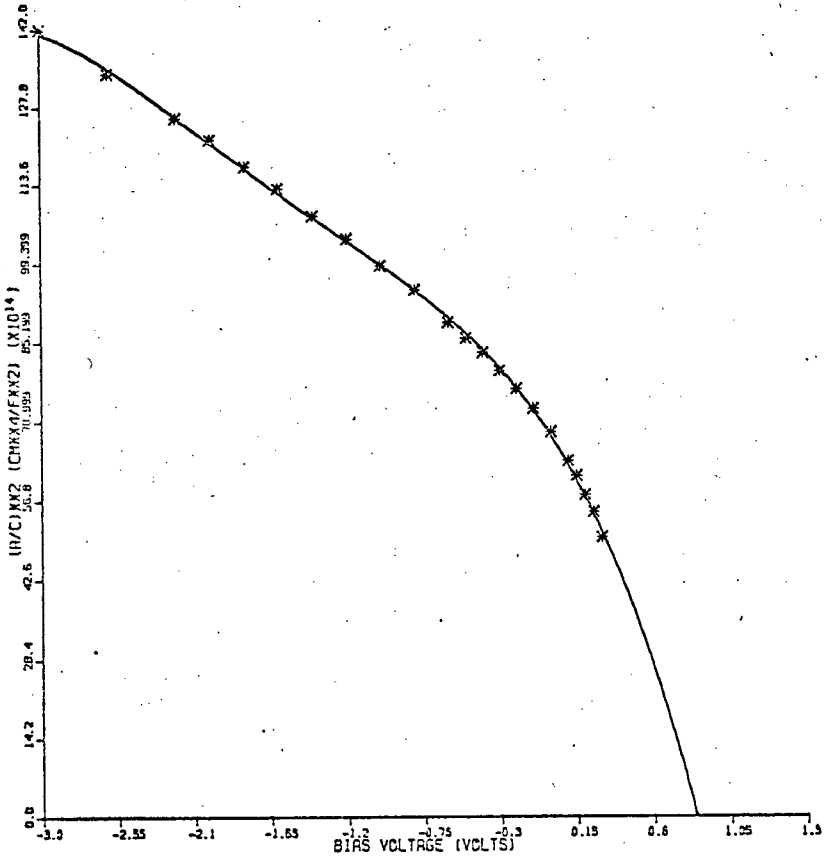

b) Diode 20, Corrected for R_S and Approximated by a 4th Degree Chebychev Polynomial

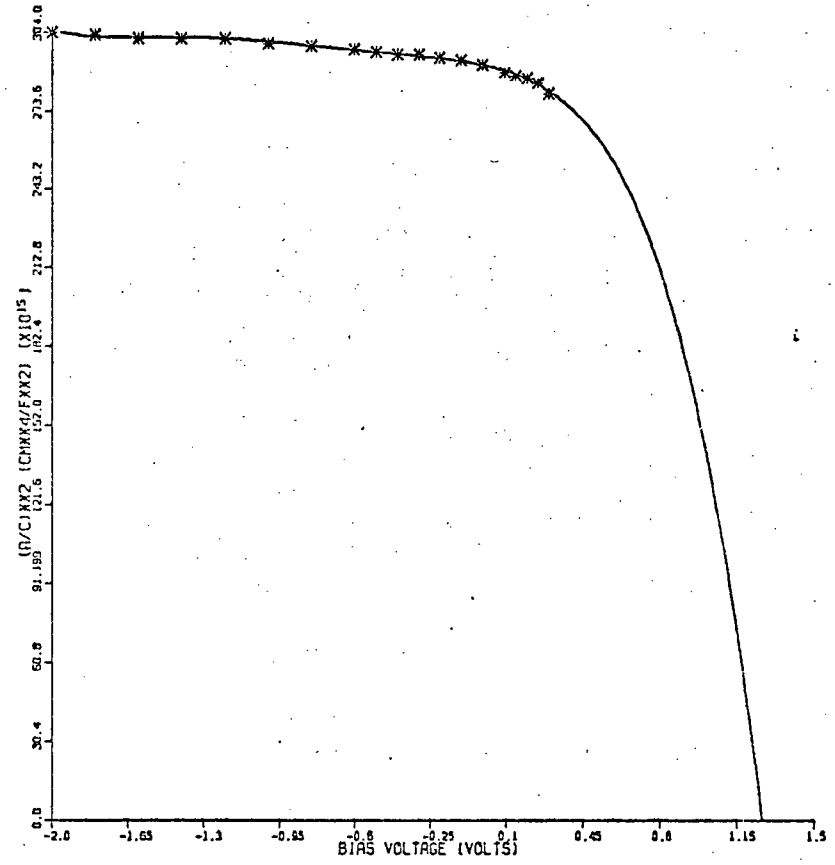

c) Diode 21, Not Corrected for R_S and Approximated by a 5th Degree Chebychev Polynomial

Fig. IVC-7b & c $(A/C)^2$ vs V of Specimen B1/II

$$[A/C']^2 = 2(V_{bi} - V - kT/q)/(qE_S N_D) + 2A^2\omega^2 R_S^2 \qquad \text{(IVC-5)}$$

The measured $(A/C')^2$ vs V curve is translated upward from the Schottky relation by a constant $2A^2\omega^2 R_S^2$. This correction was applied to the relevant diodes and used to obtain the results summarized in Table IVC-1.

To demonstrate the recorded range in C-V data, results are shown in Fig. IVC-7 for the three diodes that were used to illustrate the J-V results (Fig. IVC-2). For diode B2/II pt. 21, the series resistance was so high that no correction could be attempted. It is clear in all cases that the diode doping density profile was not uniform and that the doping density was increasing away from the Au/GaAs interface. To facilitate comparison of the various characteristics, the doping density was calculated from the C-V data using equation IVB-6 with V set to zero. The resulting doping densities are shown in Table IVC-1.

Because of the non-linearity in the $(A/C)^2$-V plots, the extrapolation of the data to the abscissa (to find ϕ_B using equation IVB-3 and 5) is of very doubtful value. However, an attempt to do this was made by fitting the data to Chebychev polynomials of degree 6 or less. The coefficients were calculated by numerical methods on an IBM 370 computer. Both the original data and the Chebychev approximation were plotted on a Calcomp plotter and the criterion for choosing the polynomial degree was the closest fit with the least error. The ϕ_B results so calculated and shown in Table IVC-1 were computed for zero bias conditions to allow comparison with the values calculated from the J-V method. To do this the image force lowering $\Delta\phi$ was calculated at V = 0 and V_n was calculated for the doping concentration that coincided with V = 0 where,

$$V_n = kT\ell n \frac{N_C}{N_{D(V=0)}} \qquad \text{(IVC-6)}$$

Device	R_S (Ω)	R_{SH} (Ω)	J-V		C-V				Chebychev Polynomial Degree	C Corrected for R_S?
			n	ϕ_B (eV)	ϕ_B (eV)	$N_D(V>0)$ (cm^{-3})	$C_{(V=0)}$ (pf)	Vi (volts)		
B2/II pt. 4	20.5	7.9×10^6	1.58	.78	.77	4.0×10^{16}	200	.72	5	N
B1/III pt. 2	87.9	6.2×10^6	1.58	.74	.89	1.0×10^{16}	146	.80	5	Y
B3/I pt. 2	2010.	3.9×10^5	2.02	.67	-	1.1×10^{16}	64	1.05	4	U
B1/I pt. 9	196.	1.0×10^6	2.29	.72	1.04	1.4×10^{16}	165	.96	6	Y
B2/III pt. 17	22.9	5.7×10^6	1.50	.73	.77	5.8×10^{16}	250	.73	5	Y
B2/II pt. 2	54.0	1.1×10^7	1.66	.77	.83	3.9×10^{16}	192	.78	5	Y
B2/II pt. 20	248.	2.3×10^7	1.64	.80	.97	3.9×10^{15}	52	.85	4	Y
B2/II pt. 21	15,800.	3.2×10^7	1.85	.77	-	1.6×10^{15}	8	1.27	5	U

*N - Not necessary: $(\omega R_S C)^2 << 1$

Y - Yes: $R_S G << 1$ and $0.005 < (R_S C)^2 < 0.1$

U - Unable to correct for R_S: $R_S G \not< 1$

Table IVC-1 Electrical Properties of Au Schottky Polycrystalline-GaAs Diodes

N_C is the effective density of states in the conduction band and is equal to 4.7×10^7 cm^{-3} ([69S1], p. 57).

IV-D Discussion

Two of the major problems encountered in making solar cells from polycrystalline semiconductors involve the formation of a suitable electrostatic inhomogeneity for photocarrier separation and production of low resistivity semiconductor material. The work presented in this chapter has shown that these problems need not necessarily arise in Schottky barriers formed by the deposition of Au onto GaAs films grown by the CSVT method.

The resistivity of films grown at a substrate temperature of 710°C on Mo foil substrates has been measured to be 220 ohm·cm, which can be compared with the value of 10^{-2} Ω cm appropriate to the GaAs source material. From the C-V data presented, it is clear that the doping density profile in the films is not uniform but that a value of around 1×10^{16} donors per cm^3 is present in the better films. The equivalent single crystal resistivity for GaAs doped to this extent would be 0.15 Ω cm, indicating a reduced conduction in the polycrystalline film. This is to be expected and a number of models have been proposed to explain the phenomenon (see appendix AIV2). If the film conduction is primarily controlled by the grain boundaries, which may be appropriately modelled as a two sided abrupt junction, then the incomplete barrier height would be 0.3 eV. A detailed investigation of the temperature and magnetic dependence of the conductivity would be necessary, however, to yield further insight into the mechanisms controlling conduction.

The metal-semiconductor barrier height of the Au/polycrystalline GaAs system was found to lie in the range of 0.67-0.80 eV. These values

are a little lower than the value of 0.89 eV which is generally accepted to represent the barrier height in the Au/single crystal GaAs case. The lower value found here is most likely due to conditions at the surface of the GaAs film where surface state distributions might differ from the single crystal case. Another possibility, (Pulfrey [76P1]) is the presence of a thin interfacial insulating layer between the metal and semiconductor, although in the present investigation care was taken to avoid interfacial layer formation by ensuring that the transfer of the GaAS from the etching solution to the evaporation chamber was rapid ($\approx$ 20 secs). Under these conditions, an oxide in excess of 10 Å would not be expected to grow (see Pruniaux and Adams [72P1]). The difference in barrier height of .09 eV or so is likely due to positive surface state densities that might form on n-type GaAs films.

Using a value for ϕ_B of 0.8 eV and a film resistivity of 220 ohm cm, it can be computed from the table in appendix IVA-3 that a 5 μm thick GaAs solar cell with n = 1.5 has a maximum AM1 conversion efficiency of 10%. Such a thickness of film is easily grown by the present method and comprises essentially columnar crystals of grain size averaging around 5 μm. Hovel (Fig. 68 (75H1]), using a specific polycrystalline semiconductor model, has calculated that an AM1 efficiency of 80% of the single crystal case is possible under these circumstances. If such an efficiency could be realized in a practical cell then this would be a substantial improvement over the best figures so far reported for thin film solar cells.

The only work reported on solar cell fabrication using thin film CSVT GaAs was by Vohl et al. [67V1] who obtained AM1 efficiencies of 4.5 %, but encountered stability and series resistance problems. The

latter is also very much in evidence in the cells prepared in this work and has been found to be associated with the contact between the GaAs film and the Mo substrate on which it was grown. This contact is rectifying to a degree that apparently varies with position on the substrate. The reason for the non-uniformity is not obvious although it may be due to impurities in the Mo foil or to variations in surface state and interfacial layer properties. An ohmic contact is desirable at this interface as backwall cells are prone to uniformity problems (backwall cells using direct band gap semiconductors need to be very thin, 1-2 μm). In any event, the Mo/GaAs interface is not sufficiently rectifying for consideration of this mode of operation. Even the most rectifying contact (see Fig. IVC-4) only had an estimated barrier height of .6 eV, which would only give an AM1 conversion efficiency of 2% (from Fig. 1 [74P1]).

To improve this back contact and make it more nearly ohmic, the doping density in this region of the semiconductor must be increased. Vohl et al. [67V1] achieved this by precoating the Mo foil with a layer of tin-germanium prior to GaAs film formation. The subsequent film growth presumably allowed shallow-level donor diffusion into the interfacial region of the semiconductor. The diffusion process is apparently very critical as was discovered when an attempt was made in the present investigation to repeat this result (using a 500 Å tin-germanium layer), no rectifying action was observed. Presumably, the tin and/or germanium diffused through the film causing shorting paths. Possibly, movement of these metals can proceed along grain boundaries by electromigration which may account for the stability problems noted by Vohl et al.

In the present work, the back contact resistance has been shown to account for the deviation from linearity at high bias of the dark ℓnJ-V

characteristics. The corrected characteristics show linearity over nearly five decades of current, with a slope that gives a diode ideality factor n typically in the range of 1.5 to 2.0. These values are too high to be accounted for solely by the voltage-dependent parameters in the thermionic emission model, see equation IVB-11, but are typical of the values reported in the literature for Schottky barrier solar cells. n values of this magnitude can be associated with the presence of an interfacial oxide (see Card and Roderick [71C1]) or with the dominance of a recombination-generation component of current. In the recent solar cell work by Anderson and Milano [75A1], it has been suggested that high n values would be advantageous in Schottky barrier solar cells on account of their apparent affect on the open circuit voltage, e.g. from equation IIA-2 of appendix IVA-2 at $I_L = 0$, we have

$$V_{oc} = n\frac{kT}{q} \ln \left(\frac{I_{ph} + I_S}{I_S}\right) \qquad \text{(IVD-1)}$$

However, it must be realized that for n-values greater than about 1.1, the dark current can probably no longer be adequately expressed by the usual expression (see equation IVA-1) and thus the I_S term in equation IVD-1 needs modification, almost certainly to a higher value. This effect will cause a reduction in V_{oc} that may well offset the gain that might otherwise be expected from the high n value. It is thus unreasonable to treat n as an independent parameter and even in deliberately-formed MIS solar cells, high n values cannot be automatically used in an equation such as IVD-1, as for example, Anderson and Milano [75A1] have suggested, because the interfacial layer affects the minority carrier flow and the majority carrier flow in different ways and it is this effect that controls V_{oc} (see Card and Yang [76C1]).

n values greater than unity can also be associated with recombination-generation current flow and there is evidence for the presence of such currents in the present work. Such currents can be expected to occur on account of deep level traps formed at dislocations and impurities in the polycrystalline film. The usual expression for recombination current is

$$J_{rec} = J_r \exp [eV/2kT] \qquad \text{(IVD-2)}$$

where

$$J_r = qn_iW/\tau$$

and

$$4\ kT/q \leq V \leq V_{bi} - 10\ kT/q$$

(from Roderick [70R2], p. 1163). n_i is the intrinsic carrier concentration = $\sqrt{N_C N_V} \exp(-Eg/2kT)$ and τ is the effective lifetime. For several trapping centers at different energy positions, and possibly interacting, J_{rec} could be the sum of the individual recombination currents and thus the total current could be of the form

$$J = J_{ST} \exp (qV/kT) + J_{r_{sum}} \exp (qV/2kT) \qquad \text{(IVD-3)}$$

for moderate bias. When both currents are comparable n has a value between 1 and 2. Such behaviour has recently been reported in MIS solar cells on p-type silicon (see Pulfrey [76P2]).

In the present work, the recombination-generation currents can be represented in the equivalent circuit (see Fig. IVA-1) by a parallel resistance R_{SH}. The values reported in this work (see Table IVC-1) are, however, acceptably high. If such values could be maintained in a large area solar cell, say 5 cm^2, R_{SH} magnitudes of about 10^4 ohms would result and these would not cause any significant reduction in solar conversion

efficiency (Hovel [75H1], Fig. 52). Shunt resistance in polycrystalline solar cells can also be caused by large impurity concentrations diffused along dislocations or grain boundaries, or by the presence of fine metallic bridges through microcracks in the film. Although microcracks were observed in some films using the SEM (see Figs. IIIB-3) the high recorded values of R_{SH} indicate that these imperfections would not adversely affect solar cell performance.

V CONCLUSION

GaAs films grown by the close-spaced vapour transport method directly onto Mo substrates have been found to be polycrystalline with no preferred orientation. The crystallite area increased with the temperature at which the substrate was held during growth and at 710°C grain sizes of 100 μm^2 were observed. The crystallites formed a columnar-like structure with crystal size comparable to the film thickness. This pattern is advantageous for thin film solar cells in that carriers need to cross few grain boundaries and high conversion efficiencies are possible. No impurities or foreign intrusions existed in the films in quantities observable on the electron microprobe.

The resistivity of the GaAs films was greater than would be expected for single crystal GaAs of the same doping density ($\approx 1 \times 10^{16}$ atoms cm^{-3}), but still low enough for consideration for use in thin film solar cells. However, the GaAs-Mo contact was a mildly rectifying contact, varying in the degree of rectification across the sample but never sufficient for use as a backwall cell. Frontwall cell operation would also be adversely affected by this arrangement and the problem was thought to be associated with surface states, interfacial layers or low doping densities in the resulting GaAs films. A thin layer of Ge or Sn precoated on the Mo substrates would probably enhance the doping density of the film and experimentation with these and other dopants is suggested to try and reveal a combination that yields good ohmic contacts but does not affect the stability of the diode.

Diode junction formation was achieved by the deposition of gold onto the GaAs films and the resulting barriers showed acceptable values of barrier height and diode ideality factor. The latter values and the

low bias portion of the dark J-V characteristics suggested the presence of recombination-generation currents, but the associated value of shunt resistance was sufficiently high not to present a problem in subsequent solar cell fabrication.

REFERENCES

1950

V1 Volger, J., "Note on the Hall Potential Across an Inhomogeneous Conductor", Physical Review, Vol. 79, pp. 1023-1024.

1956

P1 Petritz, Richard L., "Theory of Photoconductivity in Semiconductor Films", Physical Review, Vol. 104, No. 6, pp. 1508-1516.

S1 Slater, J.C., "Barrier Theory of the Photoconductivity of Lead Sulfide", Physical Review, Vol. 103, No. 6, pp. 1631-1644.

1957

H1 Henisch, H.K., Rectifying Semiconductor Contacts, Oxford University Press, London.

1958

F1 Fuller, C.S. and Whelan, J.M., "Diffusion, Solubility, and Electrical Behavior of Copper in Gallium Arsenide", J. Phys. Chem. Solids, Vol. 6, pp. 173-177.

1960

C1 Cunnell, F.A., Edmond, J.T., and Harding, W.R., "Technology of GaAs", Solid State Electronics, Vol. 1, pp. 97-106.

1962

F1 Frosch, G.J. and Thurmond, C.D., "Vapour Pressure Measurements of Ga-Ga_2O_3 Mixtures", Journal of Physical Chemistry, Vol. 66, pp. 877-878.

1963

B1 Birks, L.S., Electron Probe Microanalysis, Wiley, New York.

G1 Gottlieb, G. Eugene and Carboy, John F., "Epitaxial Growth of GaAs in Water Vapor", RCA Review, Vol. 24, No. 4, pp. 591-595.

G2 Goodman, Alvin M., "Metal-Semiconductor Barrier Height Measurement by the Differential Capacitance Method-One Carrier System", Journal of Applied Physics, Vol. 34, No. 2.

N1 Nicoll, F.H., "The Use of Close-Spacing in Chemical Transport Systems for Growing Epitaxial Layers of Semiconductors", Journal of the Electrochemical Society, Vol. 110, No. 11, pp. 1165-1167.

1963 (Continued)

R1 Robinson, P.H., "Transport of Gallium Arsenide by a Close-Spaced Technique", RCA Review, Vol. 24, No. 4, pp. 574-584.

1964

M1 Madelung, O., Physics of III-V Compounds, Wiley, New York.

1965

M1 Many, Goldstein and Grover, Semiconductor Surfaces, John Wiley and Sons, New York.

P1 Padovani, F.A. and Sumner, G.G., "Experimental Study of Gold-Gallium Arsenide Schottky Barriers", J. Appl. Phys., Vol. 36, No. 12, p. 3744.

1966

P1 Pankey, Titus and John E. Davey, "Structural and Optical Characteristics of Thin Films II", J. Appl. Phys., Vol. 37, No. 4.

T1 Tucker, T.W., "The Electrical Properties of Evaporated Silicon Films", M.A.Sc. Thesis, University of British Columbia, Vancouver.

1967

S1 Seraphine, B.O. and Bennett, H.E., "Optical Constants", Semiconductors and Semimetals, Vol. 3, eds. Beer and Willardson, Academic Press, New York.

V1 Vohl, P. et al., "GaAs Thin Film Solar Cells", IEEE Transactions on Electron Devices, Vol. ED-14, No. 1.

1969

S1 Sze, S.M., Physics of Semiconductor Devices, John Wiley and Sons, New York.

1970

R1 Rideout, V.L. and Crowell, C.R., "Effects of Image Force and Tunneling on Current Transport in Metal-Semiconductor (Schottky Barrier) Contacts", Solid State Electronics, Vol. 13, pp. 993-1009.

R2 Rhoderick, E.H., "The Physics of Schottky Barriers", J. Phys. D : Appl. Phys., Vol. 3, No. 8, p. 1153.

1971

C1 Cord, H.C. and Rhoderick, E.H., "Studies of Tunnel MOS Diodes", J. Phys. D : Appl. Phys., Vol. 4, p. 1589.

1972

H1 Hubbert, M. King, "The Energy Resources of the Earth", Scientific American, Vol. 225, No. 3, pp. 61-70.

I1 International Commission on Illumination, Publication CIE No. 20 (TC-22), Paris.

J1 Joseph, J.D. and Kamins, T.I., "Resistivity of Chemically Deposited Polycrystalline Silicon Films", Solid State Electronics, Vol. 15, pp. 355-358.

M1 Milnes, A.G. and Feucht, D.L., Heterojunctions and Metal-Semiconductor Junctions, Academic Press, New York.

P1 Pruniaux, B.R. and Adams, A.C., "Dependence of Barrier Height of Metal Semiconductor Contact (Au-GaAs) on Thickness of Semiconductor Surface Layer", J. Appl. Phys., Vol. 43, No. 4, pp. 1980-1982.

1973

H1 Heime, K., Konig, U., aKohn, E. and Wortmann, A., "Very Low Resistance Ni-AuGe-Ni Contacts to n-GaAs", Solid State Electronics, Vol. 17, pp. 835-837.

1974

F1 Fang, P.H., "Polycrystalline Silicon Solar Cells for Economical and Ecological Electrical Power Systems", National Science Foundation Report No. NSF/RANN/SE/GI-34975/73/4, Washington, D.C.

M1 Maratukulam, D.J., "Options of Energy Exploitation and Utilization", M.Eng. Essay, Dept. of E.E., University of British Columbia, Vancouver, Canada.

P1 Pulfrey, D.L. and McOuat, R.F., "Schottky-Barrier Solar Cell Calculations", Applied Physics Letters, Vol. 24, No. 15, pp. 167-169.

R1 Ramakumar, R., Allison, H.J. and Hughes, W.L., "Solar Energy Conversion and Storage Systems for the Future", IEEE Power Engineering Papers on Energy Development, April, pp. 12-20.

1975

A1 Anderson, Wayne A. and Milano, R.A., "I-V Characteristics for Silicon Schottky Solar Cells", Proceedings of the IEEE, Jan., pp. 206-208.

C1 Chu, T.L. et al., "Polycrystalline Silicon Solar Cells for Terrestrial Applications", 11th IEEE Photovoltaic Specialists Conference, p. 303.

E1 Electronics, "Solar Cell Offers 21% Efficiency with GaAs", Vol. 47, No. 11.

1975 (Continued)

H1 Hovel, H.J., "Solar Cells", Semiconductors and Semimetals, edited by Beer and Willardson, Academic Press, Vol. 11.

R1 Rideout, V.L., "A Review of the Theory and Technology for Ohmic Contacts to Group III-IV Compound Semiconductors, Solid State Electronics, Vol. 18, pp. 541-550.

R2 Robinson, G.Y., "Metallurgical and Electrical Properties of Alloyed Ni/Au-Ge Films on n-Type GaAs", Solid State Electronics, Vol. 18, pp. 331-342.

S1 Stirn, R.J. and Yeh, Y.C.M., "A 15% Efficient Antireflection-Coated Metal-Oxide-Semiconductor Solar Cell", Applied Physics Letters, Vol. 27, No. 2, pp. 95-97.

W1 Wolf, M., "Outlook for Si Photovoltaic Devices for Terrestrial Solar-Energy Utilization", J. Vac. Sci. Technol., Vol. 12, No. 5, p. 984.

W2 Woodall, J.M. and Hovel, H.J., "Outlooks for GaAs Terrestrial Photovoltaics", J. Vac. Sci. Technol., Vol. 12, No. 5, p. 1000.

1976

C1 Card, H.C. and Yang, E.S., "MIS-Schottky Theory Under Conditions of Optical Carrier Generation in Solar Cells", Applied Physics Letters, Vol. 29, No. 1, pp. 51-53.

H1 Heckingbottom, R. et al., "Precise Lattice Parameter Determination of Dislocation-Free GaAs-II Chemical and Electrical Measurements", Solid State Electronics, Vol. 19, pp. 335-339.

M1 McOuat, R.F., M.A.Sc. Thesis, University of British Columbia, Vancouver, Canada.

P1 Pulfrey, D.L., "Barrier Height Enhancement in p-Silicon MIS Solar Cells", IEEE Transactions on Electron Devices, June, pp. 587-589.

P2 Pulfrey, D.L., "Surface Insulation Solar Cells Using p-Type Silicon", to be published.

APPENDICES

AI1. REVIEW OF THE ENERGY SITUATION

The future for photovoltaic solar cells is shining brighter as the energy crisis darkens. The deeper one looks into energy resources the better solar cells appear for many reasons. They use a non depletable fuel (the sun's radiation), do not emit pollutants or produce dangerous wastes, can use less surface area than hydroelectric reservoirs for producing equivalent power, are not biased towards large scale conversion, are mass production oriented and require low maintenance. So why are they still years in the future? It is the cost, which must be reduced by 100 to 1000 times. This factor is not so large as it looks considering that mass production techniques have not been implemented and research and development has, in the past, been concerned with space not terrestrial uses. If an intense program is initiated for photovoltaic power systems, such as for the transistor in the 50's, the necessary breakthroughs could result in an economic cell. But one might ask is such a large scale effort necessary? Are there not other easier methods?

For present trends of energy consumption oil will be depleted in less than half a century. After oil, coal is estimated to last two centuries but with increased cost per watt and sulfer polutants ([74M1], p.5). Even a shorter lifetime lies in store for present day nuclear reactors using uranium 238. New sources of energy must be found to replace the exhausted ones. If the drain of fuels to extinction is to be avoided, energy for the future must come from the following non depletable sources

1. Hydro

2. Wind
3. Tidal
4. Geothermal
5. Deuterium deuterium (fusion)
6. Direct solar radiation

Hydro power is the only substantial method presently in use. But it has been exploited considerably, for example in Western Europe 57% of the potential hydro is already harnessed. 8.5% of all the worlds potential hydro power was developed by 1967. Even if all sites are eventually utilized, still 2/3 of today's industrialized society's demand must be furnished by other means [74M1], p. 14). Substantial energy sources must be found to meet the ever increasing consumption (double every 7 years).

Wind, tidal and geothermal power sources are intermittant or limited to certain geographical locations. They therefore require storage and transmission facilities which reduce efficiencies and increase expenses. The worst problem with tidal and geothermal sites are their relative scarcity. To date tidal power has only been utilized at the Rance Estuary in France where the plant has a 240 MW capacity. Hubbert estimates that the global potential tidal power is less than 2% of water power ([71H1], p. 67). Geothermal energy has been more widely developed around the world with a total of over 1000 MW produced in Italy, Japan, New Zealand and U.S.S.R. But this method is just potentially comparable to tidal power and can furnish only a small fraction of our energy needs in the future [71H1, p. 67). On the other hand, energy available in the winds is more abundant (see Table AII-1). It has been noted that periods of high winds and intense solar radiation occur at different times during the

Energy Source	kWh	References
Hydroelectric	2.0×10^{13}	[74R1] p. 13
Winds over land	5.7×10^{15}	[74R1] p. 13
Tides and tidal currents	1.1×10^{11}	[71H1] p. 67
Geothermal	8.9×10^{12}*	[74R1] p. 13
Deuterium deuterium	essentially infinite	
Solar Radiation incident on land	2.0×10^{14}	[74R1] p. 13
Projected energy use in year 2000 A.D.	2.0×10^{14}	[74R1] p. 13

Table AI1-1 World Estimated Annual Potential Energy

*USA alone.

day and year. Therefore R. Ramakumar et al. [74R1] suggest combined wind generation and solar cell installations which would increase the energy supply while reducing the size of the storage system.

In the nuclear power field the fast breader reactors could be labelled as consumers of non depletable fuel. However, their ever increasing cost due to serious cooling problems and danger from using highly enriched weapons grade fuel render them less promising than originally expected. Fusion reactors are further behind in the research stage and cannot be regarded as an energy solution with certainty. No one person, now, can predict that all the fundamental scientific, technical and engineering breakthroughs, required to produce net energy, will be found. So, for the moment, other methods must be investigated in case fusion power is unattainable. Besides, no one source of power has supplied all our

energy needs in the past and it would be foolhardy to suppose an exclusive method could in the future.

The final non depletable energy source is solar radiation. It can be tapped without danger or disruption to the ecological system. Next to fusion fuels it is the most abundant source of energy known. The sun radiates 22800 x 10^{12} watts incident on land which is many orders of magnitude greater than present human consumption of 8 x 10^{12} watts. Unlike fusion it can be and is already being harnessed. The two prime methods of converting the sun's power to useful energy are thermal and photovoltaic. Both are expensive, but photovoltaic is the most direct method for conversion to electricity. Since electricity is the most adaptable form of energy existing today, research should be directed to produce cheaper photovoltaic converters.

AI2. SUMMARY OF ENERGY CONVERSION VERSUS SEMICONDUCTOR THICKNESS CALCULATION

The curves in Fig.IA-1 were plotted from computer calculations of photovoltaic energy conversion of AM1 irradiance in GaAs and Si cells. The program used Simpson's Rule to evaluate the integral of equation AI2-1 below, for semiconductor thickness from 0.1 μm to 100 μm

$$\int_{\lambda_i}^{\lambda_f} \mathscr{E}(\lambda)\ [1 - \exp\ (-\alpha(\lambda)x)]\ d\lambda \qquad \text{(AI2-1)}$$

where λ = Wavelength of radiation in m^{-1}

$\mathscr{E}(\lambda)$ = Irradiance in $Wm^{-2}\ m^{-1}$

$\alpha(\lambda)$ = Absorption coefficient in cm^{-1}

x = Thickness of semiconductor in cm

Shultz's AM1 irradiance data ([72I1], p. 47) was used for incident energy in a form converted to 100, .02 μm spectral bands by a cubic spline interpolation with tension (see McOuat [76M1]).

The absorption data for GaAs came from Seraphin and Bennett ([67S1], pp. 518-519) and the energy was summed from $\lambda_i = 0.3$ to $\lambda_f = .904$ μm.

The Si absorption information was taken from Sze ([69S1], p. 54) for wavelengths between $\lambda_i = .3$ μm and $\lambda_f = 1.13$ μm.

AIV1. DETERMINATION OF MAXIMUM EFFICIENCY OF SOLAR CELLS AS A FUNCTION OF SERIES RESISTANCE

Solar cell efficiencies are limited by their series resistance, especially for the case of high resistance materials such as polycrystalline GaAs. To give an idea of the extent of this effect, a relation between efficiency and series resistance has been derived. The solar cell has been modelled by a simple photo diode, shown in Fig. IVA-1. Both shunt resistance and recombination processes are considered negligible compared to high series resistance and therefore these effects were omitted in the calculations.

From Fig. IVA-1

$$I_L = I_{ph} - I_S\{\exp[e(V_L + R_S I_L)/nkT] - 1\} \qquad \text{(AIV1-1)}$$

where for thermionic emission over the metal/semiconductor barrier $I_S = A(A^* T^2 \exp(-e\phi_B/kT))$. For $(V_L + R_S I_L) >> .03$volts

$$V_L = n\frac{kT}{e}\ln\left(\frac{I_{ph} - I_L + I_S}{I_S}\right) - I_L R_S \qquad \text{(AIV1-2)}$$

The d.c. power at the load is $P_L \doteq I_L V_L$ (AIV1-3)

and the maximum is found by letting $\frac{dP_L}{dI_L} = 0$ (AIV1-4)

Substituting AIV1-2 in AIV1-3 and performing the operation of equation AIV1-4 yields

$$n \frac{kT}{e} \left[n\left(\frac{I_{ph} - I_L + I_S}{I_S}\right) - \frac{I_L}{I_{ph} - I_L + I_S}\right] - 2I_L R_S = 0 \qquad \text{(AIV1-5)}$$

The solution to AIV1-5 can be obtained by iteration. Let the value of the current I_L at maximum power be given by I_M, then the maximum power P_M is

$$P_M = I_M^2 \left[\frac{n \frac{kT}{e}}{I_{SC} - I_M + I_S} + R_S\right] \qquad \text{(AIV1-6)}$$

Using AM1 value of 0.112 W/cm^2 ([72I1], p. 47) as incident sunlight power, efficiency is

$$\eta_{SC} = \frac{I_M^2}{0.112} \left[\frac{n \frac{kT}{e}}{I_{ph} - I_M + I_S} + R_S\right] \qquad \text{(AIV1-7)}$$

The generated photocurrent I_{ph} can be approximated by assuming a collection efficiency of 100% for all photons with energy greater than the band gap (E_g) of GaAs. In reality the absorption by the front contact and transmission through the thickness of the semiconductor would reduce the collection efficiency to between 70 and 90%. However, the resultant lowering in efficiency is small compared to that due to series resistance, and therefore 100% collection efficiency was used for simplicity.

For $\mathcal{E}(\lambda)$ representing AM1 solar energy radiation according to Schulze (see tabulation in CIE publication No. 20 (TC 2.2) [72I1], p. 47), then

$$\mathcal{E}(\lambda) = h\nu \, V_{ph}(\lambda) \qquad \text{(AIV1-8)}$$

where $V_{ph}(\lambda)$ = spectral density of photons

ν = frequency of photons

Therefore the number of photons with energy greater than E_g is

$$\frac{1}{ch} \int_{\lambda_g}^{0.3\mu m} \lambda \mathcal{E}(\lambda)\, d\lambda$$

where c = speed of light

and $\lambda_g = \frac{hc}{E_g}$

$$\therefore \quad I_{ph} = \frac{q}{ch} \int_{\lambda_g}^{0.3\mu m} \lambda \mathcal{E}(\lambda)\, d$$

For GaAs $E_g = 1.43$ eV

$I_{SC} = 33.2$ ma/cm^2

Various values of R_S, n, ϕ_B were inserted into equation AIV1-7 and iterated using an IBM 370/168 computer yielding the results of Table AIV1. Richardson's constant and the temperature were as follows

$A^* = 8$ amps $°K^{-2}T^{-2}$

$T = 300$ °K

(Ω) R_S	.8	.8	.8	.9	.9	.9	ϕ_{Bn} (eV)
	1	2	3	1	2	3	n
.1	6.6	13.2	19.8	9.3	18.7	28.0	
.5	6.2	12.9	19.5	8.9	18.3	27.7	
1.0	5.8	12.5	19.1	8.5	17.9	27.3	
5.0	3.3	9.5	16.0	5.5	14.6	23.9	
10.	1.9	6.7	12.6	3.3	11.1	20.0	
50.	.4	1.6	3.6	.7	2.9	6.3	
100.	.2	.8	1.8	.4	1.5	3.2	
500.	.0	.2	.4	.1	.3	.7	

Table AIV1 Efficiency $\eta(\%)$ vs Series Resistance R_S (Ω)

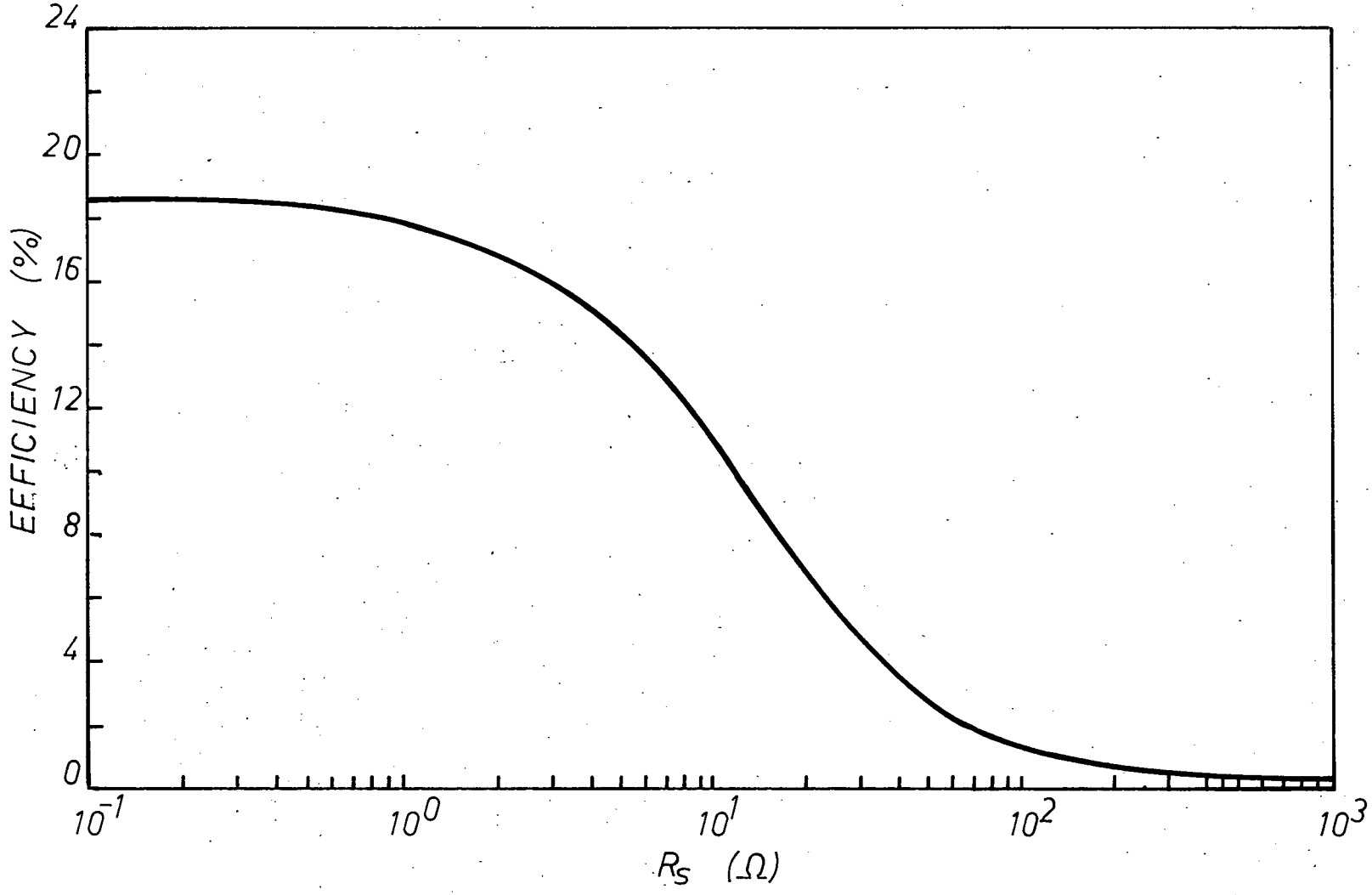

Fig. AIV1 Efficiency as a function of Series Resistance

AIV2 THEORIES OF CONDUCTION IN POLYCRYSTALLINE FILMS

The resistance of polycrystalline semiconductors is usually found to be greater than for that of the single crystal case [72J1]. No completely satisfactory theories have evolved to explain this, however, it is generally accepted that grain boundaries consist of large quantities of imperfections, and these imperfections somehow reduce conduction.

Volger [50V1] proposed a mosaic model for inhomogeneous conductors consisting of high conductance crystallites separated by thin layers (grain boundaries) of lower conductivity (see Fig. AIV2-1a). The macroscopic resistivity $\bar{\rho}$ becomes

$$\bar{\rho} \simeq \rho_B + \left(\frac{\ell_C}{\ell_B}\right) \rho_C \qquad \text{(AIV2-1)}$$

for the non trivial case of $\rho_B >> \rho_C$. Petritz [56P1] working with photoconductive PbS, has suggested that the high resistance region could arise from potential barriers of the type shown in Fig. AIV2-1b. In this model the film was composed of crystallites of n type PbS whilst the thin intercrystal barriers were p type oxides of lead. The conductivity was assumed to be limited by the potential barrier formed by the n-p-n junctions. From the current voltage relationship of a barrier like the one shown in Fig. AIV2-1b, the macroscopic conductivity $\bar{\sigma}$ was expressed in terms of the single crystal conductivity σ_{SC}

$$\bar{\sigma} = e^{-\frac{q\phi}{kT}} \sigma_{SC} \qquad \text{(AIV2-2)}$$

where ϕ is the potential height of the barriers above the conduction band edge in the bulk of the crystallites. Slater [56S1], assuming, a complete barrier model (Fig. AIV2-2b), showed that in the case of PbS films, a barrier height ϕ of 0.37 eV would be necessary to fit the experimental data.

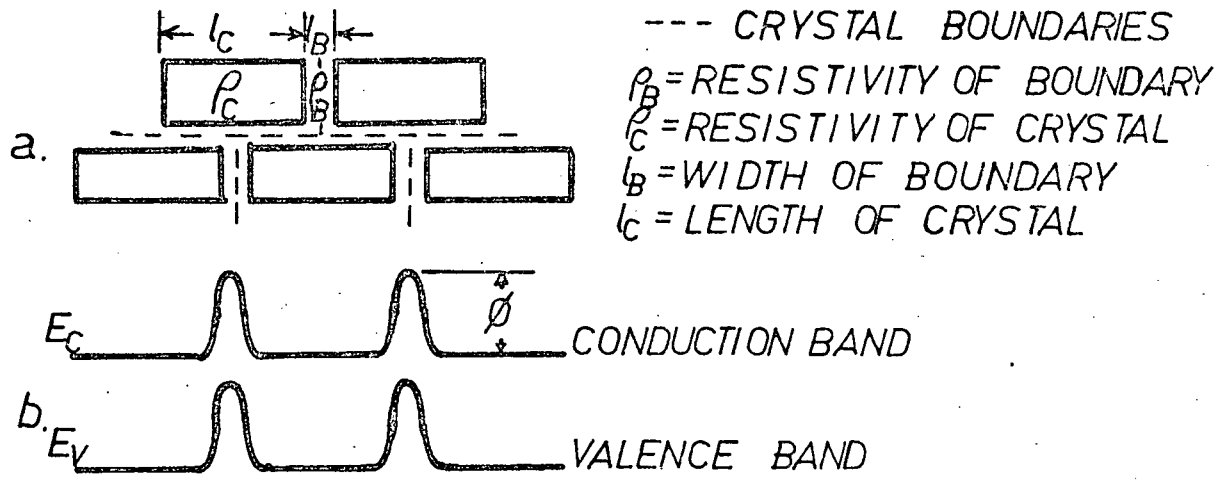

Fig. AIV2-1 The Mosaic Model and Its Band Diagram

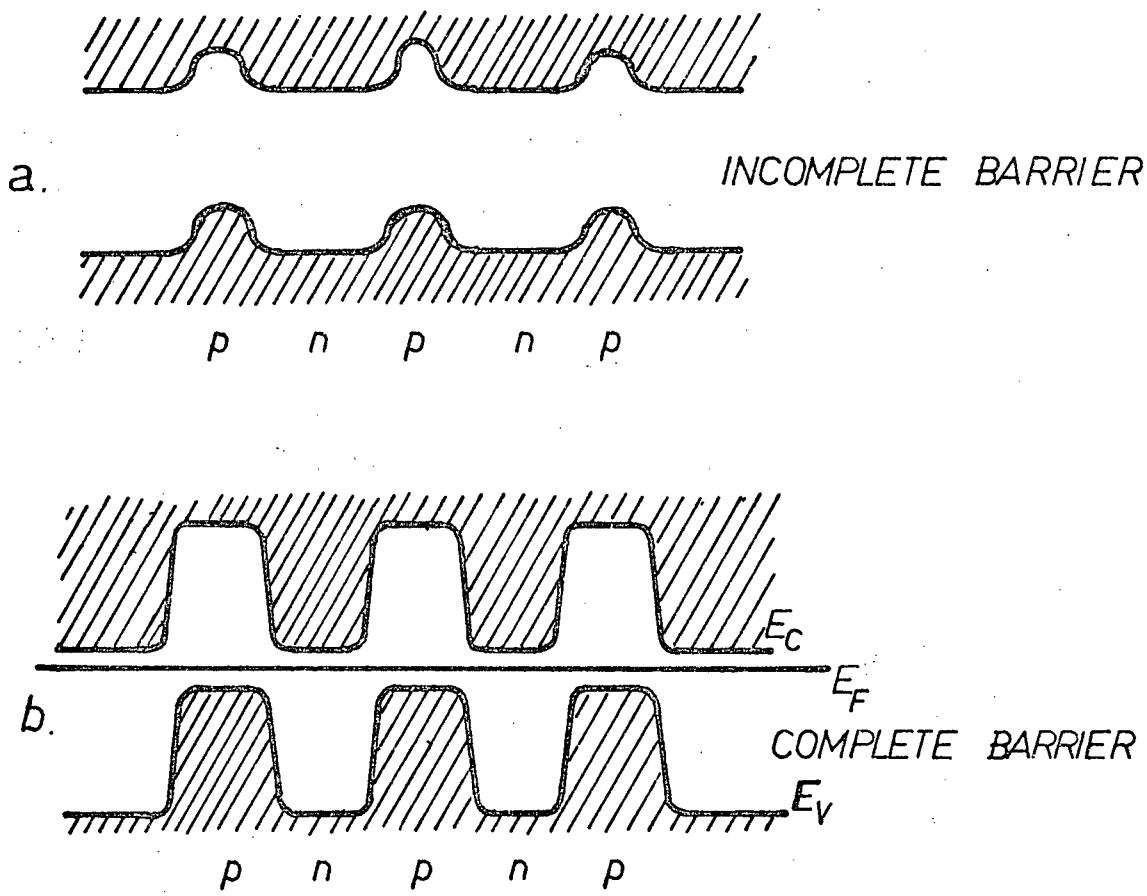

Fig. AIV2-2 Barrier Types

Incidently, polycrystalline GaAs films have been found to exhibit n-type character [63R1, 63G1, and 63N1]. This could be due to large n type crystals that contribute the bulk of the carriers separated by only thin p-type intercrystal regions. Note that the forbidden energy band for GaAs is 1.43 eV, several times larger than that for PbS (of .4eV). If complete barriers are formed, as in Petritz's mosaic model illustrated in Fig. IVA-2b, ϕ would be approximately 1.4 eV and $\bar{\sigma}$ would be orders of magnitude lower than the observed results for polycrystalline GaAs. But note that ℓ_C > 10,000 Å and ℓ_B < 200 Å (beam diameter) as was seen on the SEM and complete barriers cannot form in such a narrow intercrystal space. Therefore incomplete barriers of the type shown in Fig. AIV2-2a are expected for the case of polycrystalline GaAs.

If the grain boundary to crystal region is modelled by a two sided abrupt junction, the shape and size of the barriers would be governed as in Sze's ([69S1], p. 89) equations 10 and 15 from which the barrier height follows directly,

$$\phi = \frac{q\, W^2}{2\, \varepsilon_S \left(\frac{N_A + N_D}{N_A N_D}\right)} \qquad \text{(AIV2-3)}$$

From the resistivity measurements of chapter IVC, it was found that ϕ, by equation AIV2-2, would be approximately 0.3 eV. If it is assumed that $N_A = N_D = 10^{18} cm^{-3}$ then W = 270 Å (width of the p-type region). Keeping to this model, for any narrower p-type regions, N_A would have to be greater than N_D and

$$\phi = \frac{q\, W^2 N_D}{2\varepsilon_S} \qquad \text{for } N_A >> N_D \qquad \text{(AIV2-4)}$$

Grain boundaries are generally believed to be of the order of 10 Å to 100 Å thick (Tucker [66T1], p. 15). This suggests large variations in impurity concentrations between boundary and crystal regions.

Perhaps a more realistic model for thin grain boundaries would involve a very narrow, say 10 Å, region of structural imperfections which might include dangling bonds, dislocations and impurity atoms. An understanding of the effect of such a grain boundary can be achieved by considering the Kronig-Penney representation of a periodic lattice. Consider two adjoining crystals, each of which consists of a periodic square well potential, while the contact area between them consists of atoms that at least have periodicities other than that of the crystallites. Allowed energy levels in the forbidden band would then be produced at the joint (i.e. grain boundary). A similar model was used by Tamm and Shockley ([65M1], pp. 165-182) to account for surface states on semiconductor surfaces. However, in this work these allowed energy levels will be called grain boundary states.

Because the exact nature of the boundary states is not known, their density distribution with respect to energy is impossible to predict. However, limiting cases for the distribution of barrier states can be postulated and so indicate the range of possible interaction between the boundary regions and adjacent space-charge regions. At one limit, the density of states would be uniformly distributed over all energy levels within the band gap. At the other limit, narrow bands or discrete energy levels would exist within the band gap. For an n-type semiconductor, acceptor-like boundary states (negatively charged when occupied by electrons and neutral when empty) would form a depletion region at the edge of the crystals and donor like boundary states (positively charged when empty and neutral when occupied by electrons) would form an accumulation layer. A net density of occupied acceptor states would form a barrier potential that would reduce conduction. Similarly for p-type semiconductors,

donor states in the grain boundaries would reduce conduction.

Let us now consider in detail the charges and potentials in the grain boundary region that might result from the presence of acceptor-like states in the grain boundaries. We shall assume an n-type semiconductor in equilibrium with no externally applied bias. The situation at the grain boundaries is represented in Fig. AIV2-3 for both boundary state cases.

For the single discrete energy states case, where N_δ is the number of acceptor type boundary states per unit area (in $eV^{-1}cm^{-2}$), the grain boundary charge is

$$Q_B = -\int_{E_V(0)}^{E_C(0)} \frac{q\, N_\delta\, \delta(E - \phi_\delta - E_V(0))}{1 + \exp\,(E - E_F)/kT}\, dE$$

$$\simeq \begin{cases} -q\, N_\delta & \text{for } \phi_\delta + E_V(0) \le E_F \\ 0 & \phi_\delta + E_V(0) > E_F \end{cases} * \qquad \text{(AIV2-5)}$$

For the uniform density of states case, where N_u is the net number of acceptor and donor surface states per unit area, per unit energy (in $eV^{-1}cm^{-2}$), and ϕ_o specifies the energy level (in eV) below which all surface states are filled for charge neutrality at the surface (before equilibrium), the grain boundary charge is

$$Q_B = \int_{\phi_o + E_V(0)}^{E_C(0)} \frac{-q\, N_u}{1 + \exp\,(E - E_F)/kT}\, dE$$

$$\simeq -q\, N_u\, (E_g - \phi_B - V_n - \phi_o) * \qquad \text{(AIV2-6)}$$

For charge neutrality to exist at the grain boundaries the grain boundary charge Q_B must be balanced by a positive space charge at

---

* The approximation that $\frac{1}{1 + \exp\,(E - E_F)/kT} = 1$ for $E < E_F$ and 0 for $E > E_F$ was used since kT is small at T = 300°K.

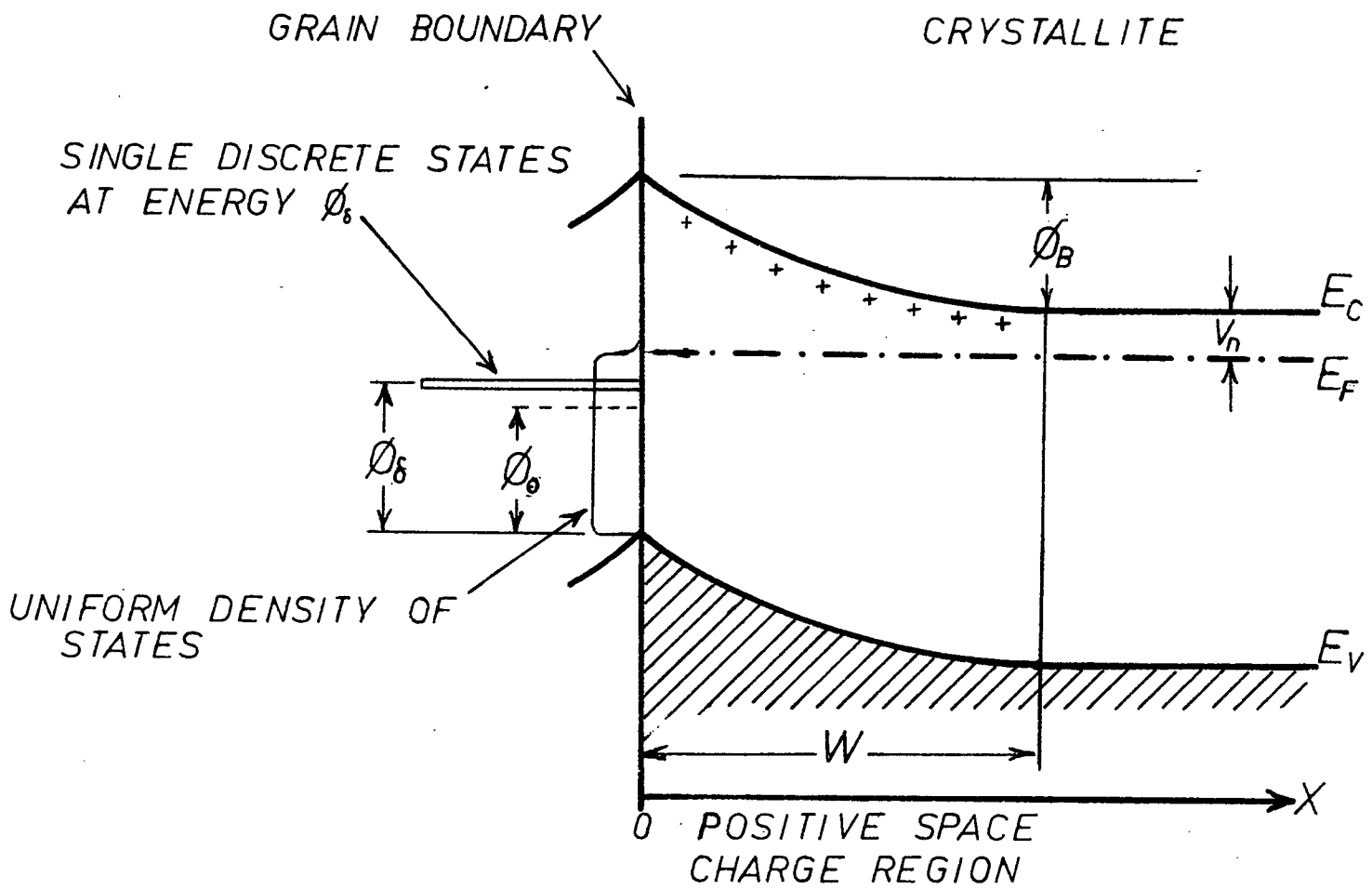

Fig. AIV2-3 Energy Diagram of a n-Type Crystallite at a Grain Boundary in the Presence of Boundary States

the crystallite surface. Assuming complete ionization in the crystallite space charge region of width W, then

$$Q_B = - qN_D W \qquad \text{(AIV2-7)}$$

The one dimensional Poisson's equation yields an intercrystal barrier height (see p. 88 Sze [69S1])

$$\phi_B = \frac{q\ N_D\ (W)^2}{2\varepsilon_S}$$

Therefore,
$$\phi_B + V_n = \frac{Q_B}{2qN_D\varepsilon_S} - \frac{kT}{q}\ \ell n\ \frac{N_D}{N_C} \qquad \text{(AIV2-8)}$$

where N_C is the effective density of states in the conduction band and is equal to $4.7 \times 10^{17} cm^{-3}$. For the discrete case, ϕ_B follows directly from equations 5 and 8 for a given N_δ, ϕ_δ and N_D. For the uniform case, equations 6 and 8 can be solved graphically for a given N_u, ϕ_o and N_D.

It can be seen that for a grain barrier height of about .3 eV (as was found by resistivity measurements and by equation AIV2-2) the density of boundary states for either discrete or uniform distribution must be about 10^{11} to 10^{13} $eV^{-1}cm^{-2}$. The conclusion to be drawn here is that the existing conductivity in polycrystalline GaAs could be explained in the forgoing model if boundary-state densities of 10^{11} to 10^{13} $eV^{-1}cm^{-2}$ were present. This number would seem reasonable on account of the magnitude of the surface atom density of GaAs (6×10^{14} atoms/cm^2).